

Marquette University

e-Publications@Marquette

Dissertations (1934 -)

Dissertations, Theses, and Professional
Projects

Immobilized Phosphate-Binding Protein Systems to remove and Recover Phosphate

Faten Bakri Hussein
Marquette University

Follow this and additional works at: https://epublications.marquette.edu/dissertations_mu



Part of the [Engineering Commons](#)

Recommended Citation

Hussein, Faten Bakri, "Immobilized Phosphate-Binding Protein Systems to remove and Recover Phosphate" (2022). *Dissertations (1934 -)*. 1598.

https://epublications.marquette.edu/dissertations_mu/1598

**IMMOBILIZED PHOSPHATE-BINDING PROTEIN SYSTEMS TO REMOVE
AND RECOVER PHOSPHATE**

by

Faten Bakri Hussein

A Dissertation submitted to the Faculty of the Graduate School,
Marquette University,
in Partial Fulfillment of the Requirements for
the Degree of Doctor of Philosophy

Milwaukee, Wisconsin

August 2022

ABSTRACT
IMMOBILIZED PHOSPHATE-BINDING PROTEIN SYSTEMS TO REMOVE AND RECOVER PHOSPHATE

Faten Bakri Hussein

Marquette University, 2022

Inorganic phosphorus (P_i) is a critical element for all life and a major component of DNA's backbone. Global agriculture requires P_i to support the rapid growth of plants and high crop productivity. Yet, the mineable P_i supply needed for global agriculture is in short supply in nature and P_i reserves are unevenly distributed around the world. In contrast, surplus P_i in water poses a serious pollution problem as it can cause eutrophication. Scarcity of non-renewable P_i resources combined with pollution in the form of overabundant P_i presents a phosphorus paradox. Tackling this issue is necessary and using innovative approaches targeting P_i removal to ultra-low levels in water/wastewater with subsequent recovery for reuse applications can help.

The purpose of this research was to investigate a novel solution utilizing the phosphate-binding protein PstS (PBP) to simultaneously remove and recover P_i from water matrices under controlled conditions. PBP is naturally expressed by many microorganisms as it is responsible for P_i transport into cells under conditions of low surrounding P_i levels. High affinity and selectivity towards P_i even at low concentrations is a superior advantage for removal and recovery efforts addressing the phosphorus paradox. Although PBP offers strong potential for use in engineered systems, more effective water/wastewater configurations are needed before it can be a potential sustainable treatment option for P_i removal and recovery. Specifically, improvements in immobilized PBP's contact with water, operation in flow-through setup, and adsorption capacity are critical.

This research investigated three prospective immobilized PBP-based systems. First, surface-displayed PBP on the outer membrane of *E. coli* was designed and tested for P_i capture and release. Previous surface displayed efforts did not address both P_i removal and recovery. Increasing temperature and ionic strength increased phosphate release by 20% and 50%, respectively. Both acidic and basic pH conditions promoted P_i release from cells induced to overexpress PBP. Surface-displayed PBP systems increased P_i release under controlled conditions compared to periplasmic PBP overexpressed in the periplasm and control cells without PBP overexpression.

Second, micro-structured immobilized PBP (PBP-NHS resin) was tested in fixed-bed column configuration, data from which is needed to support practical implementation. Highly selective P_i separation was observed, and there was no significant decline in the column's performance over three consecutive cycles for tertiary wastewater samples, substantiating PBP-NHS resin's reusability. Resin capacity was unaffected by competing anions, whereas a comparative LayneRT™ ion exchange column experienced a 20% drop in capacity in the presence of other anions.

Lastly, a PBP-loaded iron oxide particle adsorbent (PBP-IOPs) was shown to improve P_i adsorption capacity beyond the previous systems. The PBP-IOPs offered rapid P_i adsorption kinetics, with near-complete removal in less than 5 min. Higher P_i removal was observed at room temperature, low ionic strength, and slightly acidic conditions. The PBP-IOPs released 99% of total adsorbed P_i whereas IOPs alone (without immobilized PBP) released only 12%, such that PBP-IOPs offer enhanced potential for P_i recovery. Overall research findings advance understanding and system design using immobilized PBP to remove and recover P_i , supporting a more sustainable waste-to-resource paradigm.

ACKNOWLEDGEMENTS

Faten Bakri Hussein

My first and utmost gratitude goes to my creator who gave me the strength and patience to walk through this journey. With God's blessings, I was able to reach this milestone in my life and shall be for later milestones.

My heartfelt gratitude and appreciation are to my academic and research advisor Dr. Brooke Mayer. You are an amazing person to work with and to learn from. I would never thank you enough for your kind support, guidance, and patience with me during those years. Most importantly, your understanding and flexibility to deal with my hardship back in 2019 is something I will owe you forever.

The next person I owe a lot to him is Dr. Patrick McNamara. You are my gamechanger at Marquette University. If I had never had that environmental chemistry class with you, I would not have been a member and soon to be a graduate of MU. On top of that, you are an incredibly motivated scholar and amazing teacher. Dr. Brooke & Dr. Patrick (as I always like to call you), there are no words that can express my appreciation and how lucky I am to have you both as distinguished persons in my life.

My next gratitude goes to my committee members Dr. Martin St. Maurice and Dr. Marcia Silva. The story would not be completed without your willingness to serve on my committee as well as the help and guidance you provided to conduct my research work. It is my pleasure to get to know you in my professional life.

I want to thank all my colleagues in the water quality center at Marquette University, who were supportive and I had a great time around them. Many thanks to Mr. Mike Dollhopf, our lab manager, for his continuous assistance and guidance in the lab. Finally, I would like to thank the funding agents that supported my graduate study: CAREER award 1554511 from the National Science Foundation (NSF) and the NSF STEPS Center (2019435).

DEDICATION

To my life's precious gifts "My dear Mother" & "My dear late Father"

TABLE OF CONTENTS

ACKNOWLEDGEMENTS	i
LIST OF TABLES	v
LIST OF FIGURES	vi
1 INTRODUCTION.....	1
2 LITERATURE REVIEW	6
2.1 Phosphorus in the Environment: Nutrient vs. Pollutant	6
2.2 Phosphorus Removal Technologies	8
2.2.1 Physical-Chemical Removal Approaches	9
2.2.2 Biological Removal Approaches	11
2.3 Phosphorus Recovery from Water	14
2.4 Phosphate-binding Protein (PBP)	16
2.5 Prospective PBP Immobilized Systems	18
2.5.1 Microbial Cell Surface Display System.....	18
2.5.2 Micro-structured Immobilized-PBP in a Fixed-bed Column Configuration	20
2.5.3 PBP-loaded magnetic system.....	20
2.6 Summary of research needs	22
3 CELL SURFACE-EXPRESSION OF THE PHOSPHATE-BINDING PROTEIN PSTS: SYSTEM DEVELOPMENT, CHARACTERIZATION, AND EVALUATION FOR PHOSPHORUS REMOVAL AND RECOVERY	23
3.1 Introduction.....	23
3.2 Materials and Methods.....	25

3.2.1 Bacterial Strains, Plasmids, and Culture Conditions	25
3.2.2 SDS-PAGE and Western Blot Analyses.....	27
3.2.3 Outer Membrane Separation	28
3.2.4 Cell Surface Characterization	28
3.2.5 Phosphorus Desorption and Adsorption Batch Experiments.....	30
3.2.6 Statistical Analysis.....	32
3.3 Results and Discussion	32
3.3.1 Confirmation of Surface Expression Using SDS-PAGE, Western Blot Analyses, and Outer Membrane Separation.....	32
3.3.2 Cell Surface Characterization	35
3.3.3 Phosphorus Desorption Batch Experiments.....	42
3.3.4 Phosphorus Adsorption Batch Experiments	49
3.4 Conclusions.....	51
4 FIXED-BED COLUMN STUDY OF PHOSPHATE ADSORPTION USING IMMOBILIZED PHOSPHATE-BINDING PROTEIN.....	53
4.1 Introduction.....	53
4.2 Materials and Methods.....	55
4.2.1 Preparation of PBP-NHS Resin	55
4.2.2 Fixed-Bed Adsorption Studies.....	57
4.2.3 Mathematical Modeling of Breakthrough Curves	60
4.3 Results and Discussion	64
4.3.1 Fixed-Bed Adsorption Studies.....	64
4.3.2 Mathematical Modeling of Breakthrough Curves	70
4.4 Conclusions.....	74

5 PHOSPHATE-BINDING PROTEIN (PBP)-LOADED IRON OXIDE PARTICLES: ADSORPTION PERFORMANCE FOR PHOSPHORUS REMOVAL FROM WATER	75
5.1 Introduction.....	75
5.2 Materials and Methods.....	78
5.2.1 Preparation of the PBP-IOP Adsorbent	78
5.2.2 Phosphorus Adsorption Experiments.....	80
5.2.3 Selectivity and Reusability of PBP-IOPs.....	83
5.2.4 Statistical Analysis.....	85
5.3 Results and Discussion	85
5.3.1 Phosphorus Adsorption.....	85
5.3.2 Selectivity and Reusability of PBP-IOPs.....	97
5.4 Conclusions.....	100
6 CONCLUSIONS.....	102
6.1 Key Findings.....	103
6.2 Future Work	105
7 REFERENCES.....	108
APPENDICES	124
Appendix A Supporting Information - Chapter 3	124
Appendix B Supporting Information - Chapter 4	127
Appendix C Supporting Information - Chapter 5	146

LIST OF TABLES

Table 2.1 Expected years for phosphate reserve depletion for the top five producing countries (2015 data) (Rosemarin, 2016).....	7
Table 3.1 Deprotonation constants (pK_a) and point of zero charge (pH_{pzc}) as calculated with ProtoFit GIU using the constant capacitance model (CCM) and non-electrostatic model (NEM) for control cells, uninduced cells, and induced cells.	38
Table 4.1 Continuous-flow fixed-bed column experimental design.	58
Table 4.2 Adams-Bohart, Thomas, and Yoon-Nelson model parameters for varying column operating conditions.	72
Table 5.1 Parameters for the pseudo first-order and pseudo second-order kinetic models of P_i adsorption using PBP-IOPs.	87
Table 5.2 Pseudo second-order parameters for P-selective adsorbents.	88
Table 5.3 Parameters of Langmuir and Freundlich isotherm models for P_i adsorption using PBP-IOPs.	91
Table 5.4 Langmuir isotherm parameters for P-selective adsorbents.	92

LIST OF FIGURES

- Figure 2.1** (a) Configuration of a conventional wastewater treatment plant (b) Typical EBPR configuration. Blue and yellow arrows represent the fate of P_i in liquid and solid streams in the treatment system, respectively..... 12
- Figure 2.2** Illustration of phosphate-specific transporter (Pst) complex in *E. coli*. 17
- Figure 2.3** Microbial cell surface display approaches on a gram-negative bacterial cell (modified from Lee et al. (2003)). The approach of interest in this study is boxed in red. 19
- Figure 3.1** Protein verification, expression, and separation analyses. (a) Protein verification using SDS-PAGE analysis of control cells (lane 2: before IPTG induction [Control Uninduced]; lane 3: after IPTG induction [Control Induced]) and PstS cells (lane 4: before IPTG induction [PstS Cells Uninduced]; lane 5: after IPTG induction [PstS Cells Induced]). Lane 1 is the protein marker. (b) Protein expression using Western Blot analysis shows two distinguished bands for the induced cells, corresponding to INP only and INP + PstS together. (c) SDS-PAGE analysis of the outer membrane (OM) separation analysis of the induced cells showing the presence of PstS in the OM fraction rather than the cell lysate fraction. 34
- Figure 3.2** (a) Typical acid-base titration curves for induced cells (IC), uninduced cells (UC), and control cells (CC) suspended in 0.01 M NaCl with final $OD_{600} = 2$. BG = background solution (0.1 M NaCl). (b), (c), and (d) three-site (2 acid and 1 base) constant capacitance model (CCM) and three-site (2 acid and 1 base) non-electrostatic model (NEM) curve fits for CC, UC, and IC, respectively. 37
- Figure 3.3** (a) XPS spectra for freeze-dried samples of control cells, uninduced cells, and induced cells. Acquisition with pass energy 100 eV and 1 eV step size using Mg $K\alpha$ X-ray source. The inset table shows the percentage atomic concentration of C, N, O, and P on the bacterial surface calculated from the XPS spectra. (b) Infrared spectra of control cells, uninduced cells, and induced cells suspension in 10 mM Tris-HCl solution at a final $OD_{600} = 2$. The spectra are vertically offset for clarity. Peaks were identified and functional groups were assigned as shown in Appendix A (Table A2). 40
- Figure 3.4** Phosphate desorption from control cells (CC), uninduced cells (UC), and induced cells (IC) with final $OD_{600} = 1$ as a function of (a) temperature, (b) pH, and (c) ionic strength. All experiments were conducted in triplicate, and error bars denote ± 1 standard deviation. 46
- Figure 3.5** Comparison of phosphorus release using periplasmic-expressed PstS (PP-PstS) and surface-expressed PstS (SE-PstS). Data for the periplasmic-expressed-PstS from Yang et al. (2016). 48

Figure 3.6 Phosphate uptake by control cells and induced cells after desorption conditions (starvation, pH & temperature, and enzyme). Two phosphate concentrations were selected for adsorption tests (a) $7 \text{ mg PO}_4^{3-}\text{L}^{-1}$ and (b) $70 \text{ mg PO}_4^{3-}\text{L}^{-1}$. All phosphate adsorption experiments were conducted in triplicate for 3 hr at room temperature, 250 rpm mixing, and pH 6.7. Error bars denote ± 1 standard deviation. 50

Figure 4.1 Breakthrough curves (ratio of effluent to influent P_i concentration $[C_t/C_0]$ as a function of operating time) under different column operating parameters: (a) influent P_i concentration, (b) bed volume, (c) flow rate, and (d) multi-cycle column experiment at influent concentration of $1.1 \text{ mg PO}_4^{3-}\text{L}^{-1}$, bed volume of 1 mL, and flow rate of 0.2 mL min^{-1} . Note that the maximum time varies among the panels. All column tests were conducted in duplicate, as indicated by the error bars. 65

Figure 4.2 Comparison of breakthrough curves (ratio of effluent to influent P_i concentration $[C_t/C_0]$ as a function of operating time) using P_i -only solution versus multi-ion solution (containing phosphate, sulfate, chloride, nitrate, and bicarbonate ions) for two different phosphate-selective resins: (a) PBP-NHS resin, (b) LayneRT™ resin. All column tests were conducted in duplicate, as indicated by the error bars. 68

Figure 4.3 Breakthrough curves (ratio of effluent to influent P_i concentration $[C_t/C_0]$ as a function of operating time) for tertiary wastewater effluent tests: (a) single-column experiment and (b) multi-cycle column experiment. Both tests were performed using a bed volume of 0.5 mL, flow rate of 0.3 mL min^{-1} , and influent phosphate concentration of $0.75 \text{ mg PO}_4^{3-}\text{L}^{-1}$. All column tests were conducted in duplicate, as indicated by the error bars. 69

Figure 4.4 Calculated bed service time for breakthrough (10% BT; panels a and c) and exhaustion (90% BT; panels b and d). Panels a and b illustrate the impact of different influent phosphate concentrations, while panels c and d illustrate the impact of different flow rates. 73

Figure 5.1 P_i adsorption kinetics using the PBP-IOP adsorbent at room temperature and neutral pH. (a) PBP-IOP adsorbent capacity as a function of time modeled using pseudo second-order kinetics, (b) experimental data fit with linear regression using the pseudo second-order kinetic model. The model's parameters are listed in Table 5.1. 86

Figure 5.2 Phosphorus adsorption isotherms using PBP-IOPs at room temperature and neutral pH conditions. (a) experimental data fit to nonlinear isotherm models, (b) linearized Langmuir model, and (c) linearized Freundlich model. 90

Figure 5.3 Effect of experimental conditions on phosphorus adsorption using PBP-IOPs: (a) pH, (b) temperature, and (c) ionic strength (KCl). All experiments were conducted for 60 minutes in triplicate, with ± 1 standard deviation denoted by the error bars. 94

Figure 5.4 Selectivity of PBP-IOPs towards phosphorus. (a) synthetic multi-ion solution with 1 mg L^{-1} each of NaCl, Na_2SO_4 , NaNO_3 , NaHCO_3 , $\text{B}_4\text{Na}_2\text{O}_7 \cdot 10\text{H}_2\text{O}$, and KH_2PO_4 versus P_i -only solution containing 0.9 mg L^{-1} KH_2PO_4 . (b) tertiary wastewater effluent (WW) versus P_i -only solution containing 1.2 mg L^{-1} KH_2PO_4 **97**

Figure 5.5 Reusability of PBP-IOPs performed over five consecutive adsorption-desorption cycles. Only the adsorption cycles are presented. All experiments were conducted in triplicate, with ± 1 standard deviation indicated by the error bars. **99**

Figure 5.6 Comparison study of P_i adsorption/desorption capacity between IOPs modified with PBP and unmodified IOPs. All experiments were conducted in triplicate, with ± 1 standard deviation indicated by the error bars. **100**

1 INTRODUCTION

Inorganic phosphorus (P_i) is an essential nutrient for living organisms. Rapid growth and high crop productivity require substantial amounts of P_i . However, bioavailable phosphorus suitable to support cellular growth is in short supply in nature (Filippelli, 2008), necessitating mining of the non-renewable mineral rock resource. Global phosphorus deposits are predominantly confined to five countries: China, USA, Russia, Jordan, and Morocco (Elser, 2012). Depletion of phosphate reserves could be as soon as 2050 in the US (Smil, 2000), although estimates range widely.

On the other hand, phosphorus is considered a pollutant when excess concentrations of P_i in water cause eutrophication. The P_i from nonpoint runoff (e.g., urban, and agricultural lands) and point sources (e.g., municipal and industrial wastewater treatment facilities) initiates unusually high growth of algae and higher plant forms. The accelerated growth can disturb the quality of aquatic systems. Nuisance algal blooms can cause eutrophication, aging, or drinking water crises, as demonstrated by Lake Taihu in China and Lake Erie in the US/Canada (Mancini et al., 1983; Mayer et al., 2013; Withers et al., 2015). Eutrophication affects the aesthetic aspects of a waterbody (color and odor), and also alters the water's quality and habitat diversity (i.e., loss of dissolved oxygen and elimination of fish habitat) (Rittmann et al., 2011). The US Environmental Protection Agency (USEPA) identified eutrophication as the "biggest overall source of impairment of the nation's rivers and streams, lakes and reservoirs, and estuaries" (US Environmental Protection Agency, 2000). The estimated annual economic loss as a result of freshwater eutrophication in the US was reported as \$2.2 billion in 2008 (Dodds et al., 2009).

Although conventional wastewater treatment processes can achieve effluent concentrations down to about $100 \mu\text{g-P L}^{-1}$ (Blaney et al., 2007; Kuba et al., 1993), some surface waters are still prone to algal blooms even at lower P_i levels (Mayer et al., 2013). Accordingly, strict water quality guidelines and discharge standards exist in some phosphorus-sensitive locations (e.g., $5\text{-}10 \mu\text{g L}^{-1}$ in the Great Lakes and Everglades (Sengupta and Pandit, 2011)). Hence, innovations to reduce P_i to ultra-low levels in both water and wastewater are critical. Together, overabundant P_i concentrations in many waterbodies and simultaneous scarcity of P_i as a non-renewable natural resource necessary to sustain global agricultural production lead to the phosphorus paradox. Addressing this issue is necessary and using innovative approaches targeting P_i removal to ultra-low levels and subsequent recovery for reuse applications can help.

A potential sustainable solution to simultaneously remove and recover P_i under controlled conditions utilizes the phosphate-binding protein PstS (PBP). PBP is a natural part of many microorganisms' structure responsible for P_i transport into the cell under conditions of low ambient P_i levels. The protein has high affinity for P_i and can efficiently capture it even at low concentrations (Poole and Hancock, 1984; Wu et al., 1999). Moreover, P_i adsorption using PBP is reversible as a function of pH (Venkiteshwaran et al., 2018), which facilitates not only removal but recovery. Therefore, PBP-based adsorption system offers a potentially sustainable treatment option for P_i removal and recovery from water/wastewater. Although PBP offers strong potential for use in engineered systems, more effective water/wastewater configurations are needed before it can be a potential sustainable treatment option for P_i removal and recovery from

water/wastewater. Specifically, improvements in immobilized PBP's contact with the water, operation in flow-through operation, and adsorption capacity are critical.

To address these improvements, this research investigated the performance of three different configurations of PBP systems to remove and recover P_i . To the author's knowledge, there were no studies that assessed microbial surface-displayed PBP systems (bringing PBP into direct contact with the target P_i) for their potential to remove and recover P_i . Also, utilizing PBP in more practical treatment configurations (i.e., fixed-bed column) is essential to provide reliable information pertaining to breakthrough times, adsorption conditions, and the adsorbents' stability and selectivity during continuous use. This knowledge gap was addressed for immobilized PBP bead-based systems compared to an industry-standard ion exchanger. Lastly, the need for improved PBP bead P_i removal capacity led to examination of a new PBP-loaded magnetic system. This research consisted the following three objectives:

I. Synthesize and evaluate a PBP bacterial surface-displayed system to remove and recover P_i under controlled experimental conditions

Surface-displayed PBP on the outer membrane of *E. coli* cells was utilized to remove and recover P_i from water. The hypothesis was that exposing the high-binding affinity PBP directly to the water matrix would facilitate P_i capture and release in comparison to PBP's natural location in cells' periplasmic space (in which case the cell membrane and perhaps cytoplasmic regulation could impede PBP release). The proposed system was designed, verified for protein surface expression and localization, characterized, and tested for P_i capture and release. Comparison of "periplasmic-expressed

PBP” versus “surface-expressed PBP” for P_i release capacity was conducted. Objective 1 is presented in Chapter 3.

II. Perform a fixed-bed column study of a micro-structured immobilized-PBP to inform design flow-through applications

Continuous flow fixed-bed (packed-bed) column experiments for P_i removal were conducted using PBP immobilized on micro-structured beads to evaluate column design parameters. The hypothesis was that P_i removal and recovery in fixed-bed column operation using PBP resin would not be impeded by the presence of other anions and cations (whereas current industry standard ion exchange resins such as LayneRT™ are negatively impacted) due to the high selectivity of PBP-modified resin toward P_i . Therefore, breakthrough curves of the PBP-modified resin in the presence or absence of competing ions would be similar. Independent column experiments were conducted to investigate the effect of different influent P_i concentrations, bed depths (i.e., bed volumes), and flow rates on the breakthrough curve. Continuous flow fixed-bed column experiments were also conducted using tertiary wastewater effluent to investigate the water matrix effect on the overall performance of the PBP column in comparison to a LayneRT™ column. Objective 2 is presented in Chapter 4.

III. Evaluate potential improvements in capacity using a PBP-loaded magnetic particle system for P_i removal and recovery

Modified magnetic particles for PBP attachment were prepared and tested for their capacity to remove and recover P_i . The hypothesis was that the system of functionalized iron oxide particles (IOPs) loaded with PBP would provide higher capacity to remove and recover P_i compared to unmodified IOPs and previously established PBP-modified resin. The smaller particle size of IOPs compared to NHS-activated Sepharose beads would be expected to improve PBP attachment density by a factor of 10 (based on the increase in particle surface area). Also, PBP-IOPs were expected to facilitate P_i recovery compared to unmodified IOPs considering the natural binding properties of PBP. The PBP-IOP adsorbent was tested in adsorption and desorption batch experiments under different experimental conditions (pH, temperature, and ionic strength). Selectivity of the PBP-IOP adsorbent was also investigated in synthetic and wastewater matrices. The P_i adsorption and desorption capacity of PBP-IOPs was compared to unmodified IOPs. Adsorption kinetic and isotherm studies were also performed. Objective 3 is presented in Chapter 5.

2 LITERATURE REVIEW

2.1 Phosphorus in the Environment: Nutrient vs. Pollutant

Inorganic phosphorus (P_i) is an essential element for life as it serves various roles that sustain cellular vitality. P_i is a key structural component of DNA and RNA and it is also part of the cell's energy currency molecule, adenosine triphosphate (ATP). The average human body contains ~ 650 g P_i in bones (Childers et al., 2011).

Modern society is essentially dependent on phosphate rock to maintain the global food supply (Cordell et al., 2009). Increased P_i demand led to a 700% price spike in 2007-2008 (Cordell et al., 2009), which ultimately increased food prices. Hence, potential concerns for global food security would be expected as population increases. P_i is considered a nonrenewable resource, like oil, because phosphate rock requires thousands to millions of years to deposit (Filippelli, 2008). Phosphate resources could be exhausted by 2050-2080 (Smil, 2000; Steen, 1998). Declining supply in the face of increasing demand creates serious threats such as increased prices for farmers and consumers, and sociopolitical tension as 90% of the reserves are confined to only five countries (Table 2.1) (Mayer et al., 2013; Vaccari, 2009).

Table 2.1 Expected years for phosphate reserve depletion for the top five producing countries (2015 data) (Rosemarin, 2016).

Country	% Global extraction capacity	Years to depletion at current rate	Years to depletion at FAO's* 2.5% annual growth
China	44.8	37	26
USA	12.4	40	27
Russia	5.6	104	51
Jordan	3.4	173	67
Morocco	13.5	1667	150

*Food and Agriculture Organization (FAO).

Beyond availability concerns, increased P_i use leads to elevated P_i in waterbodies, causing environmental and human health concerns. Excess P_i enters surface waters and causes dangerous effects. Eutrophication is a widespread problem in aquatic ecosystems consisting of excessive growth of algae and other aquatic plants in response to over-enrichment with nutrients (nitrogen and phosphorus). Decomposition of algal blooms can lead to unpleasant odors and oxygen depletion, which can lead to fish kills. Loss of biodiversity and the presence of toxins in waterbodies are other problems associated with eutrophication (Bennett et al., 2001). To control eutrophication and its consequences, the USEPA imposed regulations that allow a maximum total phosphorus (TP) concentration of 50-100 $\mu\text{g L}^{-1}$ in streams and 25 $\mu\text{g L}^{-1}$ in lakes and reservoirs (US Environmental Protection Agency, 2000). Some phosphorus-sensitive surface water might experience excessive algal growth at P_i levels as low as 20 $\mu\text{g L}^{-1}$ (Dillon and Rigler, 1974; Schindler, 1977). Therefore, reducing P_i concentrations to ultra-low levels (less than status quo targets of 1 mg L^{-1}) using advanced treatment technologies must be investigated.

The phosphorus paradox has emerged as a result of continuously increasing demands for phosphate rock to manufacture agricultural fertilizers, which eventually will deplete nonrenewable P_i resources, and the simultaneous overabundance of P_i in water. P_i resource scarcity can be ranked as one of the most critical challenges in our lifetime as the consequences are significant. Implementing different approaches in production, usage, and reuse of P_i to manage and close its cycle is important (Cordell et al., 2011; Cordell and White, 2011). Economical water/wastewater treatment technologies that remove and recover P_i in a usable form would also help in protecting waterbodies and saving the costs of remediation. This would further contribute to a sustainable anthropogenic phosphate cycle.

2.2 Phosphorus Removal Technologies

Wastewater treatment technologies to remove phosphorus are based on physical-chemical approaches, biological approaches, or a combination thereof. Physical-chemical approaches have been utilized for decades due to their reliability and effectiveness (Bunce et al., 2018). The most common physical-chemical approaches include adsorption, ion exchange, and precipitation (chemical dosing).

Biological P_i removal approaches have a key role in wastewater treatment facilities (WWTFs). Secondary treatment processes may include conventional activated sludge, enhanced biological P removal (EBPR), or algal-based processes. The following subsections provide brief descriptions of these common processes, including their major advantages and disadvantages.

2.2.1 Physical-Chemical Removal Approaches

2.2.1.1 Adsorption and Ion Exchange

Substantial development has been achieved to remove P_i in filtration systems using functionalized media (i.e., adsorbents). Unlike traditional filtration systems that separate P_i based on size exclusion, advanced filtration systems utilize functionalized material that selectively captures P_i (Kumar et al., 2019). Adsorptive media can be prepared from natural sources such as limestone and bauxite, industrial waste material (e.g., steel slag, ash), or synthetic materials (Bunce et al., 2018). Removal mechanisms in adsorptive media may involve direct precipitation of P_i inside the material matrix or transferring onto the surface (Brix et al., 1999). Ion exchange is a subcategory of adsorption, in which P_i ions in waste streams are exchanged with other anions on the media's surface. Metal cations are attached to the polymer exchange base for polymer ligand exchanger (Bunce et al., 2018).

Adsorption and ion exchange processes have been reported to effectively remove P_i to levels $< 0.1 \text{ mg PO}_4^{3-} \text{ L}^{-1}$ (Awual et al., 2014; Luo et al., 2016; Sengupta and Pandit, 2011). Although high removal efficiency has been achieved at lab scale, implementation at larger scales is still limited (Kumar et al., 2019). Noticeably, the economic burden in adopting such technology is associated with various factors such as the cost of synthesizing adsorbents, operating conditions (i.e., temperature and pH adjustment), effect of competing ions on the adsorbents' capacity (i.e., selectivity), and the cost of regeneration (Kumar et al., 2019).

2.2.1.2 Chemical precipitation

Ferric chloride and other trivalent metal salts are commonly used to precipitate P_i from wastewater. Chemical dosing may be applied to conventional activated sludge tanks, secondary clarifier outlets, or pretreated influent (Cornel and Schaum, 2009; Oleszkiewicz et al., 2015). The solid residuals are then removed by filtration or gravity settling. Effluent concentrations of $1 \text{ mg PO}_4^{3-} \text{ L}^{-1}$ can be obtained using this process (Bunce et al., 2018); however, stringent effluent standards require more advanced separation technologies to achieve ultra-low concentrations. Also, P_i removal is proportional to the added mass of metal salts, hence, additional treatment of residual solids is required (Bunce et al., 2018). Chemical precipitation might not be suitable for small-scale plants due to limited storage space and deliveries of chemicals, pH adjustment, and excess generation of residuals (Bunce et al., 2018).

Physical-chemical P_i removal processes can be considered as “polishing” approaches in WWTFs. Reliable P_i removal outcomes are advantageous, yet, existing processes are insufficient for long-term sustainable operation and maintenance at small-scale WWTFs (Bunce et al., 2018). Integration of biological P_i removal approaches could provide more holistic treatment of wastewater.

2.2.2 Biological Removal Approaches

2.2.2.1 Enhanced Biological P Removal (EBPR)

EBPR, which alternates aerobic and anaerobic conditions, was developed to reduce phosphorous concentrations in WWTFs' effluent (Capua et al., 2022). These conditions stimulate the growth of polyphosphate accumulating organisms (PAOs), which can uptake more P_i than needed for their growth. Excess P_i is stored as intracellular granules of polyphosphate (Yuan et al., 2012). Specialized microorganisms such as *Accumulibacter* and *Tetrasphaera* are the major microorganisms driving EBPR, contributing 24%-70% of the total biomass in EBPR systems (Fernando et al., 2019; Stockholm-Bjerregaard et al., 2017). High abundance of PAOs with sufficient volatile fatty acids promoted 15-20% P_i -content by cell dry weight. However, lower abundance of PAOs promoted lower P_i content, approximately, 5-7% (Yuan et al., 2012). Figure 2.1 provides a schematic illustration of conventional wastewater treatment trains vs. typical EBPR process.

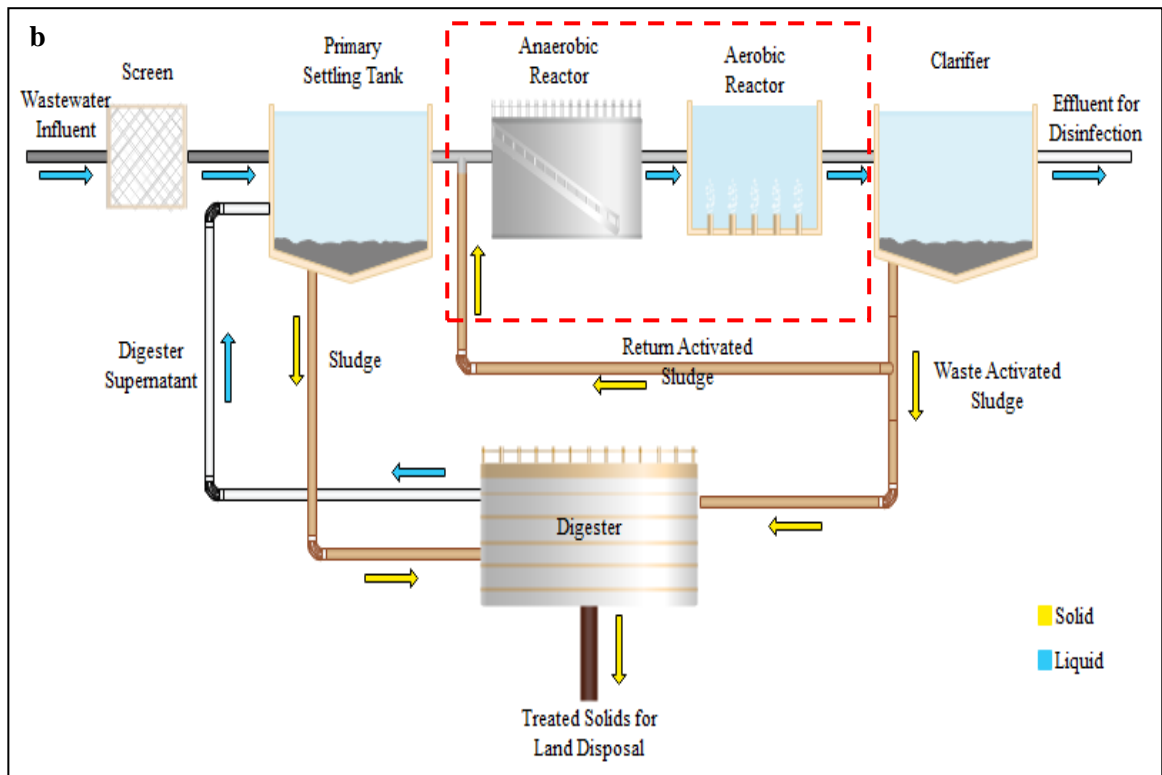
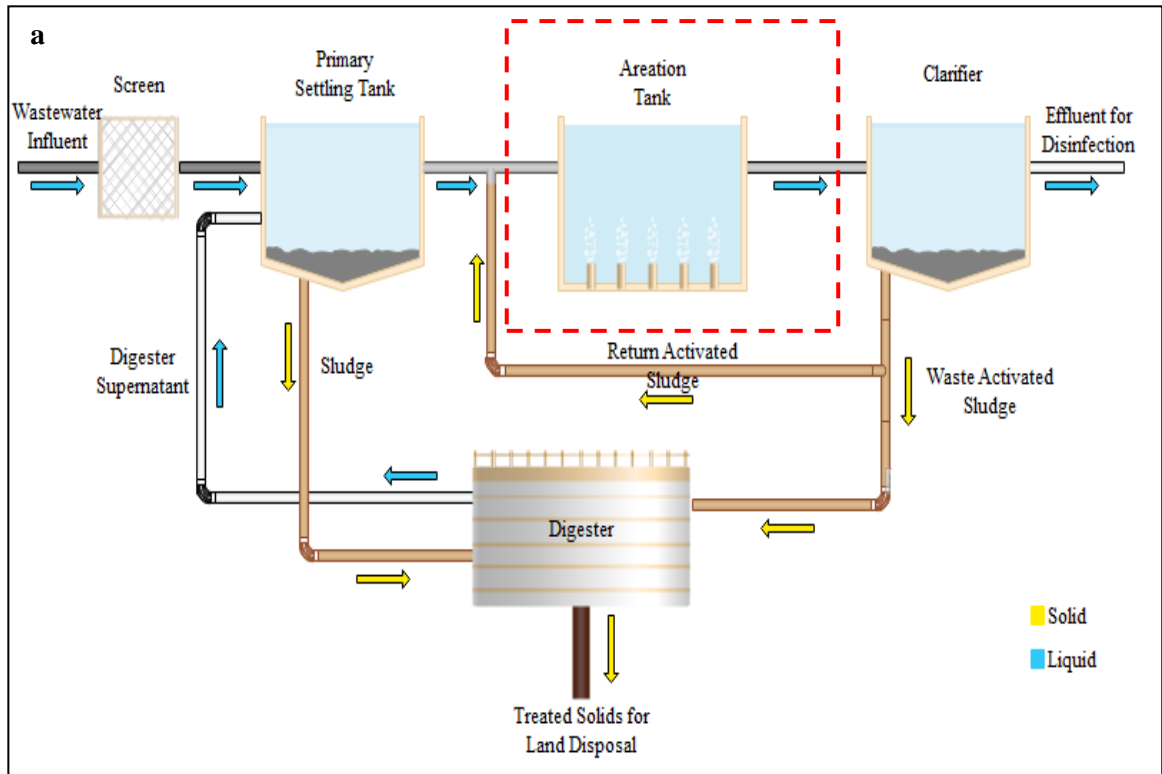


Figure 2.1 (a) Configuration of a conventional wastewater treatment plant (b) Typical EBPR configuration. Blue and yellow arrows represent the fate of P_i in liquid and solid streams in the treatment system, respectively.

While EBPR is considered an environmentally sustainable and cost-effective process compared to chemical approaches (Acevedo et al., 2012; Nguyen et al., 2013), EBPR is not fully reliable due to performance fluctuation and difficulty in process control (Bunce et al., 2018). For instance, PAOs community in EBPR system may be harmed or disadvantaged under certain operation conditions such as over aeration and aerobic-to-anaerobic contact time (Seviour et al., 2003). EBPR is less likely to be used at small scales due to the operating complexity and maintenance cost requirements (Bunce et al., 2018).

2.2.2.2 Microalgae-based Process

The synergetic relationship between microalgae and bacteria in waste stabilization ponds (WSPs) offers a natural wastewater treatment system. Heterotrophic bacteria metabolize organic compounds aerobically and produce CO₂. Meanwhile, photosynthetic microalgae utilize CO₂ and nutrients (nitrate and phosphate) for growth (Capua et al., 2022). Consequently, the O₂ produced from microalgal growth will be consumed by bacterial activity. Waste stabilization ponds can achieve 20-50% P_i removal (Abdulsada, 2014). The most common microalgae found in wastewater are *Chlorella* and *Scenedesmus*, which can grow in the presence or absence of light. The nutrient removal capacity of such species depends on the diffusion rate of dissolved nutrients, which is determined by the thickness of the boundary layer of water outside the cells (Abdulsada, 2014). Moreover, microalgae can increase pH due to CO₂ and HCO₃⁻ consumption. Basic pH will facilitate P_i precipitation with available cations and strip off the ammonia to the atmosphere (Abdulsada, 2014). Like PAOs, microalgae species can accumulate P_i as polyphosphate granules. Luxury uptake of P_i depends on nutrient concentration, pH, dissolved oxygen, temperature, and light intensity (Brown and Shilton, 2014). Accumulation of P_i occurs

when microalgae are exposed to a stressful or a nutrient-rich environment. Granular P_i accumulated inside cells can be beneficial for removal and reuse by separation and harvesting of microalgae. However, P_i removal efficiency using microalgae species is still considered low compared to chemical removal processes.

Generally, current P_i removal technologies have limited capability to achieve ultra-low effluent P_i concentrations. Unpredictable P_i removal efficiencies are associated with biological technologies (EBPR or microalgae-based processes) due to the difficulty in process control. Moreover, energy requirements and maintenance costs for small-scale treatment plant are the major challenges to adapt such technologies. For adsorption and ion exchange technologies, competing anions are a major challenge that affects the removal capacity of P_i . Also, some adsorbents and ion exchangers need energy to initiate the removal process and have multi-regeneration cycles requirement. Chemical precipitation is not suitable for highly-concentrated waste streams as it will require large amount of chemical dosage, decreasing its feasibility. Therefore, there is a need for a selective, sensitive, and reversible adsorbent to overcome the challenges associated with existing technologies. Phosphate-binding protein-based systems could offer one such strategy for water and wastewater treatment.

2.3 Phosphorus Recovery from Water

A large quantity of extracted P_i is used in agricultural applications (80-90%) and most of that P_i is lost to surface water (Rittmann et al., 2011). Losses of P_i from soil erosion and farms represent 46% of extracted phosphate, animal waste accounts for 40% of mined P_i , and human sewage has 15% losses of mined P_i (Cordell et al., 2009; Rittmann et al., 2011). Animal wastes have high-strength P_i flows where conventional treatment strategies

are more suitable and economical for P_i and energy capture and recovery (Rittmann et al., 2011). Low-strength P_i flows such as surface water and municipal wastewater might need more advanced technologies to achieve P_i recovery.

As previously described, typical water and wastewater treatment processes (physical-chemical and biological approaches) achieve P_i effluent concentrations of 1-2 mg L⁻¹, which could be reduced to 100 µg L⁻¹ effluent concentrations with advanced approaches (Blaney et al., 2007). Although many existing technologies can meet P_i effluent concentration guidelines and regulations, they are still unable to address the new sustainable P_i treatment concept that emphasizes simultaneous P_i removal and recovery (Mayer et al., 2013). Adsorption and precipitation are generally developed for P_i removal and are not fully developed for recovering P_i (Rittmann et al., 2011). Precipitation of recovered P_i produces common products used as mineral fertilizers (i.e., struvite), but requires high levels of P_i (100-200 mg L⁻¹) (Le Corre et al., 2009; Moriyama et al., 2001; Qureshi et al., 2006), ammonium, and magnesium (Ghosh et al., 1996; Johnston and Richards, 2004; Münch and Barr, 2001). P_i -specific ion exchange adsorbents could be promising approaches to concentrate P_i to promote precipitation, yet ionic competition from sulfate and arsenate as well as leaching of metal-loaded ligands over repeated use cycles hinders adsorption (An et al., 2013; Blaney et al., 2007; Rittmann, 2008; Sendrowski and Boyer, 2013; Sengupta and Pandit, 2011; Zhao and Sengupta, 1996).

In biological wastewater treatment, where activated sludge is utilized to remove nutrients, only 20-40% of P_i can be removed (Mayer et al., 2013; Morohoshi et al., 2003). Direct recovery of P_i is limited as most of the phosphate is trapped in the biosolid mass that can be used as a soil amendment, thereby minimizing its economic proposition and

contribution to a sustainable closed phosphorus cycle (Blank, 2012; Rittmann et al., 2011). Thus, there is a need for a selective and reversible adsorbent to overcome the challenges associated with existing technologies to recover P_i (i.e., low P_i recovery due to competing ions from adsorbents and limited direct recovery of P_i from biosolid mass). Engineered phosphate-binding protein-based systems for water and wastewater treatment could offer one such strategy.

2.4 Phosphate-binding Protein (PBP)

Microbes including *Escherichia coli* and *Pseudomonas aeruginosa* regulate P_i uptake through a distinct protein complex (Poole and Hancock, 1984; Wu et al., 1999). The P_i needed for cell growth is imported using one of two different phosphate transport systems: high-affinity phosphate specific transporter (Pst) and low-affinity phosphate inorganic transporter (Pit) (Blank, 2012; Santos-Beneit et al., 2008). The Pit system is responsible for P_i transport into the cell when P_i is present in excess, while Pst is responsible for P_i transport into the cell when P_i is present in low concentrations (Botero et al., 2000; Wanner, 1993). In *E. coli*, the Pst complex consists of four proteins: the dimeric ATP-binding protein (PstB), two transmembrane proteins (PstA and PstC), and the periplasmic phosphate-binding protein (PstS) (Figure 2.2). PstS functions as a high-affinity P_i receptor using twelve hydrogen bonds in its binding site (Brune et al., 1998).

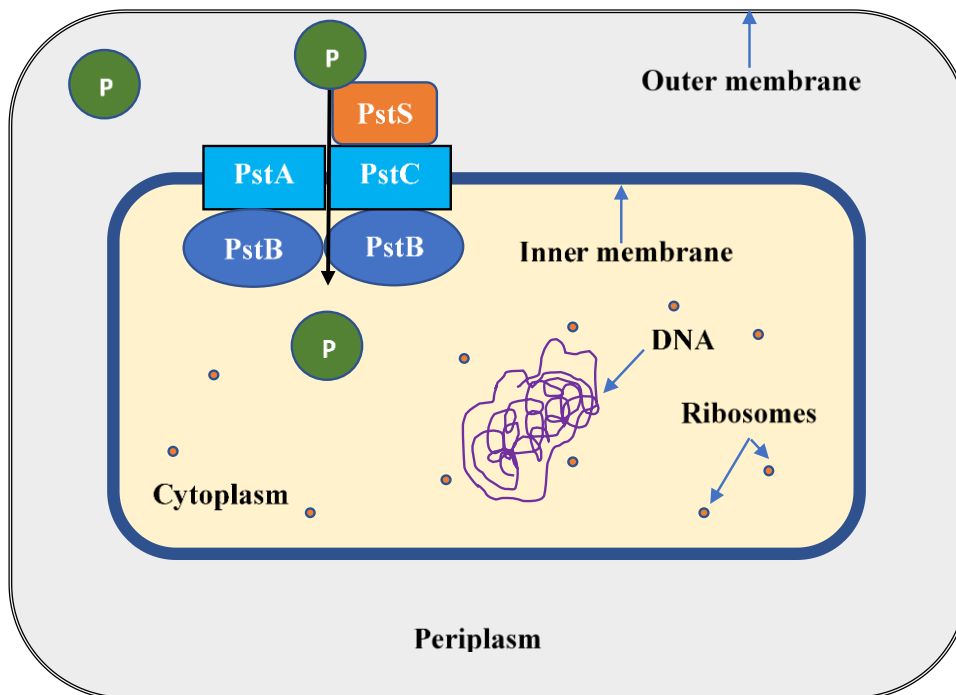


Figure 2.2 Illustration of phosphate-specific transporter (Pst) complex in *E. coli*.

Phosphate capture is strongly pH dependent (Kuroda et al., 2000; Luecke and Quioco, 1990); therefore, P_i removal and recovery could be controlled with pH adjustment in water and wastewater applications. Kuroda et al. (2000) studied P_i adsorption using PBP purified from *Pseudomonas aeruginosa* in bench-scale column tests after immobilization on polymer beads. ^{32}P -labeled pond water containing $0.5 \mu M P_i$ was tested and complete removal was achieved (Kuroda et al., 2000). Based on this proof-of-concept of PBP capabilities, immobilizing PBP may yield a more sustainable approach to remove and recover P_i . Such PBP-based adsorbents can be retained and used multiple times and P_i can be recovered under pH-controlled conditions. Prospective immobilized PBP systems are introduced in the following section.

2.5 Prospective Immobilized PBP Systems

2.5.1 Microbial Cell Surface Display System

Cell surface display is an advanced biotechnology technique that has significant application in antibody production, oral vaccines, biosensors, bio-adsorbents, and whole-cell biocatalysts for bioconversion (Lee et al., 2003). Cell surface display facilitates expression of proteins of interest (passenger proteins) on the cell's surface using anchoring motifs (carrier proteins) (Tafakori et al., 2012; van Bloois et al., 2011). Figure 2.3 (modified from Lee et al., 2003) illustrates examples of various cell surface display approaches on a gram-negative bacterial cell. The ice nucleation protein (INP) is one of the anchoring motifs used to attach various type of proteins due to its stability and ability to express large and complex passenger proteins (Lee et al., 2003). Truncated INP containing N- or C-domains (with or without internal repeating domains) is an excellent scaffold for surface display with no unfavorable effect on bacteria growth (Chen and Georgiou, 2002; Jung et al., 1998; Li et al., 2003).

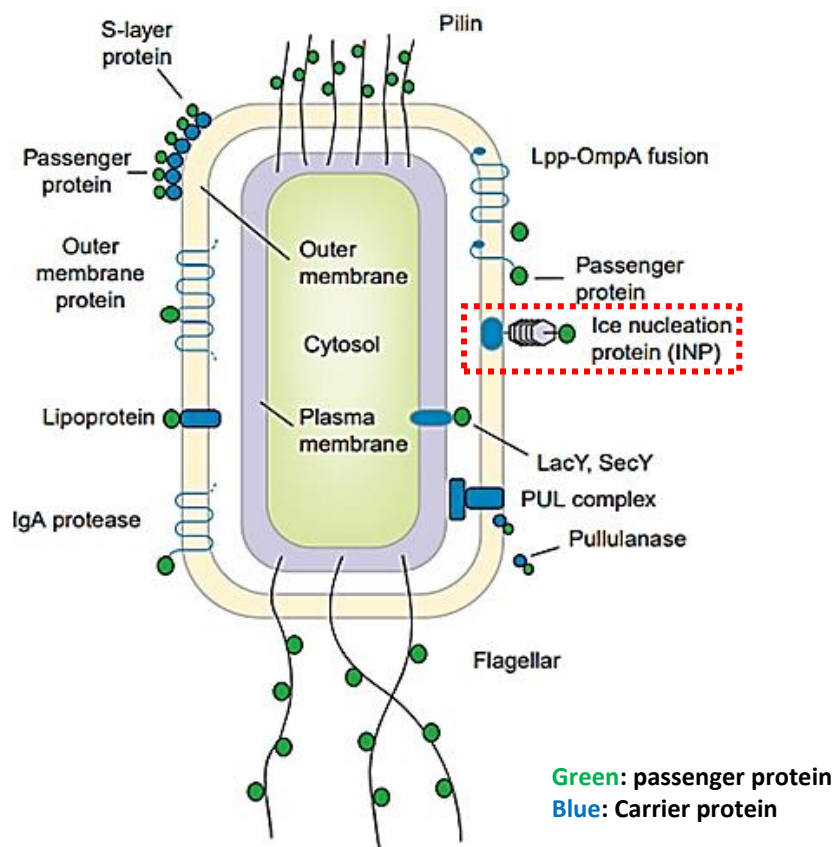


Figure 2.3 Microbial cell surface display approaches on a gram-negative bacterial cell (modified from Lee et al. (2003)). The approach of interest in this study is boxed in red.

Using INP, PBP can be immobilized on microbial surfaces (Lee et al., 2003; van Bloois et al., 2011). Li et al. (2009) utilized INP to display PBP on *E. coli* and *Pseudomonas putida* surfaces. The engineered microbes demonstrated absolute biosorption of total phosphate at 60-80 mg L⁻¹ (Li et al., 2009). However, recovery of P_i from the engineered microbes was not investigated, nor were extensive biosorption tests conducted (i.e., evaluating PBP capability to remove P_i under operating conditions such as variable pH, temperature and ionic strength). Objective 1 of this study addressed these knowledge gaps by studying P_i removal and recovery potentials for a PBP bacterial surface-displayed system. Expressing PBP on the cell surface was anticipated to facilitate P_i release in

comparison to periplasmic PstS. Surface-expressed PstS will directly interact with the water matrix, while, in the periplasmic-expressed case, the cell membrane and perhaps cytoplasmic regulation could impede P_i release.

2.5.2 Micro-structured Immobilized PBP in a Fixed-bed Column Configuration

Continuous-flow, fixed-bed columns are most convenient for wastewater treatment due to their ability to treat large volumetric flowrates (Hu et al., 2020). Fixed-bed column experiments provide reliable information pertaining to breakthrough times, adsorption conditions, and adsorbents' stability during continuous use (Satya et al., 2021; Yanyan et al., 2018). Studies of immobilized PBP in fixed-bed column configuration and assessments of its performance under a range of more realistic operating conditions have not yet been established, but are needed to determine PBP's usefulness in real-world scenarios. Additionally, information on the adsorbent's reusability in multi-cycle column operating mode and its selectivity compared to a commercially P_i -selective available ion exchange resin are not available. Objective 2 addressed these knowledge gaps by investigating a micro-structured immobilized-PBP system in a fixed-bed column configuration.

2.5.3 PBP-loaded Magnetic System

Magnetic nanoparticles (MNPs) have been extensively used in biomedical applications, such as drug delivery and enzyme conjugation, due to their unique properties such as stability, high surface area, and biocompatibility (Vallabani and Singh, 2018). MNPs have also received great consideration for environmental applications such as treating polluted water (Gómez-Pastora et al., 2014). MNPs modified with functional groups ($-NH_2$, $-COOH$, $-SH$) and inorganic/organic-coated MNPs were used to adsorb heavy metals and toxic dyes (Gómez-Pastora et al., 2014). A major advantage of MNPs is

that they can be easily collected from environmental matrices using an external magnetic field. Superparamagnetic nanomaterials exhibit strong attraction to external magnetic fields, but do not attract each other, hence reducing the risk of particle aggregation (Gómez-Pastora et al., 2014). Also, using smaller particles from micro- to nano-scale enables improved adsorbent capacity by providing higher surface area.

Improving the adsorptive capacity of immobilized PBP beyond the ability of previous systems is necessary (Venkiteshwaran et al., 2020). A new PBP-loaded magnetic system was prepared and tested for P_i removal efficiency under a range of experimental conditions (pH, temperature, and ionic strength). The reusability of this system in multiple adsorption-desorption cycles was investigated and compared to unmodified IOP system. These aspects are described in Objective 3.

2.6 Summary of research needs

New strategies to achieve sustainable P_i removal and recovery from water and wastewater are needed. Common conventional wastewater treatment technologies achieve P_i effluent concentrations of 1-2 mg L⁻¹. However, these technologies are unable to achieve ultra-low effluent concentrations (which are required in some sensitive waterbodies) and many do not recover P_i as a valuable product. Closing the P_i cycle is essential and could be achieved using innovative approaches that selectively capture and release P_i under controlled conditions.

This research utilized the natural high-affinity phosphate-binding protein PstS (PBP), which may offer significant advantages over conventional treatment processes due to its high selectivity and sensitivity toward P_i . This work aimed to evaluate immobilized PBP systems targeting selective and rapid P_i removal and subsequent recovery under controlled conditions. The PBP bacterial surface-displayed system was expected to offer an effective P_i recovery system by expressing PBP protein on the cell surface instead of in-situ, whereby bacterial proteins take P_i into the cell and use it for cellular function. The micro-structured immobilized-PBP system was expected to offer an effective filter-style system featuring continuous-flow operation suitable for realistic implementation scenarios. Finally, the PBP-magnetic particle system was proposed to increase P_i removal and recovery beyond the ability of previous systems by increasing the number of immobilized PBPs on the surface. Scaling down the particle size of the carrier material increased surface area for PBP conjugation.

3 CELL SURFACE-EXPRESSION OF THE PHOSPHATE-BINDING PROTEIN PstS: SYSTEM DEVELOPMENT, CHARACTERIZATION, AND EVALUATION FOR PHOSPHORUS REMOVAL AND RECOVERY

This chapter was published as:

Hussein, F.; Venkiteshwaran, K.; Mayer, B. (2020) Cell surface-expression of the phosphate-binding protein PstS: System development, characterization, and evaluation for phosphorus removal and recovery. *Journal of Environmental Sciences* 92, 129-140.

With permission, it was modified for inclusion in this dissertation.

3.1 Introduction

Inorganic phosphate (P_i) is an essential nutrient for all living organisms. However, its simultaneous overabundance and scarcity leads to a “phosphorus paradox,” wherein excess concentrations of P_i in water bodies cause eutrophication, while available supplies of nonrenewable phosphate rock for agricultural use are continuously depleted. Surplus P_i ultimately leads to eutrophication and the subsequent development of hypoxia (Cai et al., 2011; Mayer et al., 2013; Rittmann et al., 2011). Eutrophication affects water quality and alters ecosystem structures in freshwaters worldwide (Dodds et al., 2009). A number of technologies have been developed to remove P_i from water, e.g., selective and non-selective adsorptive materials, ion exchange resins, and biological materials (i.e., whole-cell microbes or proteins) (Mayer et al., 2013). These technologies focus on removing pollutant P_i from nonpoint sources (e.g., runoff from urban and agricultural lands) and point sources (e.g., municipal and industrial wastewater treatment facilities) to meet phosphorus regulations and guidelines in natural waters and treated discharges, respectively. The

ability of these strategies to recover and reuse the P_i removed from water is also critical in reducing demands for nonrenewable phosphate rock (Mayer et al., 2013).

One interesting approach to P_i removal and recovery from water is the development of systems harnessing the use of the high-affinity phosphate-binding protein PstS (also known by the acronym PBP) (Choi et al., 2013; Kuroda et al., 2000; Li et al., 2009; Venkiteswaran et al., 2018; Y. Yang et al., 2016). Bacterial PstS is one of four proteins that comprise the Pst complex (Luecke and Quioco, 1990). The periplasmic PstS protein binds phosphate in a deep cleft using 12 hydrogen bonds, which provides strong, highly selective binding affinity (even in the presence of other wastewater oxyanions such as sulfate and arsenate) (Ledvina et al., 1998; Luecke and Quioco, 1990). Several PstS protein systems have been tested to evaluate P_i removal efficiency from water. Kuroda et al. (2000) immobilized PstS on Sepharose beads and found removal of ^{32}P -labeled phosphate to below the detection limit (9.5 ng-P L^{-1}) using packed columns filled with the modified beads. Choi et al. (2013) evaluated *in vivo* PstS, using recombinant *E. coli* to overexpress PstS in the cell's periplasmic space. The recombinant *E. coli* efficiently removed P_i (> 94% removal), even when starting at low phosphate concentrations, ranging from 0.2 to 1.0 mg L^{-1} . In a third variation, recombinant *E. coli* was modified to express PstS on the cell surface (as opposed to the natural location in the periplasmic space) using the ice nucleation protein (INP) as an anchoring protein (Li et al., 2009). This cell surface-expressed system provided 5% phosphate removal using an influent concentration of 500 $\mu\text{g PO}_4^{3-} \text{ L}^{-1}$ (Li et al., 2009).

Beyond removal alone, our research group recently conducted P_i recovery studies using PstS proteins immobilized on beads (Venkiteshwaran et al., 2018) and recombinant *E. coli* overexpressing PstS protein in the periplasmic space (Y. Yang et al., 2016). The extracellular PstS system using proteins immobilized on the bead surface was more conducive to P_i recovery compared to the periplasmic PstS system. Thus, we hypothesized that exposing the PstS directly to the water matrix by expressing the protein on the cell surface would facilitate P_i release in comparison to periplasmic PstS (in which case the cell membrane and perhaps cytoplasmic regulation could impede P_i release). Although Li et al. (2009) developed a PBP cell surface-displayed system, no studies have yet investigated conditions targeting P_i removal and recovery using cell surface-displayed PstS proteins. Accordingly, the objectives of this study were: 1) to synthesize and characterize the cell surface-expressed PstS system and 2) to evaluate P_i removal and release using cell surface-expressed PstS under controlled experimental conditions varying temperature, pH, and ionic strength (i.e., critical parameters that affect water treatment process).

3.2 Materials and Methods

3.2.1 Bacterial Strains, Plasmids, and Culture Conditions

E. coli strain DH5 α was used as the host for the recombinant plasmid, while strain BL21 (AI) was used for protein expression. The gene sequences of INP (N terminus) and PstS were synthesized and subcloned into plasmid pTrcHis_B (as confirmed by Thermofisher, USA). INP was selected as the anchoring motif as it is characterized by stable expression and modifiable internal repeating units (Jung et al., 1998). Plasmid pTrcHis_B was used for the construction and expression of the fusion protein (INP + PstS). A hexa histidine tag (6xHis-tag) was inserted before the fusion protein gene sequence to

facilitate western blot analysis using a specific anti-His antibody [the gene map is shown in Appendix A (Figure A1)].

The recombinant plasmid was transformed into DH5 α and BL21 (AI) using a heat-shock procedure (Invitrogen Life Technologies manual C6070-03). Briefly, 2 μ L of the recombinant plasmid was added to 50 μ L of cells and gently mixed. The reaction tube was kept in ice for 30 min and then immersed in a water bath at 42°C for 45 sec. The reaction tube was then returned to ice for 2 min. Afterward, 250 μ L of Luria-Bertani (LB) medium was added to the reaction tube and incubated at 37°C for 1 hr. The incubated cells were spread on LB agar containing ampicillin and left overnight at 37°C. Isolated colonies were collected, introduced into 10 mL LB, and incubated overnight at 37°C. Aliquots of the culture were mixed with 70% glycerol (1:0.56 v/v, culture/glycerol) and stored at -80°C until use.

Recombinant cells were cultivated in LB medium amended with 100 μ g mL⁻¹ ampicillin at 37°C and vigorously agitated at 250 rpm. For protein induction, 1 mM isopropyl β -D-1-thiogalactopyranoside (IPTG) was added to the cell culture once the OD₆₀₀ reached 0.6-0.8. The IPTG was allowed to react with the culture for 3-4 hr, after which the induced cells were centrifuged and stored at -20°C until use. An uninduced sample of the cells was tested in parallel as a control. *E. coli* BL21 (AI) cells bearing an empty pTrcHis_B vector (no PstS or INP inserted) were used as negative control cells.

3.2.2 SDS-PAGE and Western Blot Analyses

SDS-polyacrylamide gel electrophoresis and western blot analyses were used to confirm the expression of PstS protein and the specificity for His-tag fusion in the induced cells. One mL of cells cultured to log phase in LB was centrifuged to prepare three different samples with final $OD_{600} = 1$ (i.e., control cells [empty vector, expected to have natural levels of periplasmic PstS], uninduced cells [no IPTG induction, expected to express low levels of surface-expressed PstS], and induced cells [expected to overexpress PstS on the cell surface]). The resulting cell pellets were resuspended in a loading buffer (100 mM Tris-HCl, pH 6.8, containing 4% SDS, 0.2% bromophenol blue, 20% glycerol, and 200 mM beta-mercaptoethanol [BME]) and heated for 15 min at 98°C. The samples were loaded onto 10% SDS-PAGE gel and analyzed under 120 V for 1.5 hr. The gel cast was stained by Coomassie brilliant blue for 30 min and de-stained in 40% methanol and 10% glacial acetic acid solution to obtain a clear gel image. For western blot, proteins on the SDS-PAGE gel were transferred to a nitrocellulose membrane under 250 mA for 1.5 hr. The membrane was blocked with 1x TBS (Tris-buffered saline) containing 5% w/v nonfat dry milk and 0.1% Tween-20 at room temperature for 1 hr. The membrane was then incubated with primary rabbit anti-His-tag monoclonal antibody (Bethyl Laboratories, Inc.) overnight at 4°C. Incubation with secondary anti-rabbit immunoglobulin G (IgG) antibody (Sigma Aldrich, US) was conducted at room temperature for 1 hr. Luminol solution was added to develop the protein signal on the films.

3.2.3 Outer Membrane Separation

To isolate the outer membrane (OM) fraction and confirm the location of the fusion protein, we followed the procedure published by Park et al. (2015). Briefly, the centrifuged *E. coli* cells were resuspended in lysozyme buffer containing 0.2 M Tris-HCl (pH 8.0), 200 $\mu\text{g mL}^{-1}$ lysozyme, 20 mM sucrose, and 0.2 mM ethylenediaminetetraacetic acid (EDTA) for 10 min at room temperature. Next, 20 $\mu\text{g mL}^{-1}$ aprotinin and 1 mM phenylmethylsulfonyl fluoride (PMSF) were added to the solution. An equivalent volume of extraction buffer (2% Triton X-100, 50 mM Tris-HCl, 10 mM MgCl_2 , and 10 $\mu\text{g mL}^{-1}$ DNase) was added to isolate the outer membrane. After incubation in ice for 30 min, the lysate was centrifuged at 5000 rpm for 5 min; the supernatant was recentrifuged at 18,000 rpm for 10 min. The presence of PstS was assessed in the collected fractions by SDS-PAGE.

3.2.4 Cell Surface Characterization

Cell surface characterization through acid-base titration, XPS, and FTIR were performed to provide information on the surface properties of *E. coli* cells. Acid-base titration provides proton-exchange properties of the surface functional groups (i.e., pK_a values). Proton and hydroxide concentrations are more precisely obtained by acid-base titration at low detection limit compared to spectroscopic techniques (Ojeda et al., 2008). FTIR spectroscopy and XPS characterize the macromolecular structure and composition of the bacterial surface. FTIR identified potential functional groups from lipids, proteins, and carbohydrates on the cell surface. XPS was used to estimate the relative elemental surface composition. The combination of analyses offers a comprehensive understanding

of the cell surface properties as an initial step toward understanding the cells' response under different conditions.

3.2.4.1 Acid-Base Titration

Cultures of control, uninduced, and induced cells were centrifuged at 6000 rpm at room temperature and the collected pellets were washed with 0.01 M NaCl. This process was repeated three times to remove LB media residue. The pellets were resuspended in a background electrolyte of 0.01 M NaCl with $OD_{600} = 2$ (≈ 0.78 g bacteria L^{-1}). Samples were purged with N_2 gas for 5 min to remove atmospheric CO_2 gas. Next, 20 mL of bacterial suspension was transferred to a polypropylene titration vessel. Titration was performed using an EasyPlusTM titrator (Mettler Toledo, Easy pH) at room temperature. All samples were initially acidified to $pH \approx 3.5$ using 0.01 M HCl, followed by titration with 0.01 M NaOH to ultimately reach pH 10.5.

ProtoFit GUI 2.1 rev1 software using surface complexation models such as the constant capacitance model (CCM) and non-electrostatic model (NEM) was used to determine pKa values. The CCM requires one fit parameter (i.e., capacitance of electrical double layer) while the NEM does not require any parameters (Turner and Fein, 2006). The extended Debye-Huckel activity coefficient model was used as it is considered the most accurate model for ionic strength up to 0.1 M (Langmuir, 1997). Three-site functional group and four-site functional group specifications were applied and compared for best fit simulation. The surface area of *E. coli* was calculated using an average cell length of 2 μm and 1 μm diameter. The cell number from the optical density reading and the dry weight of the cells were used to calculate the specific surface area (16.2 m^2 g^{-1} dry weight).

3.2.4.2 Macromolecular Structure and Composition of the Bacterial Surface

For X-ray photoelectron spectroscopy (XPS) analysis, *E. coli* cells were suspended in 10 mM Tris-HCl and 1 mM MgCl₂ at pH 7, frozen at -20°C, and freeze-dried, as previously reported (van der Mei et al., 2000). Frozen samples of control cells, uninduced cells, and induced cells were mounted on the bench-top freeze dryer manifold (Millrock Technology BT85A) at 150 mT and -48°C for 48 hr. The resulting powder was analyzed using a Perkin-Elmer PHI 5400 ESCA system equipped with a Mg K α X-ray source (1253.6 eV). A wide survey scan with pass energy 100 eV and 1 eV step size was conducted for each sample, providing a path depth 2-5 nm into the surface layer. CasaXPS 2.3.19 software was used to generate the XPS spectra for all samples and calculate the surface atomic concentrations of C, N, O, and P.

For Fourier transform infrared spectroscopy (FTIR) analysis, bacterial suspensions (in 10 mM Tris-HCl and 1 mM MgCl₂ at pH 7) were examined using an IR Tracer-100 FTIR spectrometer (Shimadzu Scientific Instruments) with a KBr beam splitter. Spectra for all samples were obtained over 50 scans with a resolution of 2 cm⁻¹ and a wavenumber range from 4000 to 400 cm⁻¹. The spectrum of the background solution was subtracted from the bacterial suspensions' spectra. Functional group presence was ascertained using corresponding peak wavenumbers.

3.2.5 Phosphorus Desorption and Adsorption Batch Experiments

To run the batch experiments, desorption tests were initially performed to remove legacy P_i since the cells were cultured in highly concentrated P_i medium (150-170 mg PO₄³⁻ L⁻¹). The cell pellets were washed with buffer (10 mM Tris-HCl and 1 mM MgCl₂ at pH 7) and centrifuged twice at 6000 rpm. The pellets were then resuspended in the same

buffer at $OD_{600} = 2$. The desorption capacity of the control, uninduced, and induced cells was investigated at different buffer pH (3.5, 5.5, 7, 8.5, and 10.5). The effects of temperature (20, 30, and 40°C) and ionic strength (0.1, 0.3, 0.5, 0.7, 1 M KCl) were also studied. In all tests, cell concentrations were maintained at $OD_{600} = 1$. All tests were conducted in triplicate at room temperature for 3 hr and 250 rpm mixing in Tris-HCl buffer unless otherwise specified. The final phosphate concentration in all tests was measured using the standard ascorbic acid method (APHA, 2005).

To facilitate comparisons of the surface-expressed system performance to periplasmic-expressed PstS (periplasmic data from Y. Yang et al. 2016), an additional surface-expressed PstS desorption test was performed at the same conditions as the previous periplasmic-expressed PstS tests (i.e., $OD_{600} = 0.5$, 3 hr, room temperature, and pH 6.8 and pH 3.5).

For adsorption tests, three different treatment conditions were initially applied to initiate phosphate desorption from the cells before conducting the adsorption experiments: cell starvation under low- P_i conditions, variable pH and temperature, and enzymatic treatments. One set of cells was suspended in Tris-HCl buffer at pH 7 for 15 hr (starvation treatment). A second set of cells was suspended in Tris-HCl solution at pH 10 and 40°C for 3 hr (pH and temperature treatment). The last set of cells was suspended in Tris-HCl at pH 7 with 1 unit per mL purine nucleotide phosphorylase (PNP) and 1 mM of 7-methylguanosine for 3 hr (enzymatic treatment). In this way, free P_i can be removed by converting it into ribose 1-phosphate (Brune et al., 1994). All treated cells were centrifuged at 6000 rpm and resuspended in phosphate solution (either 7 mg $PO_4^{3-} L^{-1}$ or 70 mg $PO_4^{3-} L^{-1}$) for 3 hr.

3.2.6 Statistical Analysis

Two-way ANOVA followed by Tukey post-hoc analysis was performed to assess the differences in phosphate capture and release due to test factors, i.e., temperature, pH, ionic strength, and cell type. Nonparametric Kolmogorov-Smirnov analysis was used to compare the acid-base titration curves. All statistics were performed using GraphPad Prism with a significance level of $\alpha = 0.05$.

3.3 Results and Discussion

3.3.1 Confirmation of Surface Expression Using SDS-PAGE, Western Blot Analyses, and Outer Membrane Separation

Expression of the fusion protein (INP + PstS) in the recombinant *E. coli* BL21 (AI) cells was confirmed via SDS-PAGE analysis (Figure 3.1a). A distinct band is visible for the induced PstS cells at a molecular weight (MW) of 60 kDa, which is the expected size of the PstS and INP proteins together. Two other notable bands are present at a MW of 35 kDa for PstS and 25 kDa for INP. Separation of the two proteins might result from protease attack on the N-terminal of the INP protein, as observed by Li et al. (2003) and Li et al. (2009).

The specificity of the His-tag fusion was confirmed via western blotting. As shown in Figure 3.1b, no bands were observed in the expected size ranges for either the control cells or the uninduced cells. The induced cell sample was characterized by two distinct bands at 60 kDa (full size of INP + PstS) and 25 kDa (size of INP only). These results confirmed expectations since the His-tag region of the constructed plasmid was located ahead of the InaK-N gene sequence (associated with the INP protein). Quantification of the western blot results was performed using Image Studio Lite software (version 5.2.5)

and indicated that approximately 27% of the overexpressed protein was present in the full fusion form (Appendix A, Table A1).

To verify the location of the PstS protein, an outer membrane fractionation procedure was performed to isolate cellular fractions (Park et al., 2015). The outer membrane fraction was obtained by enzymatic treatment with lysozyme to hydrolyze the peptidoglycan layer followed by liposome isolation using Triton X-100 as a detergent. Figure 3.1c shows the SDS-PAGE results from the outer membrane fraction and the cell lysate (from the internal cellular constituents) fractions. A distinct band is visible at 35 kDa for the outer membrane fraction, corresponding to the size of the PstS protein. Alternately, low levels of PstS protein are indicated by weak bands for the duplicate cell lysate samples (although future work could include analyzing with western blot to further assess the relative amount in the cell lysate). The fusion protein detected in the cell lysate fraction showed signs of proteolysis (Li et al., 2003). The N-terminal of INP might be susceptible to protease attack and that degradation would result in free PstS being detected in the outer membrane fraction of the induced cell (Li et al., 2003). Altogether, the SDS-PAGE, western blot, and outer membrane separation analyses demonstrated successful PstS protein expression and localization on the outermost surface of the *E. coli* cells.

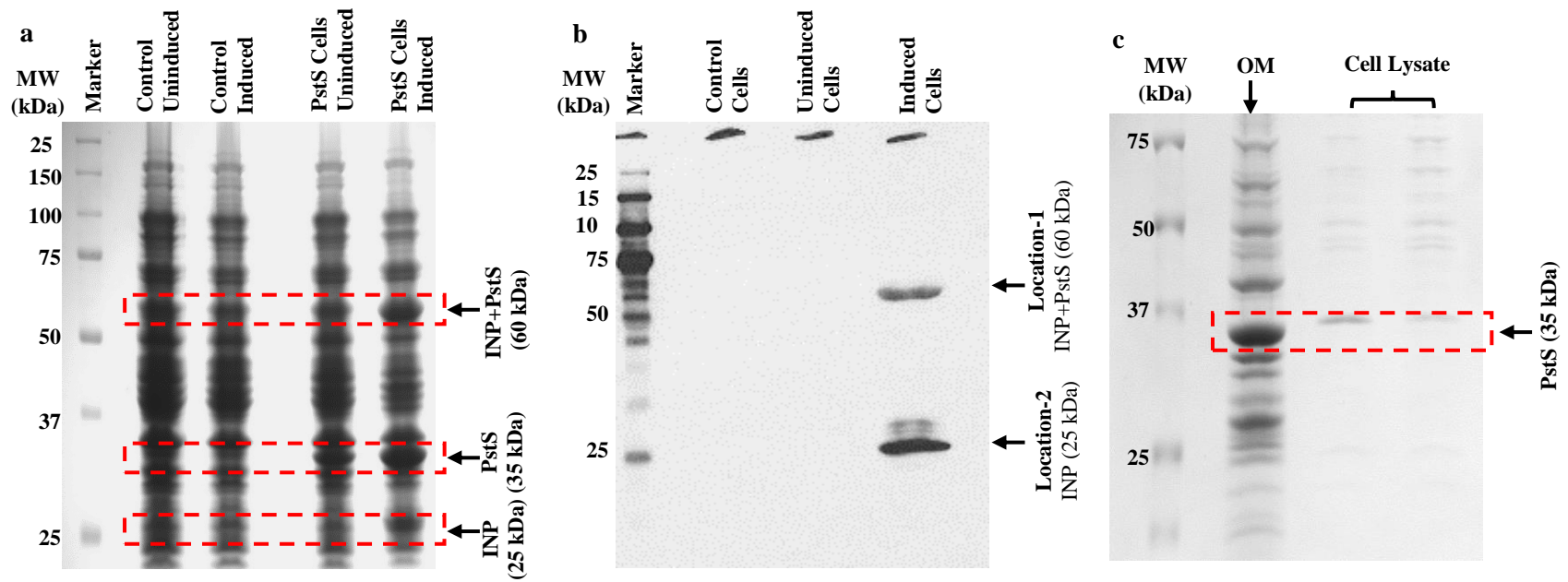


Figure 3.1 Protein verification, expression, and separation analyses. (a) Protein verification using SDS-PAGE analysis of control cells (lane 2: before IPTG induction [Control Uninduced]; lane 3: after IPTG induction [Control Induced]) and PstS cells (lane 4: before IPTG induction [PstS Cells Uninduced]; lane 5: after IPTG induction [PstS Cells Induced]). Lane 1 is the protein marker. (b) Protein expression using Western Blot analysis shows two distinguished bands for the induced cells, corresponding to INP only and INP + PstS together. (c) SDS-PAGE analysis of the outer membrane (OM) separation analysis of the induced cells showing the presence of PstS in the OM fraction rather than the cell lysate fraction.

3.3.2 Cell Surface Characterization

3.3.2.1 Acid-Base Titration

The typical titration curve for all cells - control cells (CC), uninduced cells (UC), and induced cells (IC) - is illustrated in Figure 3.2a. The curves for all cell types shifted toward the right starting at $\text{pH} \approx 5.5$ compared to the titration curve for the background solution (electrolyte solution 0.1 M NaCl). Thus, the presence of the bacteria provided additional buffering capacity. The active functional groups on the cell surfaces provide buffering capacity as they consume additional base via deprotonation (Ngwenya et al., 2003). The titration data for the control cells was significantly different than uninduced and induced cells. The titration curve for the control cells suggests a higher presence of protonated functional groups (greater buffering capacity) on the surface compared to either the induced or uninduced cells. Figure 3.2a also shows four regions characterized by different behavior, possibly indicative of different surface pK_a values (i.e., below $\text{pH} \approx 5$, between $\text{pH} \approx 5$ and $\text{pH} \approx 6.2$, between $\text{pH} \approx 6.2$ and $\text{pH} \approx 9.4$, and above $\text{pH} \approx 9.4$), in accordance with procedures described by Dittrich and Sibling (2005), Guiné et al. (2006), Haas (2004); Hong and Brown (2006), and Ojeda et al. (2008).

Figures 3.2b, 3.2c, and 3.2d show the three-site constant capacitance model (CCM) and three-site non-electrostatic model (NEM) fits for the raw titration data for the control cells, uninduced cells, and induced cells, respectively. The control and uninduced cells were best fit using the CCM, whereas the induced cells were best fit using the NEM. The CCM assumes that surface charge is homogeneously distributed over the bacterial surface, giving rise to relatively simple electrostatic field behavior (Ojeda et al., 2008). Therefore, the existence of extra charged molecules on the surface (i.e., protein) might disturb the

homogeneity of the surface charge distribution. The calculated pK_a values from both models are listed in Table 3.1. Regardless of cell type, the two models predicted similar values for pK_{a2} . However, the predicted pK_{a1} values using the CCM were consistently lower than the values from the NEM, whereas the opposite was true for the predicted pK_{a3} values (where CCM results were consistently higher than NEM). Sites with pK_a values of 3.15 to 4.5 may be indicative of the presence of carboxyl groups, sites with pK_a 5.36-6.15 would be assigned to the phosphate group, and sites with pK_a 7.46-9.75 could be tentatively assigned to hydroxyl and amine groups (Dittrich and Sibling, 2005; Guiné et al., 2006; Haas, 2004; Hong and Brown, 2006; Ojeda et al., 2008). Reported pK_a values vary for the carboxyl group from 2-6, for the phosphate group from 5.6-7.2, for the amine group 8.6-9, and for hydroxyl from 8-12 (Dittrich and Sibling, 2005; Guiné et al., 2006; Haas, 2004; Hong and Brown, 2006; Ojeda et al., 2008).

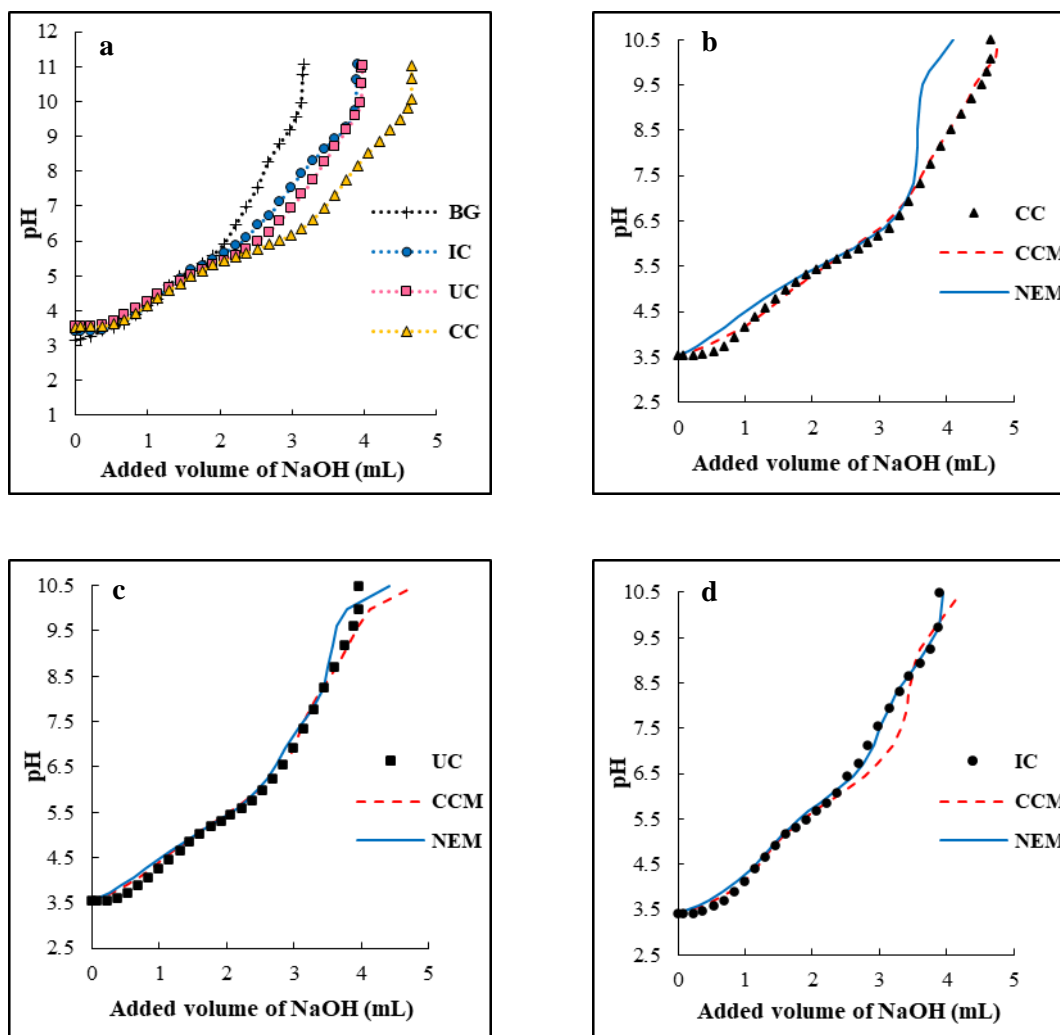


Figure 3.2 (a) Typical acid-base titration curves for induced cells (IC), uninduced cells (UC), and control cells (CC) suspended in 0.01 M NaCl with final $OD_{600} = 2$. BG = background solution (0.1 M NaCl). (b), (c), and (d) three-site (2 acid and 1 base) constant capacitance model (CCM) and three-site (2 acid and 1 base) non-electrostatic model (NEM) curve fits for CC, UC, and IC, respectively.

Considerable difference was observed between the pK_{a3} values for the induced cells compared to other cells. The higher value may correlate to the presence of PstS protein on the surface of *E. coli*, which may provide additional deprotonated functional groups based on the theoretical isoelectric point (pH_{pzc}) of PstS of 8.39 (calculated based on the sequence of amino acids, https://web.expasy.org/compute_pi/). Alternately, the average pH_{pzc} for unmodified *E. coli* cells is 6.6 (strain K12, from the proteome isoelectric point database

(Kozłowski, 2016)). This is further demonstrated through the calculated pH_{pzc} for the cells (Table 3.1), which demonstrated that the induced cells have a higher pH_{pzc} value compared to the uninduced and control cells. Notably, acid-base titration analysis might not convey all existing pK_a values on the cell surface.

Table 3.1 Deprotonation constants (pK_a) and point of zero charge (pH_{pzc}) as calculated with ProtoFit GIU using the constant capacitance model (CCM) and non-electrostatic model (NEM) for control cells, uninduced cells, and induced cells.

Cell Type	Constant Capacitance Model (CCM)				Non-Electrostatic Model (NEM)			
	pK_{a1}	pK_{a2}	pK_{a3}	pH_{pzc}	pK_{a1}	pK_{a2}	pK_{a3}	pH_{pzc}
Control Cells	3.88	5.81	8.08	5.91	4.50	5.50	6.15	6.11
Uninduced Cells	3.15	5.45	8.05	5.54	4.45	5.36	7.46	6.75
Induced Cells	3.20	5.99	9.75	6.08	4.40	6.00	8.58	7.73

3.3.2.2 Macromolecular Structure and Composition of the Bacterial Surface

The XPS wide scan for the control cells, uninduced cells, and induced cells is shown in Figure 3.3a. The overlying spectra reveal many peaks identified as C, N, and O elements, with other peaks identified as Cl, S, and P. Notably, the outermost cell surface (2-5 nm penetration depth) contains mainly C, N, and O. The carbon peak can indicate a carboxylic group R-COO^- , and the oxygen peak may be attributed to a single-bond oxygen in hydroxide or an acetal group (Ojeda et al., 2008). The nitrogen peak likely represents amine or amide groups characteristic of proteins, and the phosphorus can be attributed to phosphate groups (Dufrière et al., 1997; Omoike and Chorover, 2004; van der Mei et al., 2000). The atomic composition of the bacterial surface resulting from the integration of the C_{1s} , N_{1s} , O_{1s} , and P_{1s} peaks is listed in Figure 3.3a. The values of total carbon were similar

for induced and uninduced cells, at approximately 10% more than the control cells. Other compositions varied amongst the cell types. The oxygen content was higher in control cells compared to induced and uninduced cells, whereas the nitrogen content was lower in control cells compared to the other cells. This ostensibly stems from the addition of the fusion protein (the backbone structure of which is a combination of amino acids, i.e., carbon and nitrogen constituents) in the induced and uninduced cells. In the uninduced cells, the fusion protein may present as a result of “leaking protein expression” due to the existence of lactose in the LB medium that triggers transcription of the lac operon. Although XPS analysis provided quantitative characterization of the surface composition, the results are highly sensitive and can vary due to minor variations such as OD₆₀₀ readings, peak limits, and the cell pellet washing procedure.

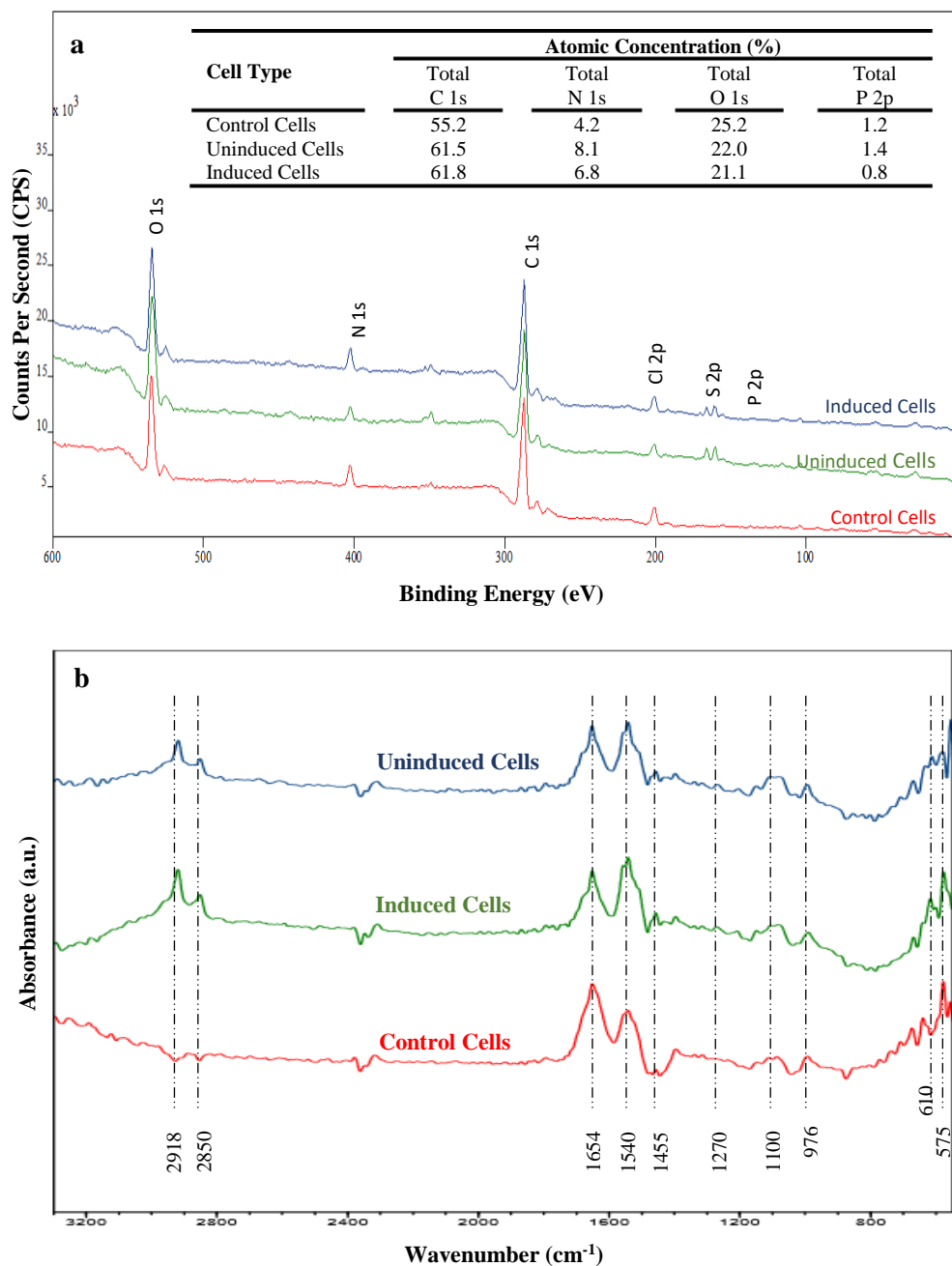


Figure 3.3 (a) XPS spectra for freeze-dried samples of control cells, uninduced cells, and induced cells. Acquisition with pass energy 100 eV and 1 eV step size using Mg K α X-ray source. The inset table shows the percentage atomic concentration of C, N, O, and P on the bacterial surface calculated from the XPS spectra. (b) Infrared spectra of control cells, uninduced cells, and induced cells suspension in 10 mM Tris-HCl solution at a final OD₆₀₀ = 2. The spectra are vertically offset for clarity. Peaks were identified and functional groups were assigned as shown in Appendix A (Table A2).

The FTIR spectrum conveys molecular-level information about the functional groups on the cell surface (Figure 3.3b; peak functional group assignments are listed in Appendix A (Table A2). As all cells were from the same strain, similar FTIR spectra were expected, with slight differences between the cell types as a result of protein overexpression. The spectrum for the induced cells exhibited higher intensity peaks in the protein region ($\approx 1400\text{-}1700\text{ cm}^{-1}$). Three functional groups were identified in this region: C=O stretching in amides (amide I at wavenumber $\approx 1654\text{ cm}^{-1}$), N-H bending and C-N stretching in amides (amide II at wavenumber $\approx 1540\text{ cm}^{-1}$), and C-H deformation of methylene (CH_2) or methyl (CH_3) groups of proteins at wavenumber $\approx 1455\text{ cm}^{-1}$. Additionally, a hydroxyl group peak was identified (COOH at wavenumber $\approx 1270\text{ cm}^{-1}$). The outcomes of FTIR spectra were consistent with previous examinations of cell surfaces of different bacterial strains (Dittrich and Sibler, 2005; Filip et al., 2008; Jiang et al., 2004).

Results from the cell surface characterization analyses can inform understanding of the differences in the surface chemical composition and functionality of different type of cells. For example, acid-base titration analysis showed that protein expression could shift the total surface charge of modified cells, affecting the electrostatic interaction between P and PstS at different pH values.

3.3.3 Phosphorus Desorption Batch Experiments

Before initiating adsorption tests, P_i desorption was performed to prepare the proteins for effective P_i capture, analogous to the regeneration phase of phosphate ion exchange media. Thus, desorption tests were initially conducted to remove legacy P_i since the cells were cultured in highly concentrated P_i medium (150-170 mg PO_4^{3-} L⁻¹). As detailed in the following sections, the use of an active cell-based system introduced potential for variations in the influence of temperature, pH, and ionic strength not only on phosphate capture and release using the surface-expressed PstS proteins, but also on the cell's basic functions related to P_i uptake and release. For simplicity, we have adopted the terms “adsorption” and “desorption” to characterize P_i capture and release, while recognizing that multiple mechanisms are actually at play in this cellular system.

3.3.3.1 Effect of Temperature

Phosphorus desorption from control cells, uninduced cells, and induced cells as a function of temperature is illustrated in Figure 3.4a. Increasing the temperature to 40°C promoted release of P_i from all cells, yielding approximately 5-6 times greater release than at 20°C. Yang et al. (2016) also reported an increase in P_i release by *E. coli* cells as a function of temperature. At 40°C, the induced cells desorbed approximately 20% more P_i compared to the control cells. There was a significant difference between P_i release among the three cell types as a function of temperature, with higher temperatures promoting desorption ($p = 0.001$). However, there was no significant difference between P_i desorbed from the uninduced cells and control cells at 20°C ($p = 0.64$) and 30°C ($p = 0.29$).

induced cells' ability to release higher levels of P_i compared to other cells may relate to the presence of overexpressed PstS protein on the cell surface. As extra P_i ions

can be attached to PstS proteins on the surface, higher levels of P_i are released once the binding affinity is disrupted (e.g., structural disruption in PstS protein) by an external factor. Therefore, increasing the temperature will facilitate P_i release and recovery.

3.3.3.2 Effect of pH

Adjusting pH significantly affected P_i release amongst the cell types, as shown in Figure 3.4b (two-way ANOVA, $p = 0.0092$). At pH 5.5 and 7, there was no significant difference in the amount of P_i released amongst the cell types ($p = 0.087$). This pH range has no impact on the intracellular pH of *E. coli* cells, so metabolism, ion transport, and other cellular functions will perform regularly (Slonczewski et al., 2009). Furthermore, no difference was expected between the cell types as proteins are structurally stable in the circumneutral pH range. In contrast, acidic and basic conditions noticeably impacted P_i release.

At pH 3.5, the control and uninduced cells released approximately 50% more P_i than the induced cells. In order to lessen the deleterious effects of high proton levels under low pH conditions, several molecular strategies are employed for acid resistance (Lund et al., 2014). The most well-known strategies are proton pumping, cell membrane modification, production of ammonia and proton-consuming decarboxylation reactions, repairing or damage prevention of proteins, and urea breakdown (Kanjee and Houry, 2013; Lund et al., 2014). Proton pumping could be a reason for the increases in P_i release at low pH observed here. Through this mechanism, protons are exported from the cytoplasm to the extracellular space, which requires energy provided by ATP hydrolysis (Lund et al., 2014). Potential pathways for release of free P_i ions produced during this reaction might be (i) phosphorylation reactions inside the cell or (ii) active transport outside the cell to

neutralize external surface charges. The strong acidic condition affects the surface charge of proteins, providing a positive net surface charge. Consequently, the protein's structure is destabilized, and the protein's functionality is lost (Appling et al., 2016). Although the PstS protein's phosphate-binding site might be disrupted, it is possible that free P_i ions would be electrostatically attracted to the PstS protein's surface. Hence, less P_i would be released by the induced cells. Phosphate ions are negatively charged above pH 2.15 (i.e., the acid dissociation constants are $pK_{a1}=2.15$, $pK_{a2}=7.2$, and $pK_{a3}=12.33$) (Ajmal et al., 2018).

Under basic pH conditions, induced cells offered the highest P_i release ($p = 0.0092$). For all cell types, increasing the pH from 8.5 to 10.5 increased P_i release by approximately 60-70%. Similar to acidic conditions, *E. coli* cells may be capable of several possible passive and active responses to high pH conditions. Three possible categories of actions include chemical processes, metabolic responses, and cell wall destabilization (Claessens et al., 2004). In metabolic responses, proton pumping can be used to prevent proton leakage by actively transporting protons against the concentration gradient. This utilizes ATP as an energy source to initiate proton transport. ATP hydrolysis reactions provide additional free P_i ions in the cytoplasm. Proton pumping might be responsible for the increased release of P_i ions. Strong basic conditions affect proteins' surface charge, providing a negative net surface charge. Therefore, the protein's structure will be destabilized, and the protein's functionality will be lost (Appling et al., 2016). The phosphate-binding site of the PstS protein would thus be disrupted, and the bound P_i ions would be released.

Overall, acidic and basic pH conditions promoted P_i release, with the PstS protein releasing more P_i at basic pH levels compared to acidic conditions. These results show that basic conditions may be used for P_i release and recovery using the cell surface-displayed system. Interestingly, the P_i release mechanism from PstS protein (i.e., disruption of hydrogen bonds in the binding site) agreed with previous findings (Venkiteshwaran et al., 2021), even though it was difficult to predict how intact cells would behave under variable pH and temperature due to the bioenergetic and metabolic regulation mechanisms.

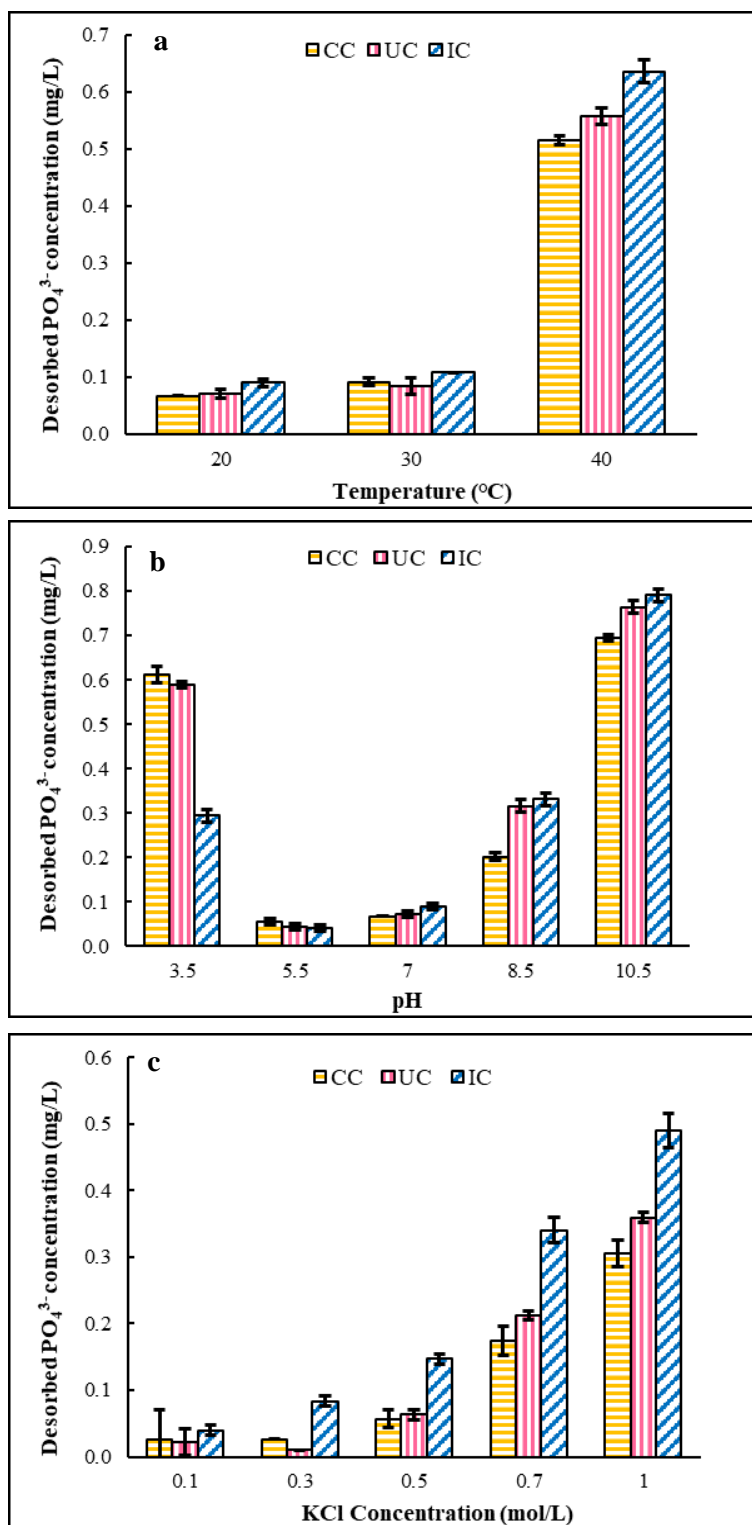


Figure 3.4 Phosphate desorption from control cells (CC), uninduced cells (UC), and induced cells (IC) with final $OD_{600} = 1$ as a function of (a) temperature, (b) pH, and (c) ionic strength. All experiments were conducted in triplicate, and error bars denote ± 1 standard deviation.

3.3.3.3 Effect of Ionic Strength

The impact of ionic strength on P_i release from all cells is shown in Figure 3.4c. Desorption of P_i from all cells significantly increased as ionic strength increased (two-way ANOVA, $p = 0.0055$). Induced cells released more P_i than control and uninduced cells at each ionic strength. The induced cells' P_i release capacity was approximately 30% to 70% greater than the other cells.

Normally, *E. coli* responds to ionic stress by ion transport and osmotic adjustment (Shabala et al., 2009). Ions can be exchanged (influx/efflux) between the extracellular space and the cytoplasmic pool of ions; cells can also synthesize anions and osmolytes to restore turgor pressure and the normal ionic strength inside the cells (Shabala et al., 2009). Two intracellular possibilities could explain the effect of ionic strength on P_i desorption. First, simple diffusion of P_i ions might occur considering that the intracellular concentration of PO_4^{3-} is higher than the extracellular concentration. Second, ion exchange with Cl^- would happen (i.e., Cl^- influx and PO_4^{3-} L^{-1} efflux). These explanations would affect induced, uninduced, and control cells.

The binding affinity of PstS is also affected by ionic strength (Wang et al., 1994). The dissociation constant of the PstS- P_i complex (K_d) increases approximately 20-fold at 0.3 M NaCl compared to no-salt solution (Ledvina et al., 1998). Affinity of PstS for anions was found to be insensitive to the surface charge potential of the cleft region (functional site), but extremely sensitive to electrostatic effects at the level of local hydrogen bonding interactions (Ledvina et al., 1998). Thus, increased ionic strength disrupts hydrogen bonds, leading to P_i release from the binding site (Ledvina et al., 1998). Therefore, induced cells would offer greater P_i desorption compared to other cells, as observed here.

3.3.3.4 Surface-expressed PstS vs Periplasmic-expressed PstS

A comparison of P_i release using periplasmic-expressed PstS (PP-PstS) and surface-expressed PstS (SE-PstS) was performed under identical experimental conditions (i.e., pH, T, and $OD_{600} = 0.5$). Figure 3.5 shows the amount of P_i released for both PstS expressions at pH 6.8 and pH 3.8. Surface-expressed PstS released two times more P_i at both pH values, which indicates that periplasmic-expressed PstS might be affected by the intracellular activities that could impede P_i release compared to surface-expressed PstS that is located outside the cells. Notably, the amount of protein expressed in the two different systems was not assessed, but would be an important consideration for future assessments in order to normalize P_i removal/release to the amount of protein present.

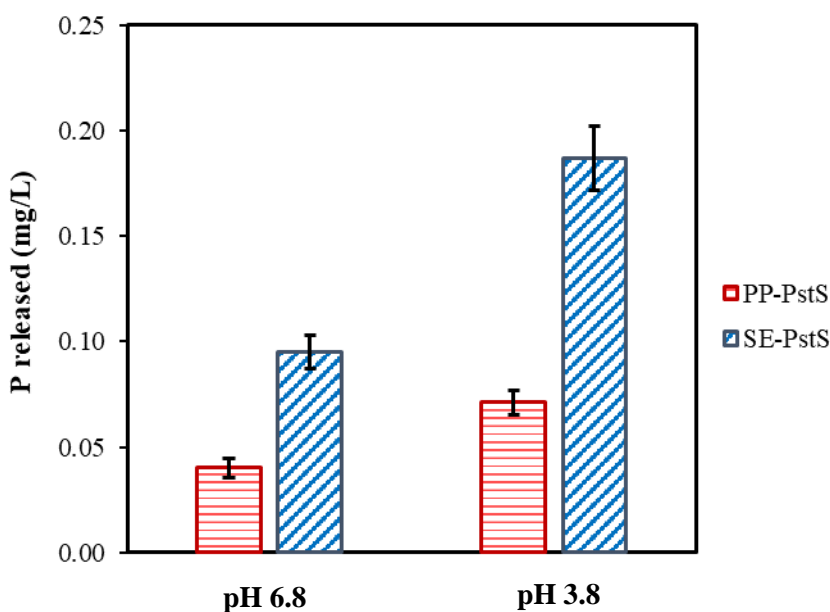


Figure 3.5 Comparison of phosphorus release using periplasmic-expressed PstS (PP-PstS) and surface-expressed PstS (SE-PstS). Data for the periplasmic-expressed-PstS is from Yang et al. (2016).

3.3.4 Phosphorus Adsorption Batch Experiments

Adsorption batch tests were conducted using control cells and induced cells (the uninduced cells were not tested as they performed similarly to the control cells in desorption experiments). The cells' capacity to remove P_i from solution was investigated following an initial desorption step (starvation, pH & temperature, or enzyme). The pH (10.5) and temperature (40°C) conditions were selected based on the previous desorption batch results. Starvation and enzyme conditions were proposed as additional approaches to be tested. Following desorption, the cells were suspended in two different phosphate solutions (7 mg $PO_4^{3-} L^{-1}$ or 70 mg $PO_4^{3-} L^{-1}$; the cells' exhibited low ability to remove P_i at low initial concentrations, i.e., 1 mg L^{-1}), and the resulting P_i removals are shown in Figure 3.6a and Figure 3.6b, respectively. Starvation, pH & temperature, and enzymatic conditions (i.e., addition of purine nucleotide phosphorylase PNP and 7-methylguanosine) were used to target minimal initial cellular/external P_i levels to prepare the *E. coli* cells for P_i adsorption.

The most effective condition to prepare cells for P_i removal was "starvation", wherein control and induced cells were suspended in 10 mM Tris-HCl solution at pH 7 for approximately 15 hr. This condition effectively released P_i for induced cells at both P_i concentrations but was not effective at 7 mg $PO_4^{3-} L^{-1}$ for control cells ($p = 0.636$). Under these conditions, additional P_i ions were released from the control cells (rather than P_i removal). The free P_i in the cytoplasm was likely still too high, preventing the cells from uptaking additional P_i . The induced cells provided approximately 48% additional P_i removal under starvation conditions with an initial concentration of 70 mg $PO_4^{3-} L^{-1}$. Starvation conditions may force the cells to consume the pool of free P_i in the cytoplasm,

of which potentially less is available in induced cells compared to control cells. Induced cells would encounter additional stresses during the induction and translocation of fusion protein (INP + PstS), which would require more production of ATP by utilizing the free P_i in the cytoplasm.

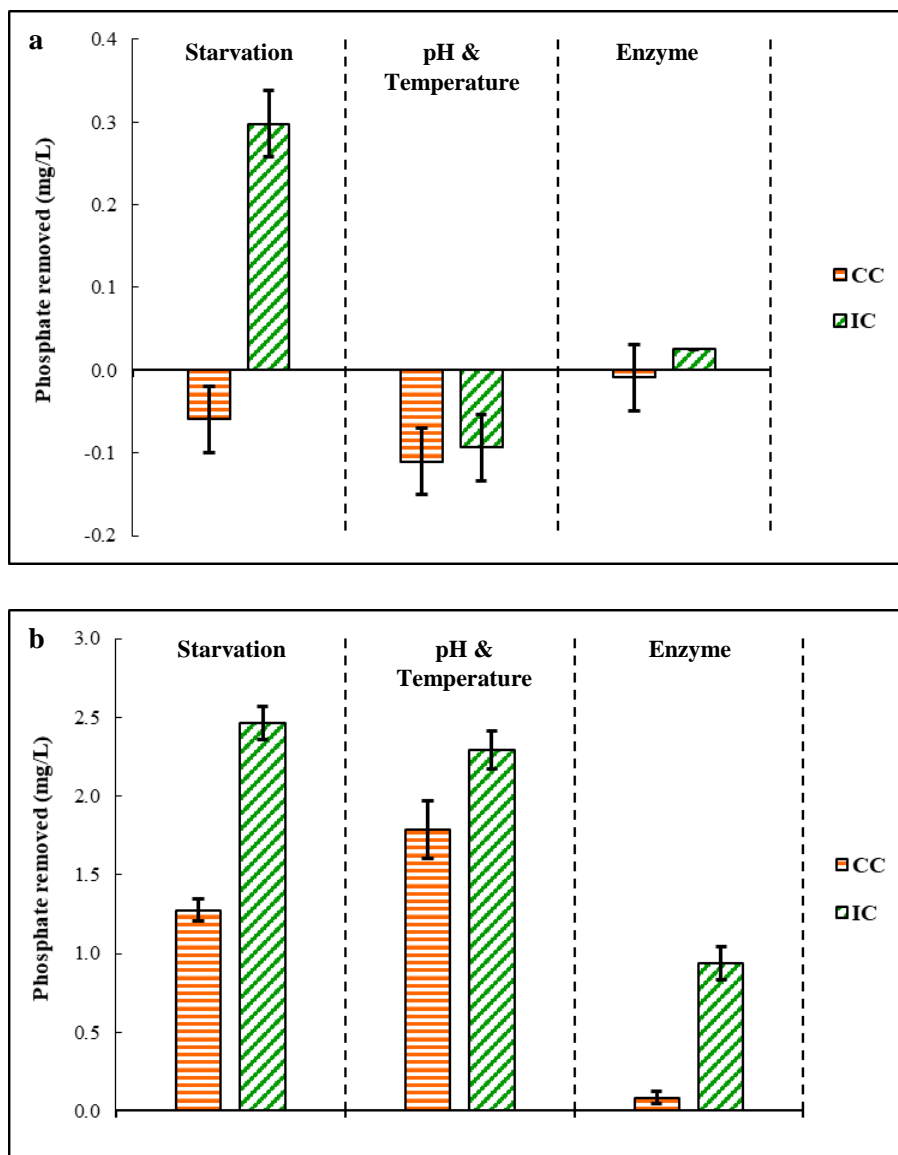


Figure 3.6 Phosphate uptake by control cells and induced cells after desorption conditions (starvation, pH & temperature, and enzyme). Two phosphate concentrations were selected for adsorption tests (a) 7 mg $PO_4^{3-} L^{-1}$ and (b) 70 mg $PO_4^{3-} L^{-1}$. All phosphate adsorption experiments were conducted in triplicate for 3 hr at room temperature, 250 rpm mixing, and pH 6.7. Error bars denote ± 1 standard deviation.

Enzymatic and pH & temperature conditions did not significantly affect adsorption at low P_i concentrations for either cell type ($p = 0.872$ and $p = 0.991$, respectively). However, pH & temperature adjustment was more effective for P_i adsorption than enzymatic treatment at higher P_i concentrations. Enzyme addition might only affect the external surrounding and the fusion protein. The PNP enzyme converts free P_i to ribose 1-phosphate (Brune et al., 1994). However, pH & temperature adjustment might affect both the internal function of *E. coli* cells and the fusion protein. Induced cells adsorbed approximately 22% more P_i than control cells under adjusted pH & temperature conditions. These general observations are in accordance with the expectation that induced cells would adsorb more P_i than control cells due to the presence of the PstS protein.

3.4 Conclusions

A cell surface-expressed PstS protein system was successfully developed and characterized for P_i removal and recovery. Increasing temperature (up to 40°C) and ionic strength (up to 1 M) increased phosphate release by 20% and 50%, respectively. Acidic and basic pH conditions also promoted phosphate release, with the PstS protein releasing $\approx 63\%$ more phosphate at basic pH levels compared to acidic conditions. Increasing phosphate removal from solution was achieved when *E. coli* cells were exposed to starvation conditions with low levels of P_i available. Induced cells provided 48% higher phosphate removal compared to control cells, although removals were generally low. Moreover, surface-expressed PstS showed 2 times higher ability to release P_i compared to periplasmic-expressed PstS.

Adsorption/desorption results provided proof-of-concept of the feasibility of P_i release and recovery using cell-surface expressed PstS. However, further studies are needed to optimize performance in order to achieve higher phosphate removal as cellular functions impeded controlled P_i recovery. Also, investigating other microorganisms targeting more stable induction of the fusion protein is recommended. Inducing mutants in the Pst transport system to confine the cellular interaction might increase the efficiency of the fusion protein in phosphate adsorption and desorption applications. The system must also be tested and optimized for future wastewater/natural water applications.

4 FIXED-BED COLUMN STUDY OF PHOSPHATE ADSORPTION USING IMMOBILIZED PHOSPHATE-BINDING PROTEIN

This chapter was published as:

Hussein, F.; Mayer, B. (2022) Fixed-Bed Column Study of Phosphate Adsorption Using Immobilized Phosphate-Binding Proteins. *Chemosphere* 295.

With permission, it was reformatted for this dissertation.

4.1 Introduction

Excessive orthophosphate (P_i) released from domestic, agricultural, and industrial activities significantly contributes to eutrophication, which affects water quality and leads to losses in biodiversity. While too much P_i is therefore problematic, conversely, too little P_i also poses major challenges. Mineable phosphate is a finite resource that, on human timescales, is being continuously depleted to supply fertilizers for food production. Therefore, it is vital to efficiently manage P_i usage, and removing and recovering P_i from waste streams whenever viable can contribute to this effort. Numerous technologies have been applied to remove P_i from water/wastewater, including ion exchange resins, chemical precipitation and crystallization, adsorption, membrane technology, and biological treatment (Bui et al., 2018; Huang et al., 2017; Mayer et al., 2013; Xu et al., 2019; S. Yang et al., 2016). Among these technologies, adsorption is a promising approach to remove P_i to low final concentrations (Jia et al., 2020; Mayer et al., 2013; Pap et al., 2020). Advantages include the adsorbents' high selectivity, low cost, and durability in batch or continuous-flow operating modes (Qiu et al., 2017). Adsorption performance, however,

depends on the material itself and system conditions such as pH and sorbate concentration (Pap et al., 2020).

Nature offers an effective P_i sorbent in the form of high-affinity phosphate-binding proteins (PBPs) such as PstS, which selectively binds P_i in a deep cleft using 12 hydrogen bonds (Ledvina et al., 1998; Luecke and Quioco, 1990). Adsorptive systems utilizing PstS have been developed for P_i removal and recovery (Choi et al., 2013; Hussein et al., 2020; Li et al., 2009; Venkiteshwaran et al., 2020, 2018; Y. Yang et al., 2016). Using such systems, effective P_i removal to ultra-low levels, even when starting at low concentrations, has been demonstrated. PBP adsorbents also offer P_i recovery via pH adjustment to desorb the captured molecules in a pure, concentrated form suitable for reuse (Hussein et al., 2020; Venkiteshwaran et al., 2020). PBP features rapid adsorption in comparison to metal oxide adsorbents (Venkiteshwaran et al., 2020). For example, P_i sorption using PBP was 30 to 240 times faster with 15 to 100 times higher adsorption affinity compared to zirconium and copper oxides. Moreover, PBP can selectively adsorb P_i even in the presence of the structurally similar arsenate ion (Venkiteshwaran et al., 2021). Previous PBP research predominantly focused on proof-of-concept tests performed in batch systems rather than the more realistic flow-through columns needed to optimize performance for practical application.

Continuous-flow, fixed-bed columns are most practical for wastewater treatment as they efficiently treat large volumetric flowrates (Hu et al., 2020). Fixed-bed column experiments provide reliable information pertaining to breakthrough times, adsorption conditions, and adsorbents' stability during continuous use (Satya et al., 2021; Yanyan et al., 2018). This study examined P_i adsorption using PBP immobilized on a resin material

(PBP-NHS resin) operated in continuous-flow, fixed-bed column mode. The research objectives were to (i) investigate the effect of column operating parameters (influent concentration, bed volume, and flow rate) to establish a basis for large-scale column design; (ii) evaluate the column's reusability in multi-cycle operating mode and examine its selectivity compared to a commercially available ion exchange resin, LayneRTTM; (iii) assess PBP-NHS resin performance treating tertiary wastewater effluent; and (iv) determine the breakthrough characteristics of the fixed-bed column using the Thomas, Adams-Bohart, Yoon-Nelson, and bed depth service time (BDST) mathematical models.

4.2 Materials and Methods

4.2.1 Preparation of PBP-NHS Resin

The packed-bed material was prepared by immobilizing a purified solution of PBP onto NHS-activated Sepharose resin [schematic illustration is shown in Appendix B (Figure B1)]. This consisted of two major steps, expression and purification followed by immobilization, as described below.

4.2.1.1 PBP Expression and Purification

The backbone overexpression plasmid pET22b including the *pstS* gene (A197C) was obtained from Addgene, USA (plasmid #78198). The plasmid was transformed into *E. coli* BL21(DE3) competent cells, as described by Solscheid et al. (2015). To express and purify PBP, recombinant cells were cultivated in Luria Broth (LB) with 100 $\mu\text{g mL}^{-1}$ ampicillin at 37°C and vigorous agitation at 250 rpm. Once the cell suspension reached an OD₆₀₀ value of 0.6-0.8, 1 mM isopropyl β -D-1-thiogalactopyranoside (IPTG) was added. The IPTG was allowed to react with the culture for 3-4 hr, after which the induced cells were centrifuged for 20 min at 1250 \times g. PBP expression in the cells was confirmed using

sodium dodecyl sulfate polyacrylamide gel electrophoresis (SDS-PAGE), as described in Hussein et al. (2020).

To obtain purified PBP solution, the PBP-expressed cell pellet was resuspended in 100 mL of binding buffer (50 mM NaH₂PO₄, 0.5 M NaCl, pH 8.0) and sonicated using a Q500 Sonicator (Qsonica, USA) set at amplitude = 45%, pulse rate = 15 sec on and 45 sec off. The lysate supernatant was collected following centrifugation at 6700 ×g for 45 min. The supernatant was then added to a Ni Sepharose™ 6 Fast Flow resin column (GE Healthcare Life Sciences, USA) to bind for 60 min at room temperature with gentle agitation. Elution buffer (50 mM NaH₂PO₄, 0.5 M NaCl, 250 mM imidazole, pH 8.0) was used to release the PBP, and 5 mL eluted fractions were collected. The protein's presence was verified in the eluted fractions using SDS-PAGE. The eluted PBP fraction was dialyzed in buffer (0.2 M NaHCO₃, 0.5 M NaCl, pH 7), and the PBP concentration was measured using a Pierce™ BCA protein assay kit (Thermo Fisher Scientific, USA). The PBP was stored with 14% glycerol solution at -80°C until use.

4.2.1.2 PBP Immobilization on NHS-activated Sepharose

To immobilize PBP on the surface of NHS-activated Sepharose, purified PBP samples were dialyzed using a Spectra/Por® 2 dialysis membrane (MWCO 12-14 kDa, Spectrum Laboratories, Inc., USA) to remove the glycerol preservative. PBP dialysis was conducted at room temperature for 2 hr with 4-6 exchanges of buffer (0.2 M NaHCO₃, 0.5 M NaCl, pH 8). The dialyzed PBP was immobilized on NHS-activated Sepharose™ 4 Fast Flow resins (GE Healthcare Life Sciences, USA) following the manufacturer's instructions (71-5000-14 AD). Briefly, NHS-activated Sepharose resin was washed with 10-15 bed

volumes of 1 mM HCl solution at 4°C. The washed resin was mixed with PBP solution at a 1:1 volumetric ratio. The coupling reaction was performed at room temperature for 4 hr.

After reaction completion, the supernatant was collected and the concentration of unbound PBP was measured using a Pierce™ BCA protein assay kit. The binding efficiency of the NHS-activated Sepharose was 60-80%. The modified resin was blocked against non-reacted groups using 2 bed volumes of 0.1 M Tris-HCl at pH 8.5 for 45 min. The resin was then washed with low pH (0.1 M acetate, 0.5 M NaCl, pH 4-5) and high pH (0.1 M Tris-HCl, pH 8-9) buffers in 3 repetitions of alternating wash cycles. To remove the legacy P_i adsorbed on the PBP during the expression and purification process, PBP-NHS resin was washed with 5 bed volumes of Tris buffer at pH 12.5, which completely desorbed P_i from the PBP-NHS resin (Venkiteshwaran et al., 2018). The PBP-NHS resin was kept at 4°C until use within 48 hr.

4.2.2 Fixed-Bed Adsorption Studies

Continuous-flow, fixed-bed column experiments were conducted to evaluate the column performance under various operating parameters: influent concentration, bed volume, flow rate, and multi-cycle operating mode. These tests were performed in well-controlled laboratory buffers. The selectivity of PBP-NHS resin was evaluated in comparison to a commercially available resin, LayneRT™. Additionally, a lab-scale experiment using tertiary wastewater effluent was performed to further assess the performance of PBP-NHS resin in more realistic settings.

4.2.2.1 The Influence of Column Operating Parameters

PBP-NHS resin was packed into Bio-Rad's Poly-Prep[®] columns (0.8 cm ID x 4 cm H). A peristaltic pump was used to maintain continuous downflow of P_i solution. Experimental conditions are listed in Table 4.1. Each set of experiments was conducted in duplicate. Effluent fractions (1.0 mL) were collected at room temperature for all experiments at regular time intervals until the bed was exhausted (i.e., the effluent P_i concentration $[C_t]$ equaled the influent P_i concentration $[C_0]$). The column's breakthrough point was determined as $C_t/C_0 = 10\%$, and the column's point of exhaustion was $C_t/C_0 = 90\%$. Influent and effluent P_i concentrations were measured using the standard ascorbic acid method (APHA, 2005).

Table 4.1 Continuous-flow fixed-bed column experimental design.

Parameter	Experimental Conditions		
	Influent Concentration, C_0 (mg PO_4^{3-} L ⁻¹)	Bed Volume, BV (mL)	Flow rate, Q (mL min ⁻¹)
Variable influent concentration	0.5	1.5	0.2
	1.0	1.5	0.2
	1.5	1.5	0.2
Variable bed volume	0.65	0.5	0.2
	0.65	1.0	0.2
	0.65	1.5	0.2
Variable flowrate	0.75	1.0	0.1
	0.75	1.0	0.2
	0.75	1.0	0.3

PBP-NHS resin must also be reusable such that the P_i binding ability of the system is restored following desorption (Kuroda et al., 2000). Moreover, the recovered P_i from desorption can be utilized for subsequent reuse. To evaluate the system's reusability,

consecutive adsorption-desorption cycles were conducted three times with an influent P_i concentration of $1.1 \text{ mg PO}_4^{3-} \text{ L}^{-1}$, 1.0 mL bed volume of drained PBP-NHS resin, and 0.2 mL min^{-1} flow rate. The desorption cycle was performed using 3 bed volumes of Tris buffer at pH 12.5. A control column experiment with only NHS resin (without PBP) was also performed to ensure no P_i adsorption was associated with NHS-activated Sepharose. The control test showed that the NHS resin by itself did not adsorb P_i , meaning that all adsorptive performance was derived from the PBP's functionality.

4.2.2.2 PBP-NHS Resin's P_i Selectivity

To compare the selectivity of PBP-NHS resin to a commercially available P -selective resin LayneRT™ (Layne Christensen Co., The Woodlands, TX), parallel experiments using P_i -only solution and multi-ion solution were conducted. For PBP-NHS resin, the fixed-bed column was operated with 0.35 g PBP-NHS resin, flow rate of 0.2 mL min^{-1} , and 1.5 mg L^{-1} P_i -only solution (spiked as KH_2PO_4). An identical column was operated with a multi-ion solution containing 1.5 mg L^{-1} each of KH_2PO_4 , MgSO_4 , CaCl_2 , KNO_3 , and NaHCO_3 . Tests using both water matrices were conducted in duplicate. Analogous experiments were conducted using LayneRT™ resin. The fixed-bed column was performed with 0.35 g LayneRT™ resin, flow rate of 0.2 mL min^{-1} , and P_i -only solution of 1.0 g L^{-1} . For multi-ion solution test, 1.0 g L^{-1} of each (KH_2PO_4 , MgSO_4 , CaCl_2 , KNO_3 , and NaHCO_3), flow rate of 0.2 mL min^{-1} , and 0.35 g LayneRT™ resin were used. Both experiments were conducted in duplicate.

A continuous-flow, fixed-bed column test was also performed using tertiary wastewater effluent to evaluate the PBP column's performance in more realistic applications. Tertiary wastewater effluent was collected from the fifth pass of the

chlorination basin at the South Shore Water Reclamation Facility (Oak Creek, WI). Tertiary wastewater samples were analyzed for water quality parameters, as shown in Appendix B (Table B1). The influent P_i concentration was $\approx 0.75 \text{ mg PO}_4^{3-} \text{ L}^{-1}$ and the column was operated with 0.5 mL drained PBP-NHS resin and a flow rate of 0.3 mL min^{-1} . Consecutive 1 mL samples were collected until the effluent concentration equaled the influent. A reusability test was conducted for tertiary wastewater effluent (three consecutive adsorption-desorption cycles) using these same fixed-bed column parameters, with desorption using 3 bed volumes of Tris buffer at pH 12.5.

4.2.2.3 Statistical Analysis

One-way ANOVA was performed to assess the differences in breakthrough curves for multi-cycle operation mode (reusability study), as well as to assess the differences in breakthrough curves for the selectivity study. All statistics were performed using Excel with a significance level of $\alpha = 0.05$.

4.2.3 Mathematical Modeling of Breakthrough Curves

Breakthrough curves showing the ratio of effluent concentration to influent concentration with respect to time (C_t/C_0 vs t) were modeled using the empirical Adams-Bohart, Thomas, Yoon-Nelson, and Bed-Depth/Service Time (BDST) models to determine the dynamic properties of fixed-bed column operation for scaling-up purposes and performance comparison (Satya et al., 2021). These models are the most widely used to analyze adsorbent-adsorbate behavior in column-mode system operation (Patel, 2019).

4.2.3.1 Adams-Bohart Model

The Adams-Bohart model was developed based on the surface reaction theory, which predicts that equilibrium is not immediate. Hence, the rate of adsorption is proportional to the remaining capacity of the adsorbent and the concentration of adsorbate (Chowdhury et al., 2015). The model equation and its linearized form are shown in Equation 4.1 and Equation 4.2, respectively.

$$\frac{C_t}{C_0} = \exp \left(K_{AB} C_0 t - K_{AB} \frac{N_0 Z}{U_0} \right) \quad (\text{eq 4.1})$$

$$\ln \frac{C_t}{C_0} = K_{AB} C_0 t - K_{AB} \frac{N_0 Z}{U_0} \quad (\text{eq 4.2})$$

where C_0 and C_t are the influent and effluent P_i concentrations (mg L^{-1}), respectively. Z is the bed height (cm), U_0 is the superficial velocity (cm min^{-1}), K_{AB} is the Adams-Bohart rate constant (L (mg-min)^{-1}), and N_0 is the saturation concentration (mg L^{-1}). Values for K_{AB} and N_0 are calculated from the slope and the intercept of Equation 4.2, respectively.

4.2.3.2 Thomas Model

The Thomas model was developed based on the assumption of the Langmuir adsorption isotherm with no axial dispersion, with second-order biosorption reaction kinetics (Recepoglu et al., 2018). The Thomas model is shown in Equation 4.3 and its linearized form is in Equation 4.4

$$\frac{C_t}{C_0} = \frac{1}{1 + \exp\left(\frac{K_{TH}q_0m}{Q} - K_{TH}C_0t\right)} \quad (\text{eq 4.3})$$

$$\ln\left(\frac{C_0}{C_t} - 1\right) = \frac{K_{TH}q_0m}{Q} - K_{TH}C_0t \quad (\text{eq 4.4})$$

where C_0 and C_t are the influent and effluent P_i concentrations (mg L^{-1}), m is the weight of PBP-resin (g), Q is the flow rate (mL min^{-1}), K_{TH} is the Thomas rate constant (L (mg-min)^{-1}), and q_0 is the adsorption capacity (mg g^{-1}). Values for K_{TH} and q_0 are calculated from the slope and the intercept of Equation 4.4, respectively.

4.2.3.3 Yoon-Nelson Model

The Yoon-Nelson model is a simple theoretical model derived based on the assumption that decreasing rate of adsorption for a molecule is proportional to adsorbate adsorption and breakthrough on the adsorbent (Chowdhury et al., 2013; Patel, 2019). The model equation and its linearized form are described in Equation 4.5 and Equation 4.6, respectively.

$$\frac{C_t}{C_0} = \frac{\exp(K_{YN}t - \tau K_{YN})}{1 + \exp(K_{YN}t - \tau K_{YN})} \quad (\text{eq 4.5})$$

$$\ln\frac{C_t}{C_0 - C_t} = K_{YN}t - \tau K_{YN} \quad (\text{eq 4.6})$$

where C_0 and C_t are the influent and effluent P_i concentrations (mg L^{-1}), K_{YN} is Yoon-Nelson rate constant (min^{-1}), and τ is the time required for 50% adsorbate breakthrough

(min). Values for K_{YN} and τ can be found from the slope and the intercept of Equation 4.6, respectively.

4.2.3.4 Bed-Depth/Service Time Model

The BDST model is used to predict how long the column's packed-bed material can last before regeneration or replacement (Samarghandi et al., 2014). The BDST model was developed based on a surface chemical reaction between the adsorbate and the unused capacity of the adsorbent, with negligible intraparticle diffusion (Oh et al., 2009; Samarghandi et al., 2014). The linear relationship of bed depth (i.e., height) to service time is given by Equation 4.7 (Oh et al., 2009).

$$t = \frac{N_0 Z}{C_0 F} - \frac{1}{K_{BDST} C_0} \ln\left(\frac{C_0}{C_t} - 1\right) \quad (\text{eq 4.7})$$

where C_0 and C_t are the influent and effluent P_1 concentrations (mg L^{-1}), K_{BDST} is the rate constant of the BDST model (L (mg-min)^{-1}), and N_0 is the adsorption capacity (mg L^{-1}), Z is the bed depth (cm), F is the linear velocity (cm min^{-1}), and t is the service time (min).

4.3 Results and Discussion

4.3.1 Fixed-Bed Adsorption Studies

To design and run fixed-bed columns for realistic full-scale operation, smaller-scale breakthrough curves tested as a function of operating parameters are needed (Manjunath and Kumar, 2021). To inform scale-up and implementation, the breakthrough curves from the continuous-flow, fixed-bed column experiments using PBP-NHS resin are discussed in the following sections.

4.3.1.1 Column Operating Parameters

Effect of Influent P_i Concentration

The effect of influent P_i concentration on the breakthrough curve was investigated for influent levels of 0.5, 1.0, and 1.5 mg $\text{PO}_4^{3-} \text{L}^{-1}$, as illustrated in Figure 4.1a. Increasing influent P_i concentration resulted in a steeper breakthrough curve due to faster mass transfer. Time to breakthrough was faster as influent P_i concentration increased, with values of 100, 55, and 45 min for 0.5, 1.0, and 1.5 mg $\text{PO}_4^{3-} \text{L}^{-1}$, respectively (145, 100, and 60 min for exhaustion). At the lowest influent P_i concentration tested (0.5 mg $\text{PO}_4^{3-} \text{L}^{-1}$) the number of treated bed volumes was 20, or approximately twice that treated when the P_i concentration doubled. This general trend (i.e., increasing the concentration expedites breakthrough) was expected because the available active PBP binding sites were more rapidly occupied in the presence of higher P_i concentration, and the column was saturated more quickly. Yet, the exact timing of column breakthrough and exhaustion under variable conditions is needed for scale-up and must be determined experimentally.

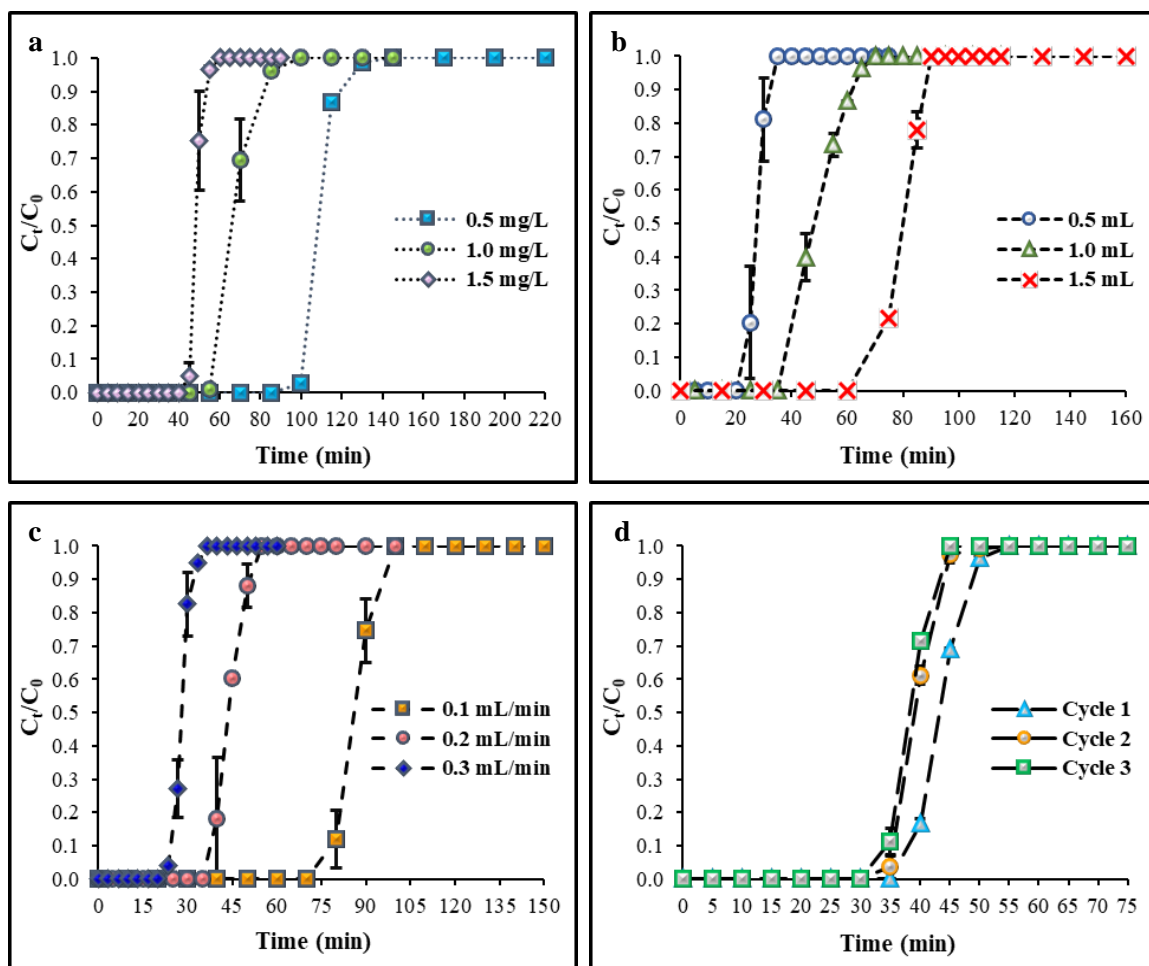


Figure 4.1 Breakthrough curves (ratio of effluent to influent P_i concentration [C_t/C_0] as a function of operating time) under different column operating parameters: (a) influent P_i concentration, (b) bed volume, (c) flow rate, and (d) multi-cycle column experiment at influent concentration of $1.1 \text{ mg } PO_4^{3-} L^{-1}$, bed volume of 1 mL , and flow rate of $0.2 \text{ mL } min^{-1}$. Note that the maximum time varies among the panels. All column tests were conducted in duplicate, as indicated by the error bars.

Effect of Bed Volume

The effect of bed volume (controlled by bed height) on the breakthrough curve is shown in Figure 4.1b. Noticeably longer time to breakthrough was obtained as the bed volume increased from 0.5 mL to 1.5 mL. Time to breakthrough was 25, 45, and 75 min for 0.5, 1.0, and 1.5 mL of drained PBP-NHS resin, respectively (35, 70, and 90 min for exhaustion). Increasing the bed volume provided more PBP active binding sites in the

column to capture P_i ; therefore, a longer time was needed to reach complete saturation (column exhaustion). The number of treated bed volumes doubled from 5 to approximately 10 as bed volume doubled, which suggests a uniform distribution of PBP adsorption on NHS-activated Sepharose. This lab-scale breakthrough data can be used to advance scaled-up design for large-scale column applications.

Effect of Feed Flow Rate

The effect of influent P_i flow rate on the breakthrough curve is shown in Figure 4.1c. As expected, time to breakthrough was more rapid as influent P_i flow rate increased. Time to breakthrough was 80, 40, and 23 min for 0.1, 0.2, and 0.3 mL min⁻¹, respectively (100, 55, and 37 min for exhaustion). The available PBP binding sites were rapidly occupied when higher rates of P_i molecules entered the column.

Reusability

To evaluate the system's reusability, consecutive adsorption-desorption cycles were conducted three times, as shown in Figure 4.1d. The desorption cycle, which consisted of three bed volumes of wash with pH 12.5 Tris buffer, released all P_i from the column. For the first cycle, the breakthrough time was 40 min, and the exhaustion time was 55 min with a treated bed volume of 8 mL. For the second cycle, the breakthrough time was 40 min, and the exhaustion time was 50 min with a treated bed volume of 8 mL. For the third cycle, the breakthrough time was 35 min, and the exhaustion time was 45 min with a treated bed volume of 7 mL. The experimental data showed slight variation in the breakthrough curves between the cycles. However, one-way ANOVA showed no significant difference between the three cycles ($p = 0.93$). Thus, there was no loss in PBP-NHS resin performance for at least three cycles of adsorption/desorption in column mode

operation. Venkiteshwaran et al. (2018) similarly showed no loss in performance over 10 cycles of adsorption/desorption in batch-mode operation.

4.3.1.2 Selectivity of PBP-NHS Resin in More Complex Matrices

Phosphate-only Versus Multi-ion Buffer

An adsorbent's selectivity is important for actual applications in which many potential competitors may be present in solution. Higher selectivity offers higher removal in the presence of other constituents, and also leads to a purer recovered product, which enhances the value of the process. The selectivity of PBP-NHS resin was investigated in parallel sets of experiments using P_i -only solution and multi-ion synthetic solution (Figure 4.2a). There was no significant difference between the breakthrough curves ($p = 0.81$), with each having a breakthrough time of 20 min with 4 mL treated bed volume and time to exhaustion of approximately 35 min. This demonstrates the high P_i -selectivity of PBP-NHS resin, in agreement with previous batch tests (Venkiteshwaran et al., 2020).

For comparison, Figure 4.2b illustrates the breakthrough curves for P_i -only solution and multi-ion solution experiments using commercially available, phosphate-selective ion exchange resin, LayneRT™. Noticeably, LayneRT™ resin's performance was affected by competing anions, where competing anions decreased the time to exhaustion by 20 min. Additionally, the LayneRT™ resin's P_i removal capacity (40 mg P per g LayneRT™ resin) dropped by 20% due to the presence of competing anions. Accordingly, although LayneRT™ resin offers much more selective P_i adsorption relative to common adsorbents such as granular activated carbon, competition due to other ions can impact performance, as also reported in other studies (Martin et al., 2018; Ownby et al., 2021; Tang, 2015; Williams et al., 2015; You et al., 2016). Conversely, the presence of other anions and cations did not impede P_i adsorption using the PBP-NHS resin.

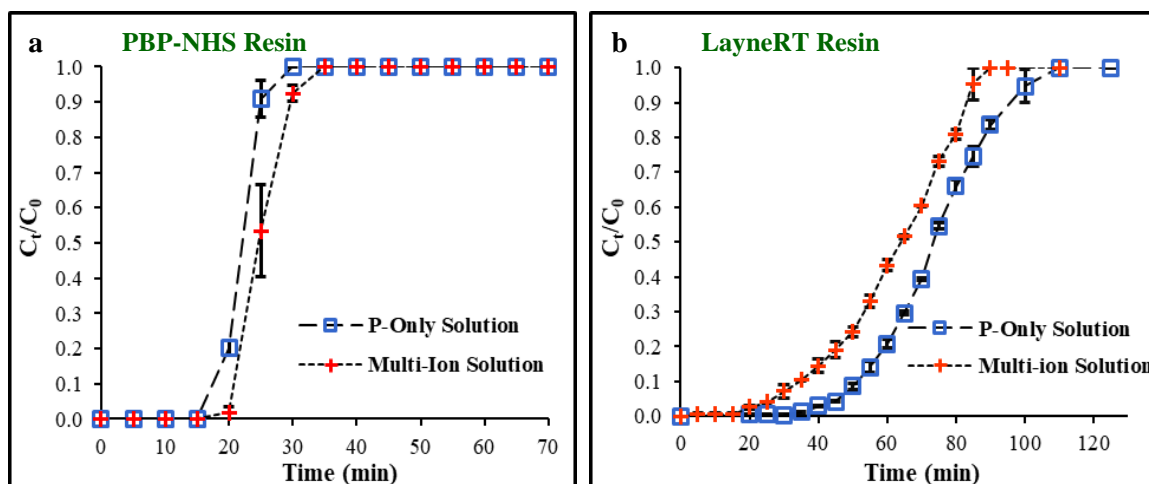


Figure 4.2 Comparison of breakthrough curves (ratio of effluent to influent P_i concentration [C_t/C_0] as a function of operating time) using P_i -only solution versus multi-ion solution (containing phosphate, sulfate, chloride, nitrate, and bicarbonate ions) for two different phosphate-selective resins: (a) PBP-NHS resin, (b) LayneRT™ resin. All column tests were conducted in duplicate, as indicated by the error bars.

Wastewater

To investigate PBP-NHS resin's performance under more realistic conditions, tertiary wastewater effluent was tested in continuous-flow, fixed-bed columns. The breakthrough curves for a single column run and multi-cycle column run are illustrated in Figure 4.3a and Figure 4.3b, respectively. Compared to the P_i synthetic solution experiments, the wastewater breakthrough curve had a typical S-shape with a breakthrough time of 20 min and exhaustion time of 43 min. The curve was more gradual (i.e., there was not a quick jump in the effluent concentration), with 23 min between breakthrough and exhaustion compared to 10 min using the P_i -only solution. The tertiary wastewater components likely served as a physical barrier, i.e., causing steric hindrance to prevent P_i from accessing the immobilized PBP's active binding, thus extending the time to exhaustion. While extending the time to exhaustion can be beneficial in application, it would be important to monitor effluent concentrations to ensure compliance with the

discharge limits during the extended cycle. Although the shape of the breakthrough curves differed, there was no difference in adsorption capacity as the PBP-NHS resin achieved 96% of its maximum theoretical capacity in both synthetic solution and wastewater ($20 \mu\text{g P per g PBP-NHS resin}$).

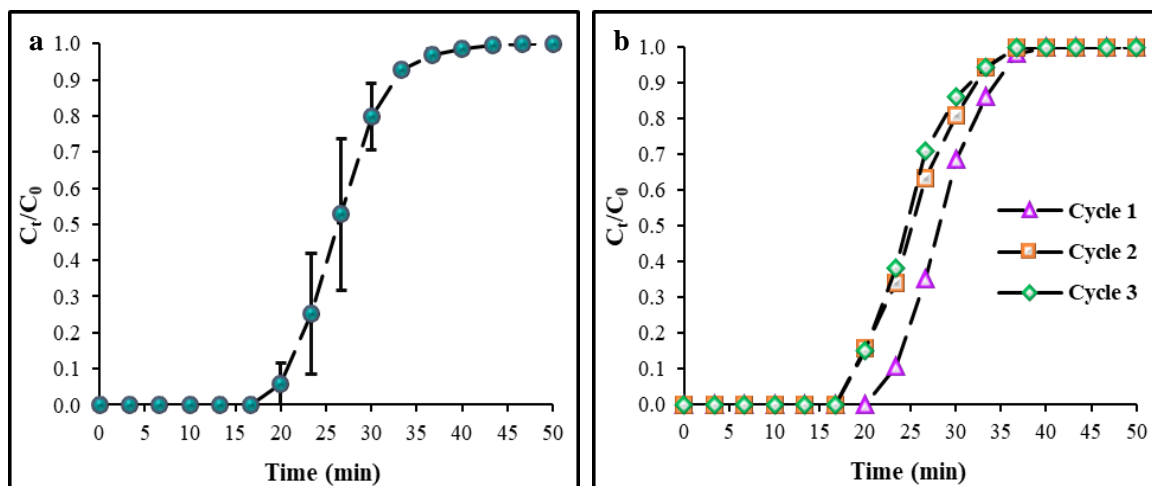


Figure 4.3 Breakthrough curves (ratio of effluent to influent P_i concentration [C_i/C_0] as a function of operating time) for tertiary wastewater effluent tests: (a) single-column experiment and (b) multi-cycle column experiment. Both tests were performed using a bed volume of 0.5 mL, flow rate of 0.3 mL min^{-1} , and influent phosphate concentration of $0.75 \text{ mg PO}_4^{3-} \text{ L}^{-1}$. All column tests were conducted in duplicate, as indicated by the error bars.

Three consecutive cycles of adsorption/desorption using the column to treat wastewater showed no significant reduction ($p = 0.91$) in the time to exhaustion and the treated bed volume. The first cycle had a breakthrough time of 23 min and exhaustion time of 40 min with a 7-mL treated bed volume. The second and third cycles had breakthrough times of 20 min and exhaustion times of 37 min with a 6-mL treated bed volume.

4.3.2 Mathematical Modeling of Breakthrough Curves

4.3.2.1 Breakthrough Curve Fitting with the Adams-Bohart, Thomas, and Yoon-Nelson Models

Parameters for the Adams-Bohart, Thomas, and Yoon Nelson models are provided in Table 4.2. A comparison between the empirical and theoretical breakthrough curves predicted using these models at different influent P_i concentration is shown in Appendix B (Figures B2-B4). The linear regression analyses and the breakthrough curve comparison at different bed volumes and flow rates for all models are shown in Appendix B (Figures B5-B10). The breakthrough curves were well fit using the Thomas and Yoon-Nelson models ($R^2 > 0.95$). The strong alignment of the experimental data with the Thomas model suggests that P_i adsorption occurs in a monolayer (Langmuir isotherm assumption) with no axial dispersion. In contrast, the Adams-Bohart model only fit well to the initial part of the breakthrough curve ($C_i/C_0 < 0.1$). This agrees with previous reports that the Adams-Bohart model is usually used to describe only the initial part of the breakthrough curve (Singh et al., 2020).

As influent P_i concentration increased, the Thomas model rate constant (K_{TH}) decreased, while the sorption capacity (q_0) increased. The same trend was observed for the Adams-Bohart model. Higher adsorbate concentration increases the resistance to mass transfer and thus decreases the rate constants (Manjunath and Kumar, 2021). Conversely, the Yoon-Nelson rate constant (K_{YN}) increased as influent P_i concentration increased. Using the Yoon-Nelson model, the time to $C_i/C_0 = 50\%$ (τ) decreased from 96.7 min to 44.2 min as P_i concentration increased from 0.5 to 1.5 mg PO_4^{3-} L⁻¹.

The percent error (ε) between τ determined using the experimental data versus the predicted model was 8% - 12%. For the Thomas model, the error between $C_t/C_0 = 50\%$ values determined using the experimental data versus the predicted model was 3% - 9%, suggesting that both Thomas and Yoon-Nelson models provide good predictions of the dynamic behavior of the PBP-NHS resin column.

All model rate constants decreased as bed volume increased, while the sorption capacity increased. Greater bed depth slows the mass transfer rate by increasing the residence time between the adsorbate and adsorbent (Manjunath and Kumar, 2021). The time required for $C_t/C_0 = 50\%$ (τ) increased from 22.4 min to 67.6 min as bed volume increased from 0.5 to 1.5 mL of drained PBP-NHS resin. The error between experimental and predicted $C_t/C_0 = 50\%$ values was 16% - 20% using the Yoon-Nelson model and 0.1% - 0.4% using the Thomas model.

The Thomas model rate constant (K_{TH}) and sorption capacity (q_0) increased as flow rate increased. The same trend was observed for the Adams-Bohart model, where the mass transfer coefficient (K_{AB}) and saturation concentration (N_0) increased as influent P_i flow rate increased. Similarly, the Yoon-Nelson rate constant (K_{YN}) increased as influent P_i flow rate increased. The time required for $C_t/C_0 = 50\%$ (τ) decreased from 76.5 min to 24.8 min as influent P_i flow rates increased from 0.1 to 0.3 mL. The error (ε) between experimental and predicted values was 11% for all operating flow rates using the Yoon-Nelson model and 0.3% - 0.7% using the Thomas model.

Table 4.2 Adams-Bohart, Thomas, and Yoon-Nelson model parameters for varying column operating conditions.

C ₀ (mg L ⁻¹)	Z (cm)	Q (mL min ⁻¹)	EBCT (min)	Adams-Bohart model			Thomas model			Yoon-Nelson model		
				K _{AB} (L [mg-min] ⁻¹)	N ₀ (mg L ⁻¹)	R ²	K _{TH} (L [mg-min] ⁻¹)	q ₀ (mg g ⁻¹)	R ²	K _{YN} (min ⁻¹)	τ (min)	R ²
0.5	3	0.2	7.5	0.209	9.51	0.78	0.458	12.1	0.95	0.260	96.7	0.95
1.0	3	0.2	7.5	0.164	10.5	0.80	0.276	13.1	0.95	0.308	57.5	0.89
1.5	3	0.2	7.5	0.203	10.5	0.81	0.429	13.8	0.97	0.630	44.2	0.97
0.65	1	0.2	2.5	0.249	8.62	0.85	0.882	10.0	1.00	0.562	22.4	1.00
0.65	2	0.2	5.0	0.055	9.01	0.90	0.266	9.32	0.97	0.137	38.2	0.96
0.65	3	0.2	7.5	0.156	8.03	0.97	0.376	10.3	1.00	0.169	67.6	1.00
0.75	2	0.1	10.0	0.139	7.45	0.85	0.404	9.43	1.00	0.308	76.5	1.00
0.75	2	0.2	5.0	0.143	8.07	0.83	0.458	9.63	1.00	0.350	39.1	1.00
0.75	2	0.3	3.3	0.433	7.00	0.88	0.857	8.78	0.99	0.625	24.8	0.99

C₀, influent P_i concentration (mg PO₄³⁻ L⁻¹); Z, bed depth (cm); Q, flow rate (mL min⁻¹); EBCT, empty bed contact time (min); K_{AB}, mass transfer coefficient (L [mg-min]⁻¹); N₀, saturation concentration (mg L⁻¹); K_{TH}, Thomas model rate constant (L [mg-min]⁻¹); q₀, sorption capacity (mg g⁻¹); K_{YN}, Yoon-Nelson rate constant (min⁻¹); τ, time required for 50% breakthrough (min).

4.3.2.2 Application of the Bed-Depth/Service Time (BDST) Model

Service time reflects the useful operating time prior to regeneration or replacing the column media under specific operating conditions and is useful to scale up and optimize a fixed-bed adsorption system (Ang et al., 2020). The predicted bed service time at different influent P_i concentrations and flow rates using the BDST model is illustrated in Figure 4.4, with 10% and 90% breakthrough. Experimental data fit to the BDST equation ($R^2 > 0.95$) are shown in Appendix B (Figures B11 and B12). For the tertiary wastewater effluent (Figure B13, Figure B14, and Table B2), the models also performed well ($R^2 = 0.99$).

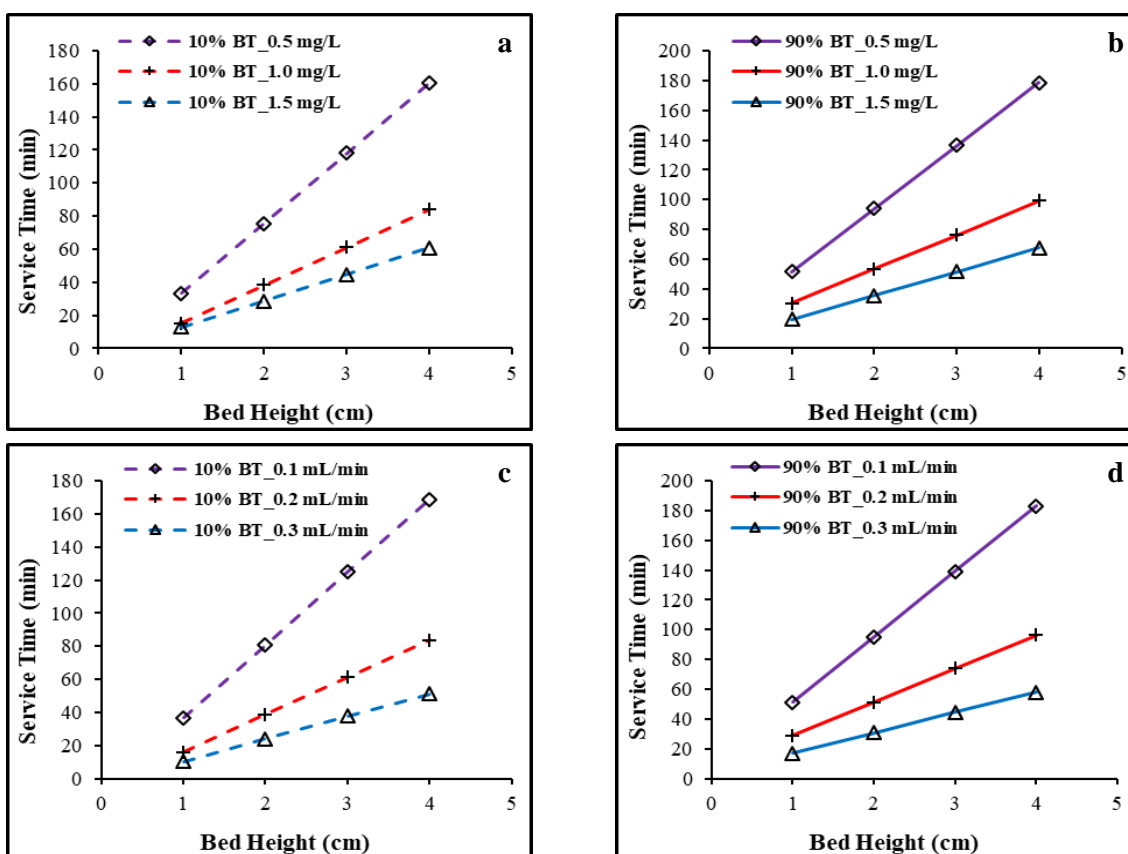


Figure 4.4 Calculated bed service time for breakthrough (10% BT; panels a and c) and exhaustion (90% BT; panels b and d). Panels a and b illustrate the impact of different influent phosphate concentrations, while panels c and d illustrate the impact of different flow rates.

4.4 Conclusions

A comprehensive lab-scale, fixed-bed column study of P_i adsorption using PBP-NHS resin was conducted in this study. Highly selective P_i separation was observed, as illustrated by the sharp S-shape of the breakthrough curves. There was no significant decline in the column's performance over three consecutive cycles in either synthetic solution or tertiary wastewater, substantiating PBP-NHS resin's reusability, as well as the potential to recover the captured P_i for subsequent reuse. Furthermore, the resin's capacity was unaffected by competing anions, whereas the LayneRT™ column capacity dropped 20% in the presence of other anions. The Thomas and Yoon-Nelson models satisfactorily described the breakthrough characteristics for PBP-NHS resin and BDST analysis predicted breakthrough service times. This study supports the potential for implementation of fixed-bed, flow through systems featuring the high-affinity PBP bio-adsorbent to effectively remove P_i to ultra-low levels while recovering P_i from wastewater. The results herein inform design and scale up of PBP-NHS resin adsorption system, although setting-specific parameters must also be accounted for during system design and implementation.

5 PHOSPHATE-BINDING PROTEIN (PBP)-LOADED IRON OXIDE PARTICLES: ADSORPTION PERFORMANCE FOR PHOSPHORUS REMOVAL FROM WATER

5.1 Introduction

Releasing excess inorganic phosphorus (P_i) from point and nonpoint sources prompts eutrophication in receiving waterbodies. While too much P_i is bad, too little is problematic as well, given that phosphate rock is a finite resource that is being continuously depleted to supply fertilizers for food production (Dodds and Smith, 2016). It is therefore important to effectively remove and recover P_i from waste streams to better manage P_i usage. Chemical and biological technologies have been applied to remove P_i from different water matrices (Bui et al., 2018; Huang et al., 2017; Mayer et al., 2013). However, some technologies such as biological processes are not able to meet strict discharge standards of $< 0.1 \text{ mg L}^{-1}$ (Oehmen et al., 2007). Chemical precipitation, which is a typical method to remove P_i from high volume biologically treated effluent, has secondary issues, e.g., an additional clarification step is needed, it produces large amounts of chemical sludge, and it has additional disposal expenses (Mahardika et al., 2018).

Adsorption is a favorable approach to remove P_i by partitioning it to surfaces, where P_i can be attached and then released under controlled conditions (Muhammad et al., 2019). Adsorption may provide high selectivity and a low-cost solution for P_i removal and recovery (Qiu et al., 2017). Adsorbent materials exhibit variable adsorptive selectivity and capacity, depending on the surface chemistry, porosity, and contact surface area (Wang and Peng, 2010). A common challenge across many adsorbents is related to selectivity (Muhammad et al., 2019). Adsorbate removal can be significantly reduced through competition for the media's active sites from other competing elements (Muhammad et al.,

2019). For instance, P_i removal from wastewater by ferric nanoparticles is likely affected by sulphate, chloride, and bicarbonate due to anion competition (Martin et al., 2018). Highly selective P_i adsorbents are therefore of great interest for improved performance. High affinity phosphate-binding proteins (PBP) may offer one means of selective adsorption.

Adsorption and recovery of P_i has been documented using several different configurations of immobilized PBP (Choi et al., 2013; Hussein et al., 2020; Hussein and Mayer, 2022; Li et al., 2009; Venkiteshwaran et al., 2021, 2020, 2018; Y. Yang et al., 2016). Effective P_i removal to ultra-low levels ($< 100 \mu\text{g L}^{-1}$) has been confirmed using such systems (Hussein and Mayer, 2022; Venkiteshwaran et al., 2020, 2018). The PBP binds P_i to amino acid residues using 12 hydrogen bonds at the binding site (Ledvina et al., 1998; Luecke and Quioco, 1990). PBP adsorbents offer P_i recovery by adjusting pH to greater than 10, which yields a concentrated P_i solution that is suitable for reuse, e.g., as fertilizer feedstock (Hussein et al., 2020). PBP provides improved adsorption in comparison to metal oxide adsorbents, offering at least 30 times faster adsorption, and at least 15 times higher affinity (Venkiteshwaran et al., 2020). Accordingly, immobilized PBP is a promising adsorbent material for P_i removal and recovery; however, previous PBP research identified the need to enhance the material's adsorption capacity to make PBP a viable alternative for implementation (Hussein and Mayer, 2022; Venkiteshwaran et al., 2020, 2018).

To increase adsorbent capacity, smaller particles from micro- to nano-scale may be used as the base material on which PBP is immobilized. A range of surfaces can be utilized for biomaterial conjugation (e.g., metals, polymers, or silica). Magnetic nanoparticles (MNPs) have been extensively used in biomedical applications, such as drug delivery and enzyme conjugation, due to their unique properties such as stability, high surface area, and biocompatibility (Vallabani and Singh, 2018). MNPs have also received great consideration for environmental applications such as treating polluted water (Gómez-Pastora et al., 2014). MNPs modified with functional groups (-NH₂, -COOH, -SH) and inorganic/organic-coated MNPs were used to adsorb heavy metals and toxic dyes (Gómez-Pastora et al., 2014). A major advantage of MNPs is that they can be easily collected from environmental matrices using an external magnetic field. Superparamagnetic nanomaterials exhibit strong attraction to external magnetic fields, but do not attract each other, hence reducing the risk of particle aggregation (Gómez-Pastora et al., 2014).

In this study, superparamagnetic NHS-activated iron oxide particles (IOPs) were modified by immobilizing PBP on the surface to study P_i adsorption potential. The hypothesis was that use of the IOPs would increase PBP attachment, in turn increasing P_i adsorption capacity compared to previously established PBP-modified resin and unmodified iron oxide particles (IOPs). It was also anticipated that PBP-IOPs would facilitate P_i recovery compared to unmodified IOPs because free P_i can be released from PBP binding site while it could be difficult to release P_i from Fe-P complex. The research objectives were to: (1) Examine P_i adsorption kinetics and isotherms using the PBP-IOP adsorbent and assess its removal capacity compared to previous PBP research; (2) Evaluate the effect of pH, temperature, and ionic strength (all of which often impact

water/wastewater treatment process performance) on P_i removal efficiency; (3) Evaluate the selectivity of the PBP-IOP adsorbent using synthetic multi-ion solution as well as tertiary wastewater effluent; and (4) Test the reusability of PBP-IOP adsorbent in multiple adsorption-desorption cycles and compare performance to IOPs without conjugated PBP.

5.2 Materials and Methods

5.2.1 Preparation of the PBP-IOP Adsorbent

The PBP-IOP adsorbent was prepared by immobilizing a purified solution of PBP onto BcMagTM NHS-activated magnetic beads (Bioclone Inc, USA). The PBP expression and purification procedures were conducted as described by Hussein and Mayer (2022). Briefly, *E. coli* BL21(DE3) competent cells containing plasmid pET22b (Addgene, USA) were grown in Luria Broth (LB) with 100 $\mu\text{g mL}^{-1}$ ampicillin at 37°C and vigorous agitation at 250 rpm. When the cell suspension reached an OD₆₀₀ value of 0.6-0.8, 1 mM final concentration isopropyl β -D-1-thiogalactopyranoside (IPTG) was added to induce PBP expression for 3-4 hr. PBP expression was confirmed by sodium dodecyl sulfate polyacrylamide gel electrophoresis (SDS-PAGE), as described by Hussein et al. (2020). The induced cells were centrifuged for 20 min at 1250 $\times g$, and the cell pellets were collected for the purification step.

To purify PBP, the cell pellets were resuspended in 100 mL of binding buffer (50 mM NaH₂PO₄, 0.5 M NaCl, pH 8.0) and sonicated to rupture the cell membrane and release the cytoplasmic content. A Q500 sonicator (Qsonica, USA) was set at amplitude = 45%, pulse rate = 15 sec on and 45 sec off. The supernatant of the cell's lysate was added to a Ni SepharoseTM 6 Fast Flow resin column (GE Healthcare Life Sciences, USA) to bind for 60 min at room temperature with gentle agitation. To release PBP from the column, elution

buffer (50 mM NaH₂PO₄, 0.5 M NaCl, 250 mM imidazole, pH 8.0) was used, and 5 mL eluted fractions were collected. The collected PBP fractions were combined and dialyzed in buffer (0.1 M NaHCO₃, 0.15 M NaCl, pH 7.4) using a Spectra/Por[®] 2 dialysis membrane (MWCO 12-14 kDa, Spectrum Laboratories, Inc., USA) at room temperature. The PBP concentration was measured using a Pierce[™] BCA protein assay kit (Thermo Fisher Scientific, USA) and the dialyzed solution was stored in 14% glycerol at -80°C until use.

BcMag[™] NHS-activated magnetic beads were used to conjugate PBP on the surface, following the manufacturer's protocol with slight modification (i.e., washing step with deionized water instead of Tris buffer and blocking with Tris buffer instead of ethanolamine). Magnetic beads of 1 μm diameter (300 mg) were transferred to a centrifuge tube and washed with deionized water before coupling. The PBP solution (10 mL at 1 mg mL⁻¹) was added to the beads and mixed well by gentle vortexing. The reaction tube was kept at room temperature for 4-6 hr with continuous rotation using a multi-purpose tube rotator (Fisherbrand[™], Model No. 88861049). A magnetic bar was used to separate the beads from the PBP solution. The PBP solution was drained and the concentration of unbound PBP was measured using a Pierce[™] BCA protein assay kit. The PBP coupling density on the BcMag[™] NHS-activated magnetic beads was 12-15 mg PBP per g IOPs. The beads were resuspended in 10 mL blocking buffer (0.05 M Tris-HCl, 0.5 M NaCl, pH 8) at room temperature for 60 min. After that, the beads were washed with washing buffer (0.01 M Tris-HCl, 1 mM MgCl₂, pH 7) 2-3 times. The PBP-IOP adsorbent was stored at 4°C until use within 48 hr. To remove the legacy P_i adsorbed on PBP during the expression and purification processes, the PBP-IOP adsorbent was washed with Tris buffer at pH 11.5-

12 prior to adsorption experiments, which was previously reported to completely desorb P_i from PBP (Venkiteshwaran et al., 2018).

5.2.2 Phosphorus Adsorption Experiments

5.2.2.1 Phosphorus Adsorption Kinetics

To examine phosphorus adsorption kinetics using the PBP-IOP adsorbent, 20 mg PBP-IOPs were placed in a 2-mL microcentrifuge tube with 1 mg $PO_4^{3-} L^{-1}$ (prepared in Tris-HCl buffer at pH 7). The samples were mixed at 30 rpm using a multi-purpose tube rotator at room temperature for 1, 5, 10, 20, or 40 min. Triplicate samples at each reaction time were conducted. The P_i concentrations before and after adsorption were measured using the standard ascorbic acid method (APHA, 2005). The data was used to calculate the adsorption capacity by applying a mass balance relationship (Equation 5.1), as described by Wu et al. (2020).

$$q_t = \frac{(C_0 - C_t)V}{m} \quad (\text{eq 5.1})$$

where q_t is the amount of phosphorus ($mg g^{-1}$) adsorbed at time (t), C_t is the phosphorus concentration in solution ($mg L^{-1}$) at time (t), C_0 is the initial phosphorus concentration ($mg L^{-1}$), V is the sample volume (mL), and m is the mass of adsorbent (mg).

Pseudo first-order (Equation 5.2) and pseudo second-order (Equation 5.3) kinetic models were used to model the data.

$$q_t = q_e (1 - e^{-k_1 t}) \quad (\text{eq 5.2})$$

$$q_t = \frac{k_2 q_e^2 t}{1 + k_2 q_e t} \quad (\text{eq 5.3})$$

where q_t is the amount of phosphorus (mg g^{-1}) adsorbed at time (t), q_e is the amount of phosphorus (mg g^{-1}) adsorbed at equilibrium time, and k_1 (min^{-1}) and k_2 ($\text{g mg}^{-1} \text{min}^{-1}$) represent the first-order kinetic rate constant and the second-order kinetic rate constant, respectively. Parameters for the pseudo first-order model were obtained from a plot of ($\ln q_t$ vs. t). Parameters for the pseudo second-order model were obtained from a plot of (t/q_t vs. t).

5.2.2.2 Phosphorus Adsorption Isotherms

Phosphorus adsorption isotherms were investigated by varying the initial concentration of P_i while keeping a constant dose of PBP-IOP adsorbent. The P_i solution was prepared in Tris buffer at pH 7 at concentrations of 0.2, 0.4, 0.6, 0.8, or 1 $\text{mg PO}_4^{3-} \text{L}^{-1}$. A dose of 20 mg PBP-IOP adsorbent was allowed to react with 1 mL phosphate solution for 60 min. The samples were mixed at 30 rpm using a multi-purpose tube rotator at room temperature. The experiments were conducted in triplicate. Once the test was completed, the reaction solution was separated from the PBP-IOP adsorbent using a magnetic bar and was analyzed for remaining P_i . The data was then modeled using Langmuir and Freundlich isotherm models (Equations 5.4 and 5.5, respectively).

$$q_e = \frac{q_{\max} K_L C_e}{(1 + K_L C_e)} \quad (\text{eq 5.4})$$

$$q_e = K_F C_e^{1/n} \quad (\text{eq 5.5})$$

where q_e is the equilibrium adsorption capacity (mg g^{-1}), q_{\max} is the maximum adsorption capacity (mg g^{-1}), C_e is the equilibrium P_i concentration (mg L^{-1}), K_L is the Langmuir constant (L mg^{-1}), K_F is the Freundlich constant (mg g^{-1}), and n defines the intensity of the adsorption process (dimensionless constant). The Langmuir model's parameters can be found from the linear plot of ($1/q_e$ vs. $1/C_e$), where the K_L constant indicates the adsorption affinity between the adsorbate and the adsorbent, and is related to energy of adsorption (ΔG) and enthalpy change (ΔH). The Freundlich model's parameters are calculated from the linear plot of ($\log q_e$ vs. $\log C_e$).

5.2.2.3 Effect of pH, Temperature, and Ionic Strength

Adsorption batch experiments were conducted to determine the effect of various experimental conditions on P_i adsorption. Temperature, pH, and ionic strength are essential factors in determining the water/wastewater treatment process performance. For all independent experiments, the test tubes were mixed at 30 rpm using a multi-purpose tube rotator. To evaluate the effect of pH on P_i adsorption, $1.1 \text{ mg PO}_4^{3-} \text{ L}^{-1}$ solution was prepared in Tris buffer at pH 4, 6, 7, 8, or 10. The reaction buffer was added to 20 mg PBP-IOP adsorbent and mixed at room temperature for 60 min.

For temperature experiments, 1.1 mg $\text{PO}_4^{3-} \text{L}^{-1}$ solution was prepared in Tris buffer at pH 7. The reaction buffer was stored at 10, 20, 30, or 40°C prior to the experiment. The reaction buffer was added to 20 mg PBP-IOP adsorbent, and the test tubes were also kept at the designated temperature.

To study the effect of ionic strength on P_i adsorption, reaction buffers at 0.01, 0.05, 0.1, or 0.5 M KCl were mixed with 1 mg $\text{PO}_4^{3-} \text{L}^{-1}$ and 20 mg PBP-IOP adsorbent. The suspension was mixed at room temperature for 60 min using a multi-purpose tube rotator. For all experiments, the reaction solution was separated from the PBP-IOP adsorbent using a magnetic bar and then analyzed for P_i concentration.

5.2.3 Selectivity and Reusability of PBP-IOPs

5.2.3.1 Selectivity of PBP-IOPs

To test the selectivity of the PBP-IOP adsorbent, parallel experiments using 20 mg PBP-IOPs were conducted using synthetic multi-ion solution and P_i -only synthetic solution. The multi-ion solution contained a final concentration of 1 mg L^{-1} each of NaCl, Na_2SO_4 , NaNO_3 , NaHCO_3 , $\text{B}_4\text{Na}_2\text{O}_7 \cdot 10\text{H}_2\text{O}$, and KH_2PO_4 . The selected anions are common competitors for P_i and common constituents of wastewater. The P_i -only synthetic solution contained 1 mg L^{-1} KH_2PO_4 . Both experiments were conducted at room temperature and the test tubes were mixed at 30 rpm for 60 min. The solution was separated from the PBP-IOP adsorbent using a magnetic bar and analyzed for P_i concentration.

To evaluate the PBP-IOP adsorbent's performance in more realistic scenarios, another batch experiment was performed using tertiary wastewater effluent compared to an equal concentration of P_i -only solution. Tertiary wastewater effluent was collected from the South Shore Water Reclamation Facility (Oak Creek, WI), and analyzed for water

quality parameters (Table C1). The initial P_i concentration was $1.2 \text{ mg PO}_4^{3-} \text{ L}^{-1}$. Other experimental conditions (adsorbent dosage, time, and mixing speed) were identical to the synthetic multi-ion solution test.

5.2.3.2 Reusability of PBP-IOPs

Recovering P_i as a concentrated solution is important for subsequent reuse. The PBP-IOP adsorbent must also be reusable such that the P_i binding ability of the system is restored following desorption (Kuroda et al., 2000). To evaluate the adsorbent's reusability, consecutive adsorption-desorption cycles were conducted five times with an initial P_i concentration of $0.9 \text{ mg PO}_4^{3-} \text{ L}^{-1}$ and 20 mg PBP-IOP adsorbent. The adsorption cycle was conducted for 30 min using 1 mL reaction buffer (pH 7) at room temperature. The desorption cycle was performed using 1 mL of Tris buffer at pH 11.5 for 10 min, which was previously reported to completely desorb P_i from PBP (Venkiteshwaran et al., 2018). After the desorption cycle, a washing step was conducted using 2 mL Tris buffer at pH 7 for 10 min, as previously recommended (Venkiteshwaran et al., 2018). All experiments were conducted in triplicate at room temperature.

In an additional comparison study for reusability, unmodified IOPs (without PBP immobilized on the surface) were tested for P_i adsorption and desorption under identical experimental conditions to the PBP-IOPs tests.

5.2.4 Statistical Analysis

One-way ANOVA followed by Tukey post-hoc analysis was performed to assess differences in P_i removal efficiency under various experimental conditions (pH, temperature, and ionic strength). One-way ANOVA was also used to assess the differences in P_i removal efficiency for the selectivity and reusability studies. All statistics were performed using GraphPad Prism with a significance level of $\alpha = 0.05$.

5.3 Results and Discussion

5.3.1 Phosphorus Adsorption

5.3.1.1 Phosphorus Adsorption Kinetics

The pseudo second-order kinetic model provided the best fit for P_i adsorption using PBP-IOPs, as shown in Figure 5.1a. Most of the adsorbed P_i was rapidly removed in less than 5 min and the system reached equilibrium after 10 min as there was no change in the adsorbed P_i over time. Figure 5.1b shows the experimental data fit to the linear regression of the pseudo second-order model (t/q_t vs t) with $R^2 \approx 1$. The experimental data did not fit the pseudo first-order model well ($R^2 = 0.56$, Supporting Information Figure C1).

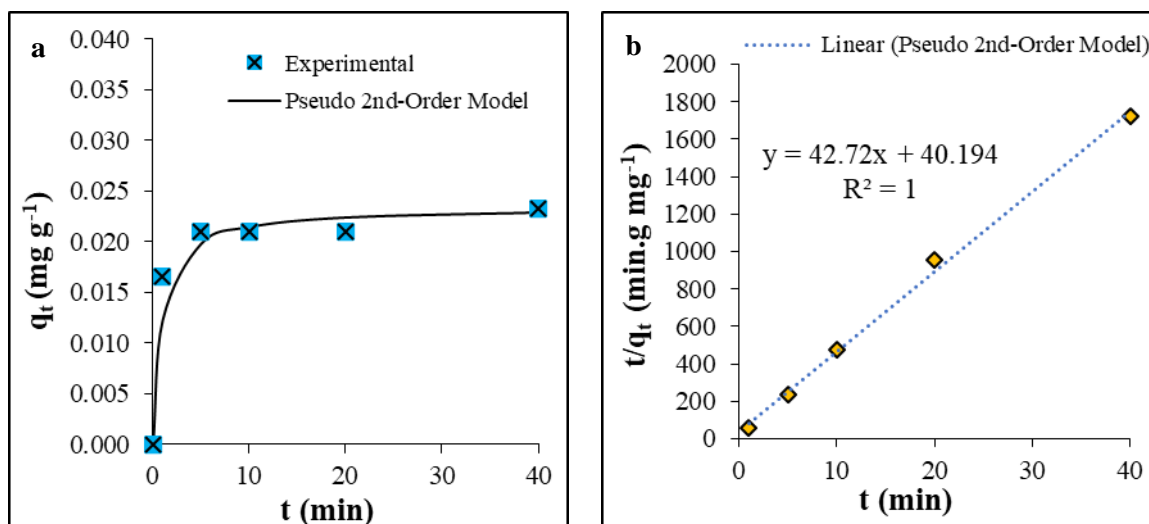


Figure 5.1 P_i adsorption kinetics using the PBP-IOP adsorbent at room temperature and neutral pH. (a) PBP-IOP adsorbent capacity as a function of time modeled using pseudo second-order kinetics, (b) experimental data fit with linear regression using the pseudo second-order kinetic model. The model's parameters are listed in Table 5.1.

The kinetic model parameters are listed in Table 5.1. The pseudo second-order kinetic results indicated that the adsorption process depends on concentrations of both P_i and PBP-IOPs. This finding is similar to a previous study by Venkiteswaran et al. (2020), in which PBP was attached to NHS activated Sepharose beads (PBP-NHS resin). However, the final values of each kinetic model parameter differed between the studies. For instance, using PBP-IOPs, the kinetic rate constant k_2 was $47 \text{ g mg}^{-1} \text{ min}^{-1}$, which was substantially higher than other adsorbents used to remove P_i such as iron oxide nanoparticles dispersed onto zeolite (Xu et al., 2020), ferrihydrite (Mallet et al., 2013), ferrihydrite-impregnated granular activated carbon (Mahardika et al., 2018), iron oxyhydroxides (Kalaitzidou et al., 2022), granular ferric hydroxide (Yousefi et al., 2019), ZnO nanoparticles (Do et al., 2020), and hybrid metal oxides (Gu et al., 2011).

Table 5.1 Parameters for the pseudo first-order and pseudo second-order kinetic models of P_i adsorption using PBP-IOPs.

Kinetic Models	Parameter	
Pseudo First-order	k_1 (min^{-1})	0.0061
	q_e (mg g^{-1})	0.019
	R^2	0.56
Pseudo Second-order	k_2 ($\text{g mg}^{-1}\text{min}^{-1}$)	47.03
	q_e (mg g^{-1})	0.023
	R^2	1

The equilibrium capacity (q_e) for PBP-IOPs (0.023 mg P_i per g PBP-IOPs) was approximately 3.5 times greater than that for PBP-NHS resin at (0.0066 mg P_i per g PBP-NHS resin, as reported by Venkiteshwaran et al. (2020)). The enhanced equilibrium capacity is related to the additional number of PBP molecules in the system (which leads to higher P_i removal). The average particle size of the IOPs was 1 μm , while NHS-activated Sepharose is 90 μm ; therefore, more surface area is available to conjugate PBP on IOPs compared to NHS-activated Sepharose. NHS-activated iron oxide has a maximum observed PBP attachment capacity of 14 mg PBP per g IOPs, while NHS-activated Sepharose has a maximum observed PBP attachment capacity 7 mg PBP per g NHS resin. However, the calculated q_e for PBP-IOPs was lower than other non-PBP adsorbents (Table 5.2).

Table 5.2 Pseudo second-order parameters for P-selective adsorbents.

Adsorbent	Pseudo Second-order		Study
	k_2 ($\text{g mg}^{-1}\text{min}^{-1}$)	q_e (mg g^{-1})	
EL-MNP@zeolite	0.013	38.61	(Xu et al., 2020)
Ferrihydrite	4×10^{-4}	40.3	(Mallet et al., 2013)
Ferrihydrite-impregnated granular activated carbon (FH@GAC)	1.85	1.26	(Mahardika et al., 2018)
FeOOHs	0.25	4.5	(Kalaitzidou et al., 2022)
Granular ferric hydroxide	0.04	0.64	(Yousefi et al., 2019)
ZnO	0.01	54.6	(Do et al., 2020)
PBP-NHS resin	4.9×10^3	0.0066	(Venkiteshwaran et al., 2020)
PBP-IOPs	47.03	0.023	This study

5.3.1.2 Phosphorus Adsorption Isotherms

Langmuir and Freundlich isotherm models were used to model the profile of the equilibrium adsorption capacity (q_e) and the equilibrium P_i concentration (C_e) (Figure 5.2a). The experimental data fit both models well, with $R^2 \geq 0.99$. Although the models had identical profiles up to 0.6 mg L^{-1} , they diverged at higher C_e values, Langmuir model provided a better fit (experimentally, working with higher initial P_i concentration would not provide differentiable C_e values for samples as the removal capacity was limited). The Langmuir model assumes monolayer adsorption, where active sites are occupied by one adsorbate molecule each. The linearized Langmuir and Freundlich models are illustrated in Figure 5.2b and Figure 5.2c, respectively.

The Langmuir constant (K_L) can be used further to determine the feasibility of P_i adsorption by calculating the dimensionless separation factor (R_L), as described in Equation 5.6 (Ayawei et al., 2017):

$$R_L = \frac{1}{1 + K_L C_0} \quad \text{eq (5.6)}$$

where $R_L = 0$ indicates irreversible adsorption, $0 < R_L < 1$ indicates favorable adsorption, $R_L = 1$ indicates a linear (q_e vs. C_e) adsorption curve, and $R_L > 1$ indicates unfavorable adsorption (Ajmal et al., 2018; Do et al., 2020). For this dataset, R_L was 0.6-0.9, indicating favorable adsorption.

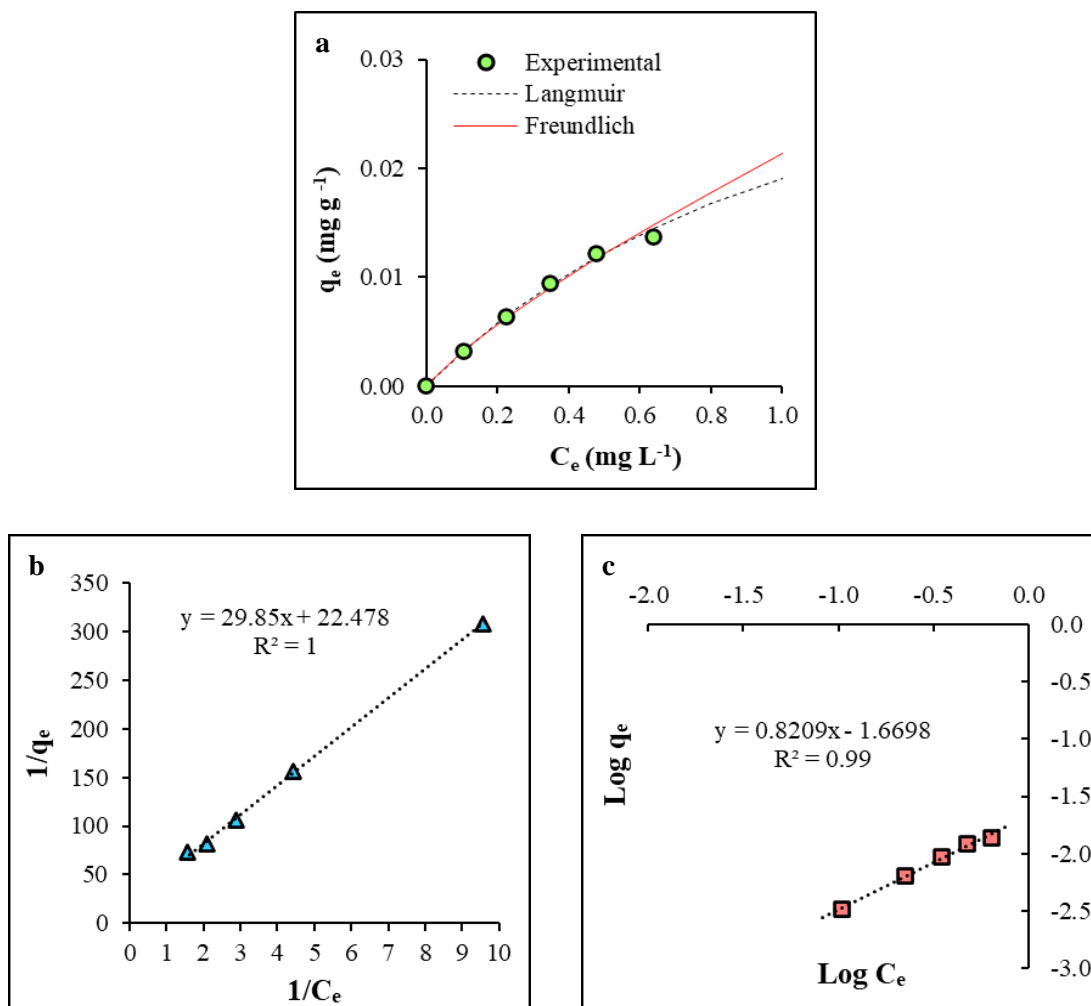


Figure 5.2 Phosphorus adsorption isotherms using PBP-IOPs at room temperature and neutral pH conditions. (a) experimental data fit to nonlinear isotherm models, (b) linearized Langmuir model, and (c) linearized Freundlich model.

The calculated Langmuir and Freundlich model parameters are listed in Table 5.3.

The maximum adsorption capacity (q_{max}) was approximately two times the experimental (q_e) value, suggesting the presence of some inactive PBP on the IOP surface or that PBP was unable to bind additional P_i due to incomplete washing. The maximum P_i adsorption capacity using PBP-IOPs (0.044 mg P_i per g PBP-IOPs) was approximately seven times higher than the P_i adsorption capacity using PBP-NHS resin (0.0062 mg P_i per g PBP-NHS resin) (Venkiteswaran et al., 2020). Increasing the number of PBP molecules attached to

IOPs (i.e., more available surface area for IOPs compared to NHS-Sepharose) increased the adsorption capacity. The average functionalized material density (NHS) was 10 times higher for IOPs (250 μmol per g IOPs) compared to Sepharose beads (25 μmol per g Sepharose). The adsorption affinity (K_L) for PBP-IOPs was 7 to 24 times higher compared to other adsorbents such as ZnFeZr-coated magnetic particles, flower-like mesoporous silica loaded with lanthanum, humic acid coated magnetite nanoparticles, and iron oxide coated granular activated carbon (Table 5.4) (Drenkova-Tuhtan et al., 2017; Huang et al., 2015; Rashid et al., 2017; Suresh Kumar et al., 2017). The calculated Freundlich constant (n) fell in the range of 0-10, indicating favorable adsorption (Mahanta and Valiyaveetti, 2013).

Table 5.3 Parameters of Langmuir and Freundlich isotherm models for P_1 adsorption using PBP-IOPs.

Isotherm Models	Parameter	
Langmuir Model	K_L (L mg^{-1})	0.753
	q_{max} (mg g^{-1})	0.044
	R^2	1
Freundlich Model	K_F (mg g^{-1})	0.021
	n	1.218
	R^2	0.99

Table 5.4 Langmuir isotherm parameters for P-selective adsorbents.

Adsorbent	Langmuir Isotherm		Study
	K_L (L mg ⁻¹)	q_{max} (mg g ⁻¹)	
FMS-0.1 La	0.11	6.1	(Huang et al., 2015)
ZnFeZr @ Fe ₃ O ₄ /SiO ₂	0.1	32.2	(Drenkova-Tuhtan et al., 2017)
HA-MNP	0.03	3.0	(Rashid et al., 2017)
Fe-GAC	0.08	21.8	(Suresh Kumar et al., 2017)
PBP-NHS resin	192	0.0062	(Venkiteshwaran et al., 2020)
PBP-IOPs	0.753	0.044	This study

5.3.1.3 Effect of pH, Temperature, and Ionic Strength

The effect of pH, temperature, and ionic strength on the P_i adsorption performance of PBP-IOPs is shown in Figure 5.3. Increasing pH from 4 to 10 significantly decreased P_i removal from 50% to less than 10% (Figure 5.3a, $p < 0.0001$). However, P_i removal at acidic conditions (pH 4 and pH 6) was not significantly different ($p = 0.64$). Solution pH affects both the degree of adsorbate dissociation and adsorbent surface charge (Nandi et al. 2009 and Choi et al. 2016). Phosphate deprotonates as pH increases, progressing from $H_3PO_4 \rightarrow H_2PO_4^- \rightarrow HPO_4^{2-} \rightarrow PO_4^{3-}$, corresponding to the acid dissociation constants ($pK_{a1}=2.15$, $pK_{a2}=7.2$, and $pK_{a3}=12.33$) (Ajmal et al., 2018). Accordingly, pH controls the distribution of dominant phosphate species and influences the strength of electrostatic attraction. Strong competition occurs between phosphate species and hydroxyl functional

groups at higher pH, consequently creating strong repulsion and reducing adsorption (Ajmal et al., 2018).

Beyond affecting P_i protonation/deprotonation state, the surface charge of the adsorbent may affect P_i adsorption as more positive charges accumulate below the point of zero charge (pH_{pzc}) and more negative charges exist above the pH_{pzc} . For the PBP-IOP adsorbent, the surface charge of the base material (i.e., iron oxide) is not subject to changes in speciation as a function of pH due to the presence of a silicon coating (Sharafi et al., 2018). Therefore, pH would more likely affect PBP's binding sites and trigger conformational changes. A fluorescent thermal shift assay of PBP showed that changes in pH did not significantly alter the thermal stability of PBP (Venkiteshwaran et al., 2018). Hence, high pH is unlikely to significantly alter PBP structure; however, changes in the coordination structure of the local binding site could affect P_i adsorption.

X-ray crystallography revealed that P_i binds to PBP through 12 hydrogen bonds from five different amino acid residues (Thr10, Thr141, Phe11, Ser38, Ser139, Ser142, Asp56, and Arg135) (Luecke and Quioco, 1990). PBP had a strong affinity for $H_2PO_4^-$ and HPO_4^{2-} , with a slight preference for the latter (Luecke and Quioco, 1990). The pK_a values of the amino acid residues range from 9.04 to 9.6, so deprotonation is most likely to occur at $pH > 10$, thereby inhibiting hydrogen bond formation between P_i and the PBP binding site.

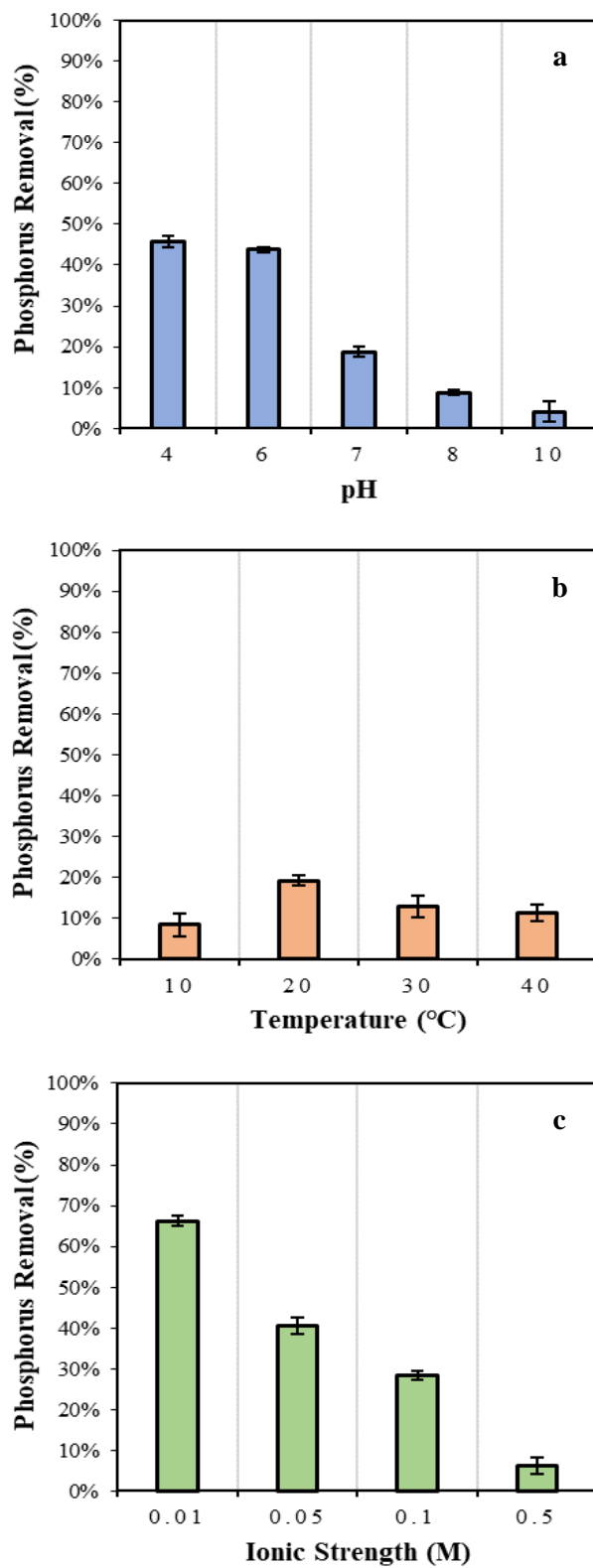


Figure 5.3 Effect of experimental conditions on phosphorus adsorption using PBP-IOPs: (a) pH, (b) temperature, and (c) ionic strength (KCl). All experiments were conducted for 60 minutes in triplicate, with ± 1 standard deviation denoted by the error bars.

Temperature is a crucial factor for adsorption at liquid-solid interfaces. Removal of P_i as a function of temperature is presented in Figure 5.3b. The highest removal was at room temperature (20°C) and the lowest at 10°C ($p = 0.003$). Tukey post hoc analysis revealed adsorption behavior was similar at 10, 30, and 40 degrees ($p \leq 0.18$), all of which were worse for P_i removal compared to room temperature. Elevated temperatures did not increase P_i removal, indicating that adsorption was exothermic (Yoon et al., 2014). Venkiteshwaran et al. (2020) showed that increasing temperature to 43°C reduced P_i adsorption affinity by $32\% \pm 8\%$ compared to 22°C. The calculated thermodynamic parameters confirmed an exothermic process: the estimated enthalpy change (ΔH) was approximately -6.3 kJ mol^{-1} , the calculated entropy change (ΔS) was $0.12 \text{ kJ mol}^{-1} \text{ K}^{-1}$, and Gibbs free energy (ΔG) was negative (Venkiteshwaran et al., 2020). Consistent with the proposed P_i -PBP interaction at the binding site (i.e., formation of 12 hydrogen bonds), noncovalent interactions such as van der Waals forces, hydrogen bonds, and ionic pairs can be indicated by low enthalpy changes ($\Delta H < 80 \text{ kJ mol}^{-1}$) (Du et al., 2016).

Alternately, P_i removal is endothermic (requiring an energy input to drive adsorption) using many other adsorbents such as ferrihydrite, magnetite, or lanthanum-doped activated carbon fiber, as indicated by an increase in phosphate uptake with increasing temperature (Ajmal et al., 2018; Liu et al., 2011). Therefore, P_i removal using PBP adsorbents is advantageous over other adsorbents as no energy addition is needed, promoting efficient P_i removal.

The effect of ionic strength on P_i removal is shown in Figure 5.3c, which shows that P_i removal significantly decreased from 66% to 6% when the concentration of KCl increased 50-fold from 0.01 to 0.5 M ($p < 0.0001$). Although there is no competition on the binding site due to the high selectivity of PBP toward P_i , the poor removal performance of PBP-IOPs towards P_i at high ionic strength (> 0.01 M KCl) may indicate an interruption in PBP binding affinity (Ledvina et al., 1998; Wang et al., 1994). The dissociation constant for the PBP- P_i complex (K_d) increased approximately 20 times for 0.3 M of NaCl solution compared to no-salt solution (Ledvina et al., 1998). The affinity of PBP for P_i was found to be insensitive to the surface charge potential of the binding site, but extremely sensitive to electrostatic effects at the level of local hydrogen bonding interactions (Ledvina et al., 1998). Therefore, increasing ionic strength impeded the formation of hydrogen bonds in the binding site and decreased P_i uptake.

Unlike PBP-IOPs, ion exchange is the proposed mechanism of P_i removal using iron oxide adsorbents, i.e., exchange occurs between hydroxide and phosphate on the adsorbent and forming ionic bond (Xue et al., 2009). High ionic strength decreases P_i removal due to competition with other anions on the active sites. Competitive anions increase the adsorption energy barrier of the active sites and reduce the interaction capacity between the adsorbent and P_i (Liu et al., 2011).

5.3.2 Selectivity and Reusability of PBP-IOPs

5.3.2.1 Selectivity of PBP-IOPs

To evaluate the PBP-IOP adsorbent's performance towards P_i removal in more practical conditions, PBP-IOPs were tested in synthetic multi-ion solution as well as tertiary wastewater effluent. The adsorption capacity of the PBP-IOP adsorbent for this test was $40 \mu\text{g-P}_i \text{ g}^{-1}$. Figure 5.4 illustrates PBP-IOP's selectivity, which was not affected by the presence of competing anions such as chloride, sulfate, nitrate, bicarbonate, and borate. The calculated P_i removal percentage was identical (22%) for P_i -only solution and multi-ion solution ($p = 0.99$). Similarly, the calculated P_i removal for tertiary wastewater effluent was the same as the corresponding P_i -only solution (17%). In both scenarios of multi-ion solution and tertiary wastewater, the amount of P_i removed was similar (0.2 mg/L).

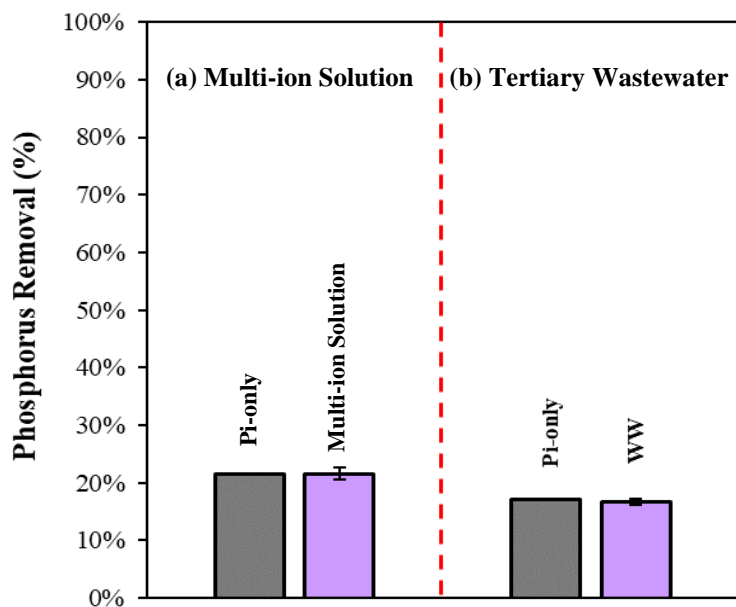


Figure 5.4 Selectivity of PBP-IOPs towards phosphorus. (a) synthetic multi-ion solution with 1 mg L^{-1} each of NaCl , Na_2SO_4 , NaNO_3 , NaHCO_3 , $\text{B}_4\text{Na}_2\text{O}_7 \cdot 10\text{H}_2\text{O}$, and KH_2PO_4 versus P_i -only solution containing 0.9 mg L^{-1} KH_2PO_4 . (b) tertiary wastewater effluent (WW) versus P_i -only solution containing 1.2 mg L^{-1} KH_2PO_4 .

The results agree with a previous selectivity study of PBP-NHS resin, in which competitive anions and cations did not impede P_i removal (Hussein and Mayer, 2022). In comparison, water constituents substantially reduced P_i removal efficiency using commercial ferric nanoparticles and hybrid anion resin (HAIX) (Muhammad et al., 2019). HAIX resin lost up to 36% of its removal capacity when preloaded with nitrate in synthetic water trials (Muhammad et al., 2019). Trials using secondary wastewater had greater impact on HAIX removal capacity since both nitrate preloading and simultaneous competition from other constituents of secondary wastewater are involved (Muhammad et al., 2019). Commercial ferric nanoparticles were also found to have 76% capacity reduction using synthetic water compared to HAIX resin (Muhammad et al., 2019). Generally, PBP-loaded iron oxide particles provide highly selective P_i removal option with no interruption from competing ions compared to HAIX or ferric nanoparticles.

5.3.2.2 Reusability of PBP-IOPs

The efficiency of adsorption-desorption of PBP-IOPs over repeated cycles is important to support its practicality. The PBP-IOP adsorbent was subjected to five consecutive adsorption-desorption cycles, as shown in Figure 5.5 (only adsorption results are included). The adsorptive performance of PBP-IOPs over the five cycles was steady at 31% to 34% ($p = 0.17$). Slight variation in P_i removal was observed for the adsorption cycles, possibly attributed to material loss during the washing (desorption) step. The results are consistent with previous studies (Hussein and Mayer, 2022; Venkiteshwaran et al., 2018), and demonstrate the viability of PBP-NHS resin as a reusable adsorbent.

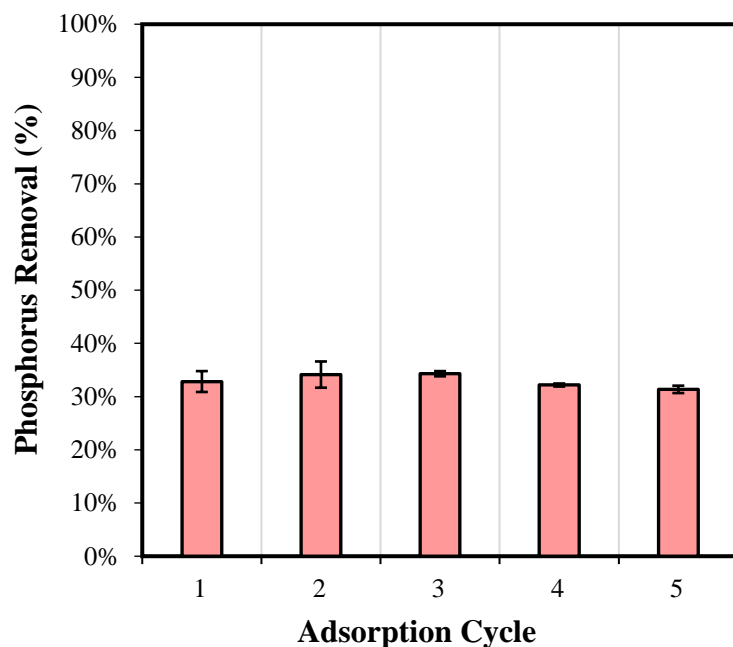


Figure 5.5 Reusability of PBP-IOPs performed over five consecutive adsorption-desorption cycles. Only the adsorption cycles are presented. All experiments were conducted in triplicate, with ± 1 standard deviation indicated by the error bars.

In additional experiments, the P_i adsorption-desorption capacity of unmodified IOPs (i.e., no PBP attached) and PBP-IOPs was assessed (Figure 5.6). PBP-IOPs were able to remove $0.30 \text{ mg PO}_4^{3-} \text{ L}^{-1}$ while IOPs alone removed $0.67 \text{ mg PO}_4^{3-} \text{ L}^{-1}$ under the same experimental condition. Perhaps, the active adsorption sites on IOPs were more than the active adsorption site of PBP-IOPs. However, for desorption, PBP-IOPs released $0.30 \text{ mg PO}_4^{3-} \text{ L}^{-1}$ (99% of total adsorbed P_i) whereas IOPs released only $0.08 \text{ mg PO}_4^{3-} \text{ L}^{-1}$ (12% of total adsorbed P_i) after exposure to Tris buffer at pH 11.5. This important finding demonstrated that PBP-IOPs may offer an improved approach to recover P_i (compared to IOPs alone) wherein nearly all adsorbed P_i can be recovered in a concentrated form.

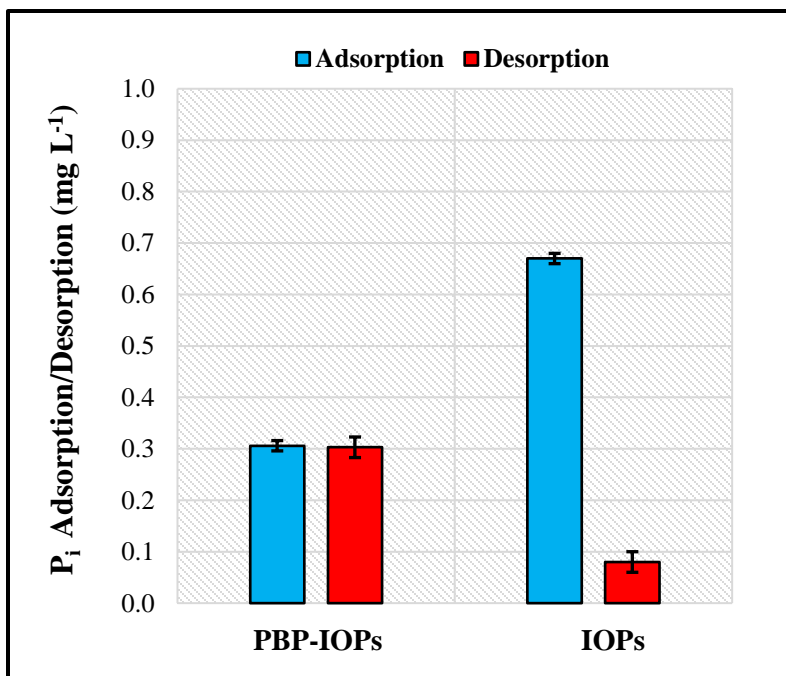


Figure 5.6 Comparison study of P_i adsorption/desorption capacity between IOPs modified with PBP and unmodified IOPs. All experiments were conducted in triplicate, with ± 1 standard deviation indicated by the error bars.

5.4 Conclusions

A PBP-loaded IOP adsorbent was hypothesized to improve the P_i adsorption capacity over previous PBP systems and to provide enhanced P_i recovery potential compared to unmodified IOPs. Using PBP-IOPs, P_i adsorption kinetics demonstrated rapid P_i removal, more than 95% adsorption within 5 min). The P_i adsorption isotherms showed that adsorption was best described as monolayer adsorption (Langmuir). Conjugation of PBP to higher surface area (i.e., smaller particle size) increased the overall attachment capacity. Iron oxide had a maximum observed PBP attachment capacity of 14 mg PBP per g IOPs, while NHS-activated Sepharose had a maximum observed PBP attachment capacity of 7 mg PBP per g NHS. The average functional group density (NHS) was 10

times higher for IOPs (250 μmol per g IOPs) compared to Sepharose beads (25 μmol per g Sepharose).

Slightly acidic pH conditions (pH 6) and low ionic strength (0.01 M KCl) demonstrated the best removal efficiency. The highest removal of P_i was observed at room temperature 20°C, indicating an exothermic process that does not need energy to drive adsorption. PBP-IOPs were tested in synthetic multi-ion solution as well as tertiary wastewater effluent. The removal capacity of PBP-IOPs was not affected by competing anions such as chloride, sulfate, nitrate, bicarbonate, and borate. In both scenarios of multi-ion solution and tertiary wastewater, the amount of P_i removed was similar (0.2 mg/L). The adsorptive performance of PBP-IOPs over five consecutive adsorption-desorption cycles was steady between 31% and 34% for P_i solution. PBP-IOPs released 99% of total adsorbed P_i whereas unmodified IOPs released only 12% of total adsorbed P_i . Altogether, the results demonstrated the ability of the PBP-IOP adsorbent to exothermically, rapidly, and selectively adsorb P_i . The PBP-IOP adsorbent effectively removed P_i from tertiary wastewater effluent.

The PBP-IOP adsorbent enhanced the removal capacity of P_i compared to previous PBP systems (i.e., PBP-NHS resin). Yet, P_i removal capacity is still low compared to other adsorbents. Future work may include working with smaller molecules such as pared down protein sequences or peptides. Designing engineered peptides to capture and release P_i would not only simulate the functionality of natural proteins but also boost P_i removal capacity by increasing the attachment density of the functionalized material.

6 CONCLUSIONS

Inorganic phosphorus (P_i) is literally a critical element for life as a major component of DNA's backbone. Rapid growth of plants and high crop productivity require large amounts of P_i . However, P_i suitable for agriculture fertilization is in short supply in nature, and global P_i reserves are unevenly distributed. On the flip side of concerns about P shortages, surplus P_i in water causes eutrophication. The simultaneous scarcity and overabundance of P_i yields a phosphorus paradox. Tackling this issue is necessary, and using innovative approaches targeting P_i removal to ultra-low levels with subsequent recovery for reuse applications can help.

The purpose of this research was to provide insights on potential sustainable solutions to simultaneously remove and recover P_i under controlled conditions utilizing immobilized phosphate-binding proteins (PBP). PBP is the constituent of many microorganisms' structure responsible for P_i transport into the cell under conditions of low ambient P_i levels. High affinity and selectivity towards P_i even at low concentrations is a superior advantage for accessing P. Utilizing PBP as an adsorptive medium could offer a potential sustainable treatment option for P_i removal and recovery from water/wastewater.

6.1 Key Findings

This research investigated three prospective immobilized PBP systems and evaluated their performance for P_i removal and recovery. Microbial surface-displayed PBP was designed, characterized, and tested for P_i capture and release. The hypothesis was that exposing the PstS directly to the water matrix by expressing the protein on the cell surface would facilitate P_i release in comparison to periplasmic PstS, in which case the cell membrane and perhaps cytoplasmic regulation could impede P_i release. In support of the hypothesis, surface-expressed PstS provided two times higher ability to release P_i compared to periplasmic-expressed PstS. Increasing temperature to 40°C and ionic strength (up to 1 M) increased phosphate release by 20% and 50%, respectively. Acidic and basic pH conditions also promoted phosphate release, with the PstS protein releasing $\approx 63\%$ more phosphate at basic pH levels compared to acidic conditions. Surface-displayed cells induced to overexpress PBP provided 48% higher phosphate removal compared to uninduced cells, although removals were generally low. Adsorption/desorption results provided proof-of-concept of the feasibility of P_i release and recovery using cell-surface expressed PstS.

A micro-structured immobilized-PBP system was tested in a fixed-bed column configuration. Fixed-bed column operation using PBP-NHS resin was hypothesized to not be impeded by the presence of other anions and cations due to the high selectivity of PBP resin toward P_i . Accordingly, similar breakthrough curves in the presence or absence of competing ions were expected. The results supported the hypothesis as the resin's capacity was unaffected by competing anions, whereas the comparison LayneRT™ ion exchange column capacity dropped 20% in the presence of other anions. Highly selective P_i

separation was observed, as illustrated by the sharp S-shape of the breakthrough curves. There was no significant decline in the column's performance over three consecutive cycles in either synthetic solution or tertiary wastewater, substantiating PBP-NHS resin's reusability, as well as the potential to recover the captured P_i for subsequent reuse. The results inform design and scale up of PBP-NHS resin adsorption systems and support the potential for PBP-NHS resin application in wastewater treatment.

Lastly, a PBP-loaded IOP adsorbent was hypothesized to improve the P_i adsorption capacity beyond previous PBP systems. Indeed, the PBP-IOP adsorbent had a maximum observed PBP attachment capacity of 14 mg PBP per g IOPs, while NHS-activated Sepharose had a maximum observed PBP attachment capacity of 7 mg PBP per g NHS. Conjugation of PBP to higher surface area (i.e., smaller particle size) increased the overall attachment capacity. Using PBP-IOPs, P_i adsorption kinetics demonstrated rapid P_i removal within less than 5 min, with pseudo second-order kinetics. The P_i adsorption isotherms showed that adsorption was best described as monolayer adsorption, informing a one-to-one interaction between P_i and PBP. The effect of pH, temperature, and ionic strength on P_i removal was investigated. Increasing pH from 4 to 10 reduced P_i removal from 50% to less than 10%. Slightly acidic pH demonstrated the best removal efficiency. The highest removal of P_i was observed at room temperature 20°C, and the lowest at 10°C. The P_i removal significantly decreased from 66% to 6% when the concentration of KCl increased from 0.01 to 0.5 M. The removal capacity of PBP-IOPs was not affected by competing anions such as chloride, sulfate, nitrate, bicarbonate, and borate. Similar P_i removal was observed in both multi-ion solution and tertiary wastewater. The adsorptive performance of PBP-IOPs over five consecutive adsorption-desorption cycles was steady

between 31% and 34%. Altogether, the results demonstrated the ability of the PBP-IOP adsorbent to rapidly and selectively adsorb P_i . The PBP-IOP adsorbent effectively removed P_i from tertiary wastewater effluent, supporting its use in actual removal and recovery applications.

6.2 Future Work

Phosphate-binding proteins have demonstrated promise as a highly selective material for P_i capture (Kuroda et al., 2000 and Li et al., 2009). Also, P_i adsorption using PBP is reversible as a function of pH (Venkiteshwaran et al., 2018), which facilitates not only removal but recovery. Therefore, PBP-based adsorption systems offer a potentially sustainable treatment option for P_i removal and recovery from water/wastewater. Although PBP offers strong potential for use in engineered systems, more effective water/wastewater configurations are needed before it can be a potential sustainable treatment option for P_i removal and recovery. Specifically, improvements in immobilized PBP's contact with the water, operation in flow-through setup, and adsorption capacity are critical.

To address these improvements, this research investigated the performance of three different configurations of PBP systems to remove and recover P_i . Microbial surface-displayed PBP systems (bringing PBP into direct contact with the target P_i) were evaluated for their potential to remove and recover P_i . Also, utilizing PBP in more practical treatment configurations (i.e., fixed-bed column) is essential to provide reliable information pertaining to breakthrough times, adsorption conditions, and the adsorbents' stability and selectivity during continuous use. This knowledge gap was addressed for immobilized PBP bead-based systems compared to an industry-standard ion exchanger. Lastly, the need for

improved PBP bead P_i removal capacity led to examination of a new PBP-loaded magnetic system.

The findings improved understanding of alternative approaches to immobilize PBP for removal/recovery applications, established flow-through column parameters, and increased the adsorbent capacity of PBP systems over previous reports. For each system, future work is needed to further advance the potential of PBP system to remove and recover P_i , as described in the following paragraphs.

For the PBP surface-displayed system, proof-of-concept of the feasibility of P_i release and recovery was provided. Nevertheless, operational complexity and performance variation are major challenges for implementation of the PBP surface-expressed system, similar to existing biological processes, such as EBPR. Possible improvements to be considered in future work include investigating other microorganisms targeting more stable induction of the fusion protein. Inducing mutants in the Pst transport system to repress the cellular interaction might increase the efficiency of the fusion protein in phosphate adsorption and desorption applications. Additionally, mutations in the PBP itself might be considered to increase the number of P_i binding sites. The system must also be tested and optimized for extended treatment applications such as wastewater, stormwater, and surface water treatment.

For the PBP-NHS resin system, protein immobilization on beads provided stable and predictable selective P_i removal and recovery potentials, even in real wastewater. Yet, improvement in PBP attachment capacity are needed to provide a more efficient solution to remove and recover P_i . The attachment procedure needs further optimization, potentially by changing the attachment conditions of pH, temperature, or initial concentration of PBP

in the buffer solution. Having the right mass ratio and functionality of attached materials is critical for successful conjugation. Also, investigating further types of functionalized beads offering greater surface area, such as polystyrene or polymethylmethacrylate (PMMA), will increase attachment capacity, considering the differences in material density, porosity, and particle size.

For the PBP-IOP system, enhanced P_i removal capacity was observed compared to previous PBP systems (i.e., PBP-NHS resin). However, the P_i removal capacity was still low compared to other adsorbents. Future work may include working with smaller molecules such as pared down protein sequences or peptides. Designing engineered peptides to capture and release P_i would not only simulate the functionality of natural proteins but also boost P_i removal capacity by increasing the attachment density of the functionalized material.

Overall, PBP-based systems offer a promising solution to selectively remove and recover P_i in a concentrated form under controlled conditions. The suggested future work may better capitalize on their potential.

7 REFERENCES

- Abdulsada, Z., 2014. Evaluation of microalgae for secondary and tertiary wastewater treatment.
- Acevedo, B., Oehmen, A., Carvalho, G., Seco, A., Borrás, L., Barat, R., 2012. Metabolic shift of polyphosphate-accumulating organisms with different levels of polyphosphate storage. *Water Research* 46, 1889–1900. <https://doi.org/10.1016/j.watres.2012.01.003>
- Ajmal, Z., Muhmood, A., Usman, M., Kizito, S., Lu, J., Dong, R., Wu, S., 2018. Phosphate removal from aqueous solution using iron oxides: Adsorption, desorption and regeneration characteristics. *Journal of Colloid and Interface Science* 528, 145–155. <https://doi.org/10.1016/j.jcis.2018.05.084>
- An, B., Nam, J., Choi, J.-W.W., Hong, S.-W.W., Lee, S.-H.H., 2013. Enhanced phosphate selectivity from wastewater using copper-loaded chelating resin functionalized with polyethylenimine. *Journal of Colloid and Interface Science* 409, 129–134. <https://doi.org/10.1016/j.jcis.2013.07.038>
- Ang, T.N., Young, B.R., Taylor, M., Burrell, R., Aroua, M.K., Baroutian, S., 2020. Breakthrough analysis of continuous fixed-bed adsorption of sevoflurane using activated carbons. *Chemosphere* 239, 124839. <https://doi.org/10.1016/j.chemosphere.2019.124839>
- Antelo, J., Fiol, S., Pérez, C., Mariño, S., Arce, F., Gondar, D., López, R., 2010. Analysis of phosphate adsorption onto ferrihydrite using the CD-MUSIC model. *Journal of Colloid and Interface Science* 347, 112–119. <https://doi.org/10.1016/j.jcis.2010.03.020>
- APHA, 2005. Standard methods for the examination of water and wastewater, 21st ed. American Public Health Association, Washington, D.C.
- Appling, D.R., Anthony-Cahill, S.J., Mathews, C.K., 2016. *Biochemistry: Concepts and Connections*, Global Edi. ed. Pearson Education Limited, Essex, England.
- Awual, Md.R., Shenashen, M.A., Jyo, A., Shiwaku, H., Yaita, T., 2014. Preparing of novel fibrous ligand exchange adsorbent for rapid column-mode trace phosphate removal from water. *Journal of Industrial and Engineering Chemistry* 20, 2840–2847.
- Ayawei, N., Ebelegi, A.N., Wankasi, D., 2017. Modelling and interpretation of adsorption isotherms. *Journal of Chemistry*. <https://doi.org/10.1155/2017/3039817>

- Bennett, E.M., Carpenter, S.R., Caraco, N.F., 2001. Human impact on erodable phosphorus and eutrophication: A global perspective. *BioScience* 51, 227–234. [https://doi.org/10.1641/0006-3568\(2001\)051\[0227:HIOEPA\]2.0.CO;2](https://doi.org/10.1641/0006-3568(2001)051[0227:HIOEPA]2.0.CO;2)
- Bischof, J., Padanilam, J., Holmes, W., Ezzell, R., Lee, R., Tompkins, R., Yarmush, M., Toner, M., 1995. Dynamics of Cell membrane Permeability Changes at Supraphysiological Temperatures. *Biophysical Journal* 68, 2608–2614.
- Blaney, L.M., Cinar, S., SenGupta, A.K., 2007. Hybrid anion exchanger for trace phosphate removal from water and wastewater. *Water Research* 41, 1603–1613. <https://doi.org/10.1016/j.watres.2007.01.008>
- Blank, L.M., 2012. The cell and P: From cellular function to biotechnological application. *Current Opinion in Biotechnology* 23, 846–851. <https://doi.org/10.1016/j.copbio.2012.08.002>
- Botero, L.M., Al-Niemi, T.S., McDermott, T.R., 2000. Characterization of two inducible phosphate transport systems in *Rhizobium tropici*. *Applied and Environmental Microbiology* 66, 15–22. <https://doi.org/10.1128/AEM.66.1.15-22.2000>
- Brix, H., Arias, C.A., Bubba, M., 1999. Media selection for sustainable phosphorus removal in subsurface flow constructed wetlands. *Water Science and Technology* 44, 47–54.
- Brown, N., Shilton, A., 2014. Luxury uptake of phosphorus by microalgae in waste stabilisation ponds: Current understanding and future direction. *Reviews in Environmental Science and Biotechnology*. <https://doi.org/10.1007/s11157-014-9337-3>
- Brune, M., Hunter, J.L., Corrie, J.E.T., Webb, M.R., 1994. Direct, Real-Time Measurement of Rapid Inorganic Phosphate Release Using a Novel Fluorescent Probe and Its Application to Actomyosin Subfragment 1 ATPase. *Biochemistry* 33, 8262–8271. <https://doi.org/10.1021/bi00193a013>
- Brune, M., Hunter, J.L., Howell, S.A., Martin, S.R., Hazlett, T.L., Corrie, J.E.T., Webb, M.R., 1998. Mechanism of inorganic phosphate interaction with phosphate binding protein from *Escherichia coli*. *Biochemistry* 37, 10370–10380. <https://doi.org/10.1021/bi9804277>
- Bui, T.H., Hong, S.P., Yoon, J., 2018. Development of nanoscale zirconium molybdate embedded anion exchange resin for selective removal of phosphate. *Water Research* 134, 22–31. <https://doi.org/10.1016/j.watres.2018.01.061>

- Bunce, J.T., Ndam, E., Ofiteru, I.D., Moore, A., Graham, D.W., 2018. A review of phosphorus removal technologies and their applicability to small-scale domestic wastewater treatment systems. *Frontiers in Environmental Science* 6, 1–15. <https://doi.org/10.3389/fenvs.2018.00008>
- Cai, W.J., Hu, X., Huang, W.J., Murrell, M.C., Lehrter, J.C., Lohrenz, S.E., Chou, W.C., Zhai, W., Hollibaugh, J.T., Wang, Y., Zhao, P., Guo, X., Gundersen, K., Dai, M., Gong, G.C., 2011. Acidification of subsurface coastal waters enhanced by eutrophication. *Nature Geoscience* 4, 766–770. <https://doi.org/10.1038/ngeo1297>
- Capua, F. di, de Sario, S., Ferraro, A., Petrella, A., Race, M., Pirozzi, F., Fratino, U., Spasiano, D., 2022. Phosphorous removal and recovery from urban wastewater: Current practices and new directions. *Proceedings of the Institution of Mechanical Engineers D: Journal of Automotive Engineering* 823, 1–18.
- Chen, W., Georgiou, G., 2002. Cell-Surface display of heterologous proteins: From high-throughput screening to environmental applications. *Biotechnology and Bioengineering* 79, 496–503. <https://doi.org/10.1002/bit.10407>
- Childers, D.L., Corman, J., Edwards, M., Elser, J.J., 2011. Sustainability Challenges of Phosphorus and Food: Solutions from Closing the Human Phosphorus Cycle. *BioScience* 61, 117–124. <https://doi.org/10.1525/bio.2011.61.2.6>
- Choi, S.S., Lee, H.M., Ha, J.H., Kang, D.G., Kim, C.S., Seo, J.H., Cha, H.J., 2013. Biological removal of phosphate at low concentrations using recombinant *Escherichia coli* expressing phosphate-binding protein in periplasmic space. *Applied Biochemistry and Biotechnology* 171, 1170–1177. <https://doi.org/10.1007/s12010-013-0187-1>
- Chowdhury, Z.Z., Hamid, S.B.A., Zain, S.M., 2015. Evaluating design parameters for breakthrough curve analysis and kinetics of fixed bed columns for Cu(II) cations using Lignocellulosic wastes zaira. *BioResources* 10, 732–749.
- Chowdhury, Z.Z., Zain, S.M., Rashid, A.K., Rafique, R.F., Khalid, K., 2013. Breakthrough curve analysis for column dynamics sorption of Mn(II) ions from wastewater by using *Mangostana garcinia* peel-based granular-activated carbon. *Journal of Chemistry* 2013, 1–8. <https://doi.org/10.1155/2013/959761>
- Claessens, J., Behrends, T., van Cappellen, P., 2004. What do acid-base titrations of live bacteria tell us? A preliminary assessment. *Aquatic Sciences* 66, 19–26. <https://doi.org/10.1007/s00027-003-0687-0>
- Cordell, D., Drangert, J.O., White, S., 2009. The story of phosphorus: Global food security and food for thought. *Global Environmental Change* 19, 292–305. <https://doi.org/10.1016/j.gloenvcha.2008.10.009>

- Cordell, D., Rosemarin, A., Schröder, J.J.J., Smit, A.L.L., 2011. Towards global phosphorus security: A systems framework for phosphorus recovery and reuse options. *Chemosphere* 84, 747–758.
<https://doi.org/10.1016/j.chemosphere.2011.02.032>
- Cordell, D., White, S., 2011. Peak phosphorus: Clarifying the key issues of a vigorous debate about long-term phosphorus security. *Sustainability* 3, 2027–2049.
<https://doi.org/10.3390/su3102027>
- Cornel, P., Schaum, C., 2009. Phosphorus recovery from wastewater: needs, technologies and costs. *Water Science & Technology* 59, 1069–1076.
- Dillon, P.J., Rigler, F.H., 1974. The phosphorus-chlorophyll relationship in lakes. *Limnology and Oceanography* 19, 767–773.
<https://doi.org/10.4319/lo.1974.19.5.0767>
- Dittrich, M., Sibling, S., 2005. Cell surface groups of two picocyanobacteria strains studied by zeta potential investigations, potentiometric titration, and infrared spectroscopy. *Journal of Colloid and Interface Science* 286, 487–495.
<https://doi.org/10.1016/j.jcis.2005.01.029>
- Dodds, W.K., Bouska, W.W., Eitzmann, J.L., Pilger, T.J., Pitts, K.L., Riley, A.J., Schloesser, J.T., Thornbrugh, D.J., 2009. Eutrophication of U. S. freshwaters: Analysis of potential economic damages. *Environmental Science and Technology*.
<https://doi.org/10.1021/es801217q>
- Dodds, W.K., Smith, V.H., 2016. Nitrogen, phosphorus, and eutrophication in streams. *Inland Waters* 6, 155–164. <https://doi.org/10.5268/IW-6.2.909>
- Do, T.H., Nguyen, V.T., Nguyen, Q.D., Chu, Nhung, M., Ngo, T.C.Q., Tan, L. van, 2020. Equilibrium, Kinetic and Thermodynamic Studies for Sorption of Phosphate from Aqueous Solutions Using ZnO Nanoparticles. *Processes* 8, 1–19.
- Drenkova-Tuhtan, A., Schneider, M., Franzreb, M., Meyer, C., Gellermann, C., SEXTL, G., Mandel, K., Steinmetz, H., 2017. Pilot-scale removal and recovery of dissolved phosphate from secondary wastewater effluents with reusable ZnFeZr adsorbent @ Fe₃O₄/SiO₂ particles with magnetic harvesting. *Water Research* 109, 77–87.
<https://doi.org/10.1016/j.watres.2016.11.039>
- Dufrêne, Y.F., van der Wal, A., Norde, W., Rouxhet, P.G., 1997. X-ray photoelectron spectroscopy analysis of whole cells and isolated cell walls of gram-positive bacteria: Comparison with biochemical analysis. *Journal of Bacteriology* 179, 1023–1028. <https://doi.org/10.1128/jb.179.4.1023-1028.1997>

- Du, X., Li, Y., Xia, Y.L., Ai, S.M., Liang, J., Sang, P., Ji, X.L., Liu, S.Q., 2016. Insights into protein–ligand interactions: Mechanisms, models, and methods. *International Journal of Molecular Sciences*. <https://doi.org/10.3390/ijms17020144>
- Elser, J.J., 2012. Phosphorus: A limiting nutrient for humanity? *Current Opinion in Biotechnology* 23, 833–838. <https://doi.org/10.1016/j.copbio.2012.03.001>
- Fernando, E.Y., McIlroy, S.J., Nierychlo, M., Herbst, F.A., Petriglieri, F., Schmid, M.C., Wagner, M., Nielsen, J.L., Nielsen, P.H., 2019. Resolving the individual contribution of key microbial populations to enhanced biological phosphorus removal with Raman–FISH. *ISME Journal* 13, 1933–1946. <https://doi.org/10.1038/s41396-019-0399-7>
- Filippelli, G.M., 2008. The global phosphorus cycle: Past, present, and future. *Elements* 4, 89–95. <https://doi.org/10.2113/GSELEMENTS.4.2.89>
- Filip, Z., Hermann, S., Demnerová, K., 2008. FT-IR spectroscopic characteristics of differently cultivated *Escherichia coli*. *Czech Journal of Food Sciences* 26, 458–463.
- Ghosh, G.K., Mohan, K.S., Sarkar, A.K., 1996. Characterization of soil-fertilizer P reaction products and their evaluation as sources of P for gram (*Cicer arietinum* L.). *Nutrient Cycling in Agroecosystems* 46, 71–79. <https://doi.org/10.1007/BF00210225>
- Gómez-Pastora, J., Bringas, E., Ortiz, I., 2014. Recent progress and future challenges on the use of high performance magnetic nano-adsorbents in environmental applications. *Chemical Engineering Journal* 256, 187–204. <https://doi.org/10.1016/j.cej.2014.06.119>
- Gu, A.Z., Liu, L., Neethling, J.B., Stensel, H.D., Murthy, S., 2011. Treatability and fate of various phosphorus fractions in different wastewater treatment processes. *Water Science and Technology* 63, 804–810. <https://doi.org/10.2166/wst.2011.312>
- Guiné, V., Spadini, L., Sarret, G., Muris, M., Delolme, C., Gaudet, J.P., Martins, J.M.F., 2006. Zinc sorption to three gram-negative bacteria: Combined titration, modeling, and EXAFS study. *Environmental Science and Technology* 40, 1806–1813. <https://doi.org/10.1021/es0509811>
- Haas, J.R., 2004. Effects of cultivation conditions on acid-base titration properties of *Shewanella putrefaciens*. *Chemical Geology* 209, 67–81. <https://doi.org/10.1016/j.chemgeo.2004.04.022>
- Hong, Y., Brown, D., 2006. Cell surface acid-base properties of *E. coli* and *Bacillus brevis* and variation as a function of growth phase, nitrogen source and C:N ratio. *Colloids and Surfaces B: Biointerfaces* 50, 112–119.

- Huang, H., Zhang, D.D., Li, J., Guo, G., Tang, S., 2017. Phosphate recovery from swine wastewater using plant ash in chemical crystallization. *Journal of Cleaner Production* 168, 338–345. <https://doi.org/10.1016/j.jclepro.2017.09.042>
- Huang, W., Yu, X., Tang, J., Zhu, Y., Zhang, Y., Li, D., 2015. Enhanced Adsorption of Phosphate by Flower-like Mesoporous Silica Spheres Loaded with Lanthanum. *Microporous and Mesoporous Materials* 217, 225–232. <https://doi.org/10.1016/j.funbio.2012.12.004>.This
- Hu, A., Ren, G., Che, J., Guo, Y., Ye, J., Zhou, S., 2020. Phosphate recovery with granular acid-activated neutralized red mud: Fixed-bed column performance and breakthrough curve modelling. *Journal of Environmental Sciences (China)* 90, 78–86. <https://doi.org/10.1016/j.jes.2019.10.018>
- Hussein, F.B., Mayer, B.K., 2022. Fixed-bed column study of phosphate adsorption using immobilized phosphate-binding protein. *Chemosphere* 295, 133908. <https://doi.org/10.1016/j.chemosphere.2022.133908>
- Hussein, F.B., Venkiteshwaran, K., Mayer, B.K., 2020. Cell surface-expression of the phosphate-binding protein PstS: System development, characterization, and evaluation for phosphorus removal and recovery. *Journal of Environmental Sciences (China)* 92, 129–140. <https://doi.org/10.1016/j.jes.2020.02.016>
- Jiang, W., Saxena, A., Song, B., Ward, B.B., Beveridge, T.J., Myneni, S.C.B., 2004. Elucidation of functional groups on gram-positive and gram-negative bacterial surfaces using infrared spectroscopy. *Langmuir* 20, 11433–11442. <https://doi.org/10.1021/la049043+>
- Jia, Z., Zeng, W., Xu, H., Li, S., Peng, Y., 2020. Adsorption removal and reuse of phosphate from wastewater using a novel adsorbent of lanthanum-modified platanus biochar. *Process Safety and Environmental Protection* 140, 221–232. <https://doi.org/10.1016/j.psep.2020.05.017>
- Johnston, A.E., Richards, I.R., 2004. Effectiveness of different precipitated phosphates as phosphorus sources for plants. *Phosphorus Research Bulletin* 15, 52–59. <https://doi.org/10.1079/SUM2002162>
- Jung, H.C., Park, J.H., Park, S.H., Lebeault, J.M., Pan, J.G., 1998. Expression of carboxymethylcellulase on the surface of *Escherichia coli* using *Pseudomonas syringae* ice nucleation protein. *Enzyme and Microbial Technology* 22, 348–354. [https://doi.org/10.1016/S0141-0229\(97\)00224-X](https://doi.org/10.1016/S0141-0229(97)00224-X)
- Jung, K.W., Jeong, T.U., Choi, J.W., Ahn, K.H., Lee, S.H., 2017. Adsorption of phosphate from aqueous solution using electrochemically modified biochar calcium-alginate beads: Batch and fixed-bed column performance. *Bioresource Technology* 244, 23–32. <https://doi.org/10.1016/j.biortech.2017.07.133>

- Kalaitzidou, K., Zouboulis, A., Mitrakas, M., 2022. Thermodynamic Study of Phosphate Adsorption and Removal from Water Using Iron Oxyhydroxides. *Water (Basel)* 14, 1–14.
- Kanjee, U., Houry, W.A., 2013. Mechanisms of Acid Resistance in *Escherichia coli*. *Annual Review of Microbiology* 67, 65–81. <https://doi.org/10.1146/annurev-micro-092412-155708>
- Kozłowski, L.P., 2016. Proteome-pI: Proteome isoelectric point database. *Nucleic Acids Research* 45, D1112–D1116. <https://doi.org/10.1093/nar/gkw978>
- Kuba, T., Smolders, G., van Loosdrecht, M.C.M., Heijnen, J.J., 1993. Biological phosphorus removal from wastewater by anaerobic-anoxic sequencing batch reactor, in: *Water Science and Technology*. pp. 241–252. <https://doi.org/10.2166/wst.1993.0504>
- Kumar, P.S., Korving, L., van Loosdrecht, M.C.M., Witkamp, G.J., 2019. Adsorption as a technology to achieve ultra-low concentrations of phosphate: Research gaps and economic analysis. *Water Research X* 4, 100029. <https://doi.org/10.1016/j.wroa.2019.100029>
- Kuroda, A., Kunimoto, H., Morohoshi, T., Ikeda, T., Kato, J., Takiguchi, N., Miya, A., Ohtake, H., 2000. Evaluation of phosphate removal from water by immobilized phosphate-binding protein PstS. *Journal of Bioscience and Bioengineering* 90, 688–690. [https://doi.org/10.1016/S1389-1723\(00\)90020-3](https://doi.org/10.1016/S1389-1723(00)90020-3)
- Langmuir, D., 1997. *Aqueous Environmental Geochemistry*. Prentice Hall, Upper Saddle River, N.J.
- Le Corre, K.S., Valsami-Jones, E., Hobbs, P., Parsons, S.A., 2009. Phosphorus recovery from wastewater by struvite crystallization: A review. *Critical Reviews in Environmental Science and Technology* 39, 433–477. <https://doi.org/10.1080/10643380701640573>
- Ledvina, P.S., Tsai, A.L., Wang, Z., Koehl, E., Quioco, F.A., 1998. Dominant role of local dipolar interactions in phosphate binding to a receptor cleft with an electronegative charge surface: Equilibrium, kinetic, and crystallographic studies. *Protein Science* 7, 2550–2559. <https://doi.org/10.1002/pro.5560071208>
- Lee, S.Y., Choi, J.H., Xu, Z., 2003. Microbial cell-surface display. *Trends Biotechnol* 21, 45–52. [https://doi.org/10.1016/S0167-7799\(02\)00006-9](https://doi.org/10.1016/S0167-7799(02)00006-9)
- Li, L., Kang, D.G., Cha, H.J., 2003. Functional Display of Foreign Protein on Surface of *Escherichia coli* Using N-Terminal Domain of Ice Nucleation Protein. *Biotechnology and Bioengineering* 85, 214–221. <https://doi.org/10.1002/bit.10892>

- Li, Q., Yu, Z., Shao, X., He, J., Li, L., 2009. Improved phosphate biosorption by bacterial surface display of phosphate-binding protein utilizing ice nucleation protein. *FEMS Microbiology Letters* 299, 44–52. <https://doi.org/10.1111/j.1574-6968.2009.01724.x>
- Liu, J., Wan, L., Zhang, L., Zhou, Q., 2011. Effect of pH, ionic strength, and temperature on the phosphate adsorption onto lanthanum-doped activated carbon fiber. *Journal of Colloid and Interface Science* 364, 490–496. <https://doi.org/10.1016/j.jcis.2011.08.067>
- Luecke, H., Quioco, F., 1990. High specificity of a phosphate transport protein determined by hydrogen bonds. *Letters To Nature* 347, 402–406. <https://doi.org/10.1038/346183a0>
- Lund, P., Tramonti, A., de Biase, D., 2014. Coping with low pH: Molecular strategies in neutralophilic bacteria. *FEMS Microbiology Reviews* 38, 1091–1125. <https://doi.org/10.1111/1574-6976.12076>
- Luo, X., Wang, X., Bao, S., Liu, X., Zhang, W., Fang, T., 2016. Adsorption of phosphate in water using one-step synthesized zirconium-loaded reduced graphene oxide. *Scientific Reports* 6.
- Mahanta, N., Valiyaveetti, S., 2013. Functionalized poly (vinyl alcohol) based nanofibers for the removal of arsenic from water. *RSC Advances* 3, 2776–2783.
- Mahardika, D., Park, H.S., Choo, K.H., 2018. Ferrihydrite-impregnated granular activated carbon (FH@GAC) for efficient phosphorus removal from wastewater secondary effluent. *Chemosphere* 207, 527–533. <https://doi.org/10.1016/j.chemosphere.2018.05.124>
- Mallet, M., Barthélémy, K., Ruby, C., Renard, A., Naille, S., 2013. Investigation of phosphate adsorption onto ferrihydrite by X-ray Photoelectron Spectroscopy. *Journal of Colloid and Interface Science* 407, 95–101. <https://doi.org/10.1016/j.jcis.2013.06.049>
- Mancini, J.L., Kaufman, G.C., Mangarella, P.A., Driscoll, E.D., 1983. *Technical Guidance Manual for Performing Waste Load Allocations*. Washington, D.C.
- Manjunath, S. v., Kumar, M., 2021. Simultaneous removal of antibiotic and nutrients via *Prosopis juliflora* activated carbon column: Performance evaluation, effect of operational parameters and breakthrough modeling. *Chemosphere* 262. <https://doi.org/10.1016/j.chemosphere.2020.127820>

- Martin, B.D., De Kock, L., Gallot, M., Guery, E., Stanowski, S., MacAdam, J., McAdam, E.J., Parsons, S.A., Jefferson, B., 2018. Quantifying the performance of a hybrid anion exchanger/adsorbent for phosphorus removal using mass spectrometry coupled with batch kinetic trials. *Environmental Technology (United Kingdom)* 39, 2304–2314. <https://doi.org/10.1080/09593330.2017.1354076>
- Mayer, B.K., Gerrity, D., Rittmann, B.E., Reisinger, D., Brandt-Williams, S., 2013. Innovative strategies to achieve low total phosphorus concentrations in high water flows. *Critical Reviews in Environmental Science and Technology* 43, 409–441. <https://doi.org/10.1080/10643389.2011.604262>
- Moriyama, K., Kojima, T., Minawa, Y., Matsumoto, S., Nakamachi, K., 2001. Development of artificial seed crystal for crystallization of calcium phosphate. *Environmental Technology (United Kingdom)* 22, 1245–1252. <https://doi.org/10.1080/09593330.2001.9619163>
- Morohoshi, T., Yamashita, T., Kato, J., Ikeda, T., Takiguchi, N., Ohtake, H., Kuroda, A., 2003. A method for screening remove polyphosphate-accumulating mutants which remove phosphate efficiently from synthetic wastewater. *Journal of Bioscience and Bioengineering* 95, 637–640. [https://doi.org/10.1016/S1389-1723\(03\)80177-9](https://doi.org/10.1016/S1389-1723(03)80177-9)
- Muhammad, A., Soares, A., Jefferson, B., 2019. The impact of background wastewater constituents on the selectivity and capacity of a hybrid ion exchange resin for phosphorus removal from wastewater. *Chemosphere* 224, 494–501. <https://doi.org/10.1016/j.chemosphere.2019.01.085>
- Münch, E. V, Barr, K., 2001. Controlled struvite crystallisation for removing phosphorus from anaerobic digester sidestreams. *Water Research* 35, 151–159. [https://doi.org/10.1016/S0043-1354\(00\)00236-0](https://doi.org/10.1016/S0043-1354(00)00236-0)
- Nguyen, T.T., Ngo, H.H., Guo, W., 2013. Pilot scale study on a new membrane bioreactor hybrid system in municipal wastewater treatment. *Bioresource Technology* 141, 8–12. <https://doi.org/10.1016/j.biortech.2013.03.125>
- Ngwenya, B.T., Sutherland, I.W., Kennedy, L., 2003. Comparison of the acid-base behaviour and metal adsorption characteristics of a gram-negative bacterium with other strains. *Applied Geochemistry* 18, 527–538. [https://doi.org/10.1016/S0883-2927\(02\)00118-X](https://doi.org/10.1016/S0883-2927(02)00118-X)
- Oehmen, A., Lemos, P.C., Carvalho, G., Yuan, Z., Keller, J., Blackall, L.L., Reis, M.A.M., 2007. Advances in enhanced biological phosphorus removal: From micro to macro scale. *Water Research*. <https://doi.org/10.1016/j.watres.2007.02.030>

- Oh, H.-J., Choung, Y.-K., Lee, S., Choi, J.-S., Hwang, T.-M., Kim, J.H., 2009. Adsorption of methylene blue by phoenix tree leaf powder in a fixed-bed column: experiments and prediction of breakthrough curves. *Desalination* 238, 333–346. <https://doi.org/10.1016/j.desal.2009.05.011>
- Ojeda, J.J., Romero-González, M.E., Bachmann, R.T., Edyvean, R.G.J., Banwart, S.A., 2008. Characterization of the Cell Surface and Cell Wall Chemistry of Drinking Water Bacteria by Combining XPS, FTIR Spectroscopy, Modeling, and Potentiometric Titrations. *Langmuir* 24, 4032–4040. <https://doi.org/10.1021/la702284b>
- Oleszkiewicz, J., Kruk, D., Devlin, T., Lashkarizadeh, M., Yuan, Q., 2015. Options for improved nutrient removal and recovery from municipal wastewater in the canadian context. Winnipeg, MN.
- Omoike, A., Chorover, J., 2004. Spectroscopic study of extracellular polymeric substances from *Bacillus subtilis*: Aqueous chemistry and adsorption effects. *Biomacromolecules* 5, 1219–1230. <https://doi.org/10.1021/bm034461z>
- Ownby, M., Desrosiers, D.A., Vaneckhaute, C., 2021. Phosphorus removal and recovery from wastewater via hybrid ion exchange nanotechnology: a study on sustainable regeneration chemistries. *npj Clean Water* 4, 1–8. <https://doi.org/10.1038/s41545-020-00097-9>
- Pap, S., Kirk, C., Bremner, B., Turk Sekulic, M., Shearer, L., Gibb, S.W., Taggart, M.A., 2020. Low-cost chitosan-calcite adsorbent development for potential phosphate removal and recovery from wastewater effluent. *Water Research* 173, 115573. <https://doi.org/10.1016/j.watres.2020.115573>
- Park, M., Yoo, G., Bong, J.H., Jose, J., Kang, M.J., Pyun, J.C., 2015. Isolation and characterization of the outer membrane of *Escherichia coli* with autodisplayed Z-domains. *Biochimica et Biophysica Acta - Biomembranes* 1848, 842–847. <https://doi.org/10.1016/j.bbamem.2014.12.011>
- Patel, H., 2019. Fixed-bed column adsorption study; a comprehensive review. *Applied Water Science* 9, 1–17. <https://doi.org/10.1007/s13201-019-0927-7>
- Pidou, M., Parsons, S.A., Raymond, G., Jeffrey, P., Stephenson, T., Jefferson, B., 2009. Fouling control of a membrane coupled photocatalytic process treating greywater. *Water Research* 43, 3932–3939. <https://doi.org/10.1016/j.watres.2009.05.030>
- Poole, K., Hancock, R.E.W., 1984. Phosphate transport in *Pseudomonas aeruginosa*. *European Journal of Biochemistry* 144, 607–612. <https://doi.org/10.1111/j.1432-1033.1984.tb08508.x>

- Qiu, H., Liang, C., Yu, J., Zhang, Q., 2017. Preferable phosphate sequestration by nano-La(III) (hydr)oxides modified wheat straw with excellent properties in regeneration. *Chemical Engineering Journal* 230315, 345–354.
- Qureshi, A., Lo, K.V., Mavinic, D.S., Liao, P.H., Koch, F., Kelly, H., 2006. Dairy manure treatment, digestion and nutrient recovery as a phosphate fertilizer. *Journal of Environmental Science and Health - Part B Pesticides, Food Contaminants, and Agricultural Wastes* 41, 1221–1235. <https://doi.org/10.1080/03601230600857098>
- Rashid, M., Price, N.T., Gracia Pinilla, M.Á., O’Shea, K.E., 2017. Effective removal of phosphate from aqueous solution using humic acid coated magnetite nanoparticles. *Water Research* 123, 353–360. <https://doi.org/10.1016/j.watres.2017.06.085>
- Recepoğlua, Y.K., Kabay, N., Ipek, I.Y., Arda, M., Yüksel, M., Yoshizuka, K., Nishihama, S., 2018. Packed bed column dynamic study for boron removal from geothermal brine by a chelating fiber and breakthrough curve analysis by using mathematical models. *Desalination* 437, 1–6. <https://doi.org/https://doi.org/10.1016/j.desal.2018.02.022>
- Rittmann, B.E., 2008. Opportunities for renewable bioenergy using microorganisms. *Biotechnology and Bioengineering* 100, 203–212. <https://doi.org/10.1002/bit.21875>
- Rittmann, B.E., Mayer, B., Westerhoff, P., Edwards, M., 2011. Capturing the lost phosphorus. *Chemosphere* 84, 846–853. <https://doi.org/10.1016/j.chemosphere.2011.02.001>
- Rosemarin, A., 2016. Global Status of Phosphorus [WWW Document]. URL https://d1pdf7a38rpjk8.cloudfront.net/fileadmin/user_upload/1600_Arno_Rosemarin_Stockholm_Environment_Institute.pdf
- Rosen, B.P., Silver, S., 1987. *Ion Transport in Prokaryotes*. Academic Press, Inc., California.
- Samarghandi, M.R., Hadi, M., McKay, G., 2014. Breakthrough curve analysis for fixed-bed adsorption of azo dyes using novel pine cone-derived active carbon. *Adsorption Science and Technology* 32, 791–806. <https://doi.org/10.1260/0263-6174.32.10.791>
- Santos-Beneit, F., Rodríguez-García, A., Franco-Domínguez, E., Martín, J.F., 2008. Phosphate-dependent regulation of the low- and high-affinity transport systems in the model actinomycete *Streptomyces coelicolor*. *Microbiology (N Y)* 154, 2356–2370. <https://doi.org/10.1099/mic.0.2008/019539-0>

- Satya, A., Harimawan, A., Sri Haryani, G., Johir, M.A.H., Nguyen, L.N., Nghiem, L.D., Vigneswaran, S., Ngo, H.H., Setiadi, T., 2021. Fixed-bed adsorption performance and empirical modeling of cadmium removal using adsorbent prepared from the cyanobacterium *Aphanothece* sp cultivar. *Environmental Technology and Innovation* 21, 101194. <https://doi.org/10.1016/j.eti.2020.101194>
- Schindler, D.W., 1977. Evolution of phosphorus limitation in lakes. *Science* (1979) 195, 260–262. <https://doi.org/10.1126/science.195.4275.260>
- Sendrowski, A., Boyer, T.H., 2013. Phosphate removal from urine using hybrid anion exchange resin. *Desalination* 322, 104–112. <https://doi.org/10.1016/j.desal.2013.05.014>
- Sengupta, S., Pandit, A., 2011. Selective removal of phosphorus from wastewater combined with its recovery as a solid-phase fertilizer. *Water Research* 45, 3318–3330. <https://doi.org/10.1016/j.watres.2011.03.044>
- Seviour, R.J., Mino, T., Onuki, M., 2003. The microbiology of biological phosphorus removal in activated sludge systems. *FEMS Microbiology Reviews*. [https://doi.org/10.1016/S0168-6445\(03\)00021-4](https://doi.org/10.1016/S0168-6445(03)00021-4)
- Shabala, L., Bowman, J., Brown, J., Ross, T., McMeekin, T., Shabala, S., 2009. Ion transport and osmotic adjustment in *Escherichia coli* in response to ionic and non-ionic osmotica. *Environmental Microbiology* 11, 137–148.
- Sharafi, Z., Bakhshi, B., Javidi, J., Adrangi, S., 2018. Synthesis of silica-coated iron oxide nanoparticles: Preventing aggregation without using additives or seed pretreatment. *Iranian Journal of Pharmaceutical Research* 17, 386–395.
- Singh, S., Chandra Srivastava, V., Goyal, A., Deo Mall, I., 2020. Breakthrough modeling of furfural sorption behavior in a bagasse fly ash packed bed. *Environmental Engineering Research* 25, 104–113. <https://doi.org/10.4491/eer.2018.407>
- Slonczewski, J.L., Fujisawa, M., Dopson, M., Krulwich, T.A., 2009. Cytoplasmic pH Measurement and Homeostasis in Bacteria and Archaea. *Advances in Microbial Physiology* 55, 1–317. [https://doi.org/10.1016/S0065-2911\(09\)05501-5](https://doi.org/10.1016/S0065-2911(09)05501-5)
- Smil, V., 2000. Phosphorus in the environment: Natural flows and human interferences. *Annual Review of Energy and the Environment* 25, 53–88. <https://doi.org/10.1146/annurev.energy.25.1.53>
- Solscheid, C., Kunzelmann, S., Davis, C.T., Hunter, J.L., Nofer, A., Webb, M.R., 2015. Development of a reagentless biosensor for inorganic phosphate, applicable over a wide concentration range. *Biochemistry* 54, 5054–5062. <https://doi.org/10.1021/acs.biochem.5b00449>

- Steen, I., 1998. Phosphorus availability in the 21st Century: management of a non-renewable resource. *Phosphorus and Potassium*.
- Stokholm-Bjerregaard, M., McIlroy, S.J., Nierychlo, M., Karst, S.M., Albertsen, M., Nielsen, P.H., 2017. A critical assessment of the microorganisms proposed to be important to enhanced biological phosphorus removal in full-scale wastewater treatment systems. *Frontiers in Microbiology* 8.
<https://doi.org/10.3389/fmicb.2017.00718>
- Suresh Kumar, P., Prot, T., Korving, L., Keesman, K.J., Dugulan, I., van Loosdrecht, M.C.M., Witkamp, G.J., 2017. Effect of pore size distribution on iron oxide coated granular activated carbons for phosphate adsorption – Importance of mesopores. *Chemical Engineering Journal* 326, 231–239.
<https://doi.org/10.1016/j.cej.2017.05.147>
- Tafakori, V., Torktaz, I., Doostmohammadi, M., 2012. Microbial cell surface display; its medical and environmental applications. *Iranian Journal of Biotechnology* 10, 231–239.
- Tang, Y., 2015. Parameters affecting phosphate sorption from sludge liquors by hybrid anion sorbents. the Karlsruhe Institute of Technology.
- Turner, B.F., Fein, J.B., 2006. Proffit: A program for determining surface protonation constants from titration data. *Computers and Geosciences* 32, 1344–1356.
<https://doi.org/10.1016/j.cageo.2005.12.005>
- US Environmental Protection Agency, 2000. Ambient water quality criteria recommendations of state and tribal nutrient criteria rivers and streams in nutrient ecoregion II. US Environmental Protection Agency EPA 822-B-00-016.
[https://doi.org/EPA 822-B-00-014](https://doi.org/EPA%20822-B-00-014)
- Vaccari, D.A., 2009. Phosphorus: A Looming Crisis. *Sci Am* 300, 54–59.
<https://doi.org/10.1038/scientificamerican0609-54>
- Vallabani, N.V.S., Singh, S., 2018. Recent advances and future prospects of iron oxide nanoparticles in biomedicine and diagnostics. *3 Biotech* 8, 1–23.
<https://doi.org/10.1007/s13205-018-1286-z>
- van Bloois, E., Winter, R.T., Kolmar, H., Fraaije, M.W., 2011. Decorating microbes: Surface display of proteins on *Escherichia coli*. *Trends in Biotechnology*.
<https://doi.org/10.1016/j.tibtech.2010.11.003>
- van der Mei, H.C., de Vries, J., Busscher, H.J., 2000. X-ray photoelectron spectroscopy for the study of microbial cell surfaces. *Surface Science Reports* 39, 1–24.
[https://doi.org/10.1016/S0167-5729\(00\)00003-0](https://doi.org/10.1016/S0167-5729(00)00003-0)

- Venkiteshwaran, K., Pokhrel, N., Hussein, F., Antony, E., Mayer, B.K., 2018. Phosphate removal and recovery using immobilized phosphate binding proteins. *Water Research X* 1, 1–9. <https://doi.org/10.1016/j.wroa.2018.09.003>
- Venkiteshwaran, K., Wells, E., Mayer, B.K., 2021. Immobilized phosphate-binding protein can effectively discriminate against arsenate during phosphate adsorption and recovery. *Water Environment Research* 93, 1173–1178. <https://doi.org/10.1002/wer.1498>
- Venkiteshwaran, K., Wells, E., Mayer, B.K., 2020. Kinetics, Affinity, Thermodynamics, and Selectivity of Phosphate Removal Using Immobilized Phosphate-Binding Proteins. *Environmental Science and Technology* 54, 10885–10894. <https://doi.org/10.1021/acs.est.0c02272>
- Wang, S., Peng, Y., 2010. Natural zeolites as effective adsorbents in water and wastewater treatment. *Chemical Engineering Journal*. <https://doi.org/10.1016/j.cej.2009.10.029>
- Wang, Z., Choudhary, A., Ledvina, P.S., Quioco, F.A., 1994. Fine tuning the specificity of the periplasmic phosphate transport receptor. Site-directed mutagenesis, ligand binding, and crystallographic studies. *The Journal of Biological Chemistry* 269, 25091–25094.
- Wanner, B.L., 1993. Gene regulation by phosphate in enteric bacteria. *Journal of Cellular Biochemistry* 51, 47–54. <https://doi.org/10.1002/jcb.240510110>
- Williams, A.T., Zitomer, D.H., Mayer, B.K., 2015. Ion exchange-precipitation for nutrient recovery from dilute wastewater. *Environmental Science: Water Research and Technology* 1, 832–838. <https://doi.org/10.1039/c5ew00142k>
- Withers, P.J.A., Elser, J.J., Hilton, J., Ohtake, H., Schipper, W.J., Van Dijk, K.C., 2015. Greening the global phosphorus cycle: How green chemistry can help achieve planetary P sustainability. *Green Chemistry* 17, 2087–2099. <https://doi.org/10.1039/c4gc02445a>
- Wu, H., Kosaka, H., Kato, J., Kuroda, A., Ikeda, T., Takiguchi, N., Ohtake, H., 1999. Cloning and characterization of *Pseudomonas putida* genes encoding the phosphate-specific transport system. *Journal of Bioscience and Bioengineering* 87, 273–279. [https://doi.org/10.1016/S1389-1723\(99\)80031-0](https://doi.org/10.1016/S1389-1723(99)80031-0)
- Wu, L., Zhang, S., Wang, J., Ding, X., 2020. Phosphorus retention using iron (II/III) modified biochar in saline-alkaline soils: Adsorption, column and field tests. *Environmental Pollution* 261, 114223. <https://doi.org/10.1016/j.envpol.2020.114223>

- Xue, Y., Hou, H., Zhu, S., 2009. Characteristics and mechanisms of phosphate adsorption onto basic oxygen furnace slag. *Journal of Hazardous Materials* 162, 973–980. <https://doi.org/10.1016/j.jhazmat.2008.05.131>
- Xu, Q., Chen, Z., Wu, Z., Xu, F., Yang, D., He, Q., Li, G., Chen, Y., 2019. Novel lanthanum doped biochars derived from lignocellulosic wastes for efficient phosphate removal and regeneration. *Bioresource Technology* 289, 121600. <https://doi.org/10.1016/j.biortech.2019.121600>
- Xu, Q., Li, W., Ma, L., Cao, D., Owens, G., Chen, Z., 2020. Simultaneous removal of ammonia and phosphate using green synthesized iron oxide nanoparticles dispersed onto zeolite. *Science of the Total Environment* 703, 1–8. <https://doi.org/10.1016/j.scitotenv.2019.135002>
- Yang, S., Jin, P., Wang, X., Zhang, Q., Chen, X., 2016. Phosphate recovery through adsorption assisted precipitation using novel precipitation material developed from building waste: Behavior and mechanism. *Chemical Engineering Journal* 292, 246–254. <https://doi.org/10.1016/j.cej.2016.02.006>
- Yang, Y., Ballent, W., Mayer, B.K., 2016. High-affinity phosphate-binding protein (PBP) for phosphorous recovery: Proof of concept using recombinant *Escherichia coli*. *FEMS Microbiology Letters* 363, 1–6. <https://doi.org/10.1093/femsle/fnw240>
- Yanyan, L., Kurniawan, T.A., Zhu, M., Ouyang, T., Avtar, R., Dzarfan Othman, M.H., Mohammad, B.T., Albadarin, A.B., 2018. Removal of acetaminophen from synthetic wastewater in a fixed-bed column adsorption using low-cost coconut shell waste pretreated with NaOH, HNO₃, ozone, and/or chitosan. *Journal of Environmental Management* 226, 365–376. <https://doi.org/10.1016/j.jenvman.2018.08.032>
- Yoon, S.Y., Lee, C.G., Park, J.A., Kim, J.H., Kim, S.B., Lee, S.H., Choi, J.W., 2014. Kinetic, equilibrium and thermodynamic studies for phosphate adsorption to magnetic iron oxide nanoparticles. *Chemical Engineering Journal* 236, 341–347. <https://doi.org/10.1016/j.cej.2013.09.053>
- Yousefi, M., Nabizadeh, R., Alimohammadi, M., Mohammadi, A.A., Mahvi, A.H., 2019. Removal of phosphate from aqueous solutions using granular ferric hydroxide process optimization by response surface methodology. *Desalination and Water Treatment* 158, 290–300. <https://doi.org/10.5004/dwt.2019.24281>
- You, X., Farran, A., Guaya, D., Valderrama, C., Soldatov, V., Cortina, J.L., 2016. Phosphate removal from aqueous solutions using a hybrid fibrous exchanger containing hydrated ferric oxide nanoparticles. *Journal of Environmental Chemical Engineering* 4, 388–397. <https://doi.org/10.1016/j.jece.2015.11.032>

- Yuan, Z., Pratt, S., Batstone, D.J., 2012. Phosphorus recovery from wastewater through microbial processes. *Current Opinion in Biotechnology* 23, 878–883.
- Zhao, D., Sengupta, A.K., 1996. Selective removal and recovery of phosphate in a novel fixed-bed process. *Water Science and Technology* 33, 139–147.
[https://doi.org/10.1016/0273-1223\(96\)00415-5](https://doi.org/10.1016/0273-1223(96)00415-5)

APPENDICES

Appendix A Supporting Information - Chapter 3

Figure A1 describes the gene map of recombinant plasmid pTrcHis_B

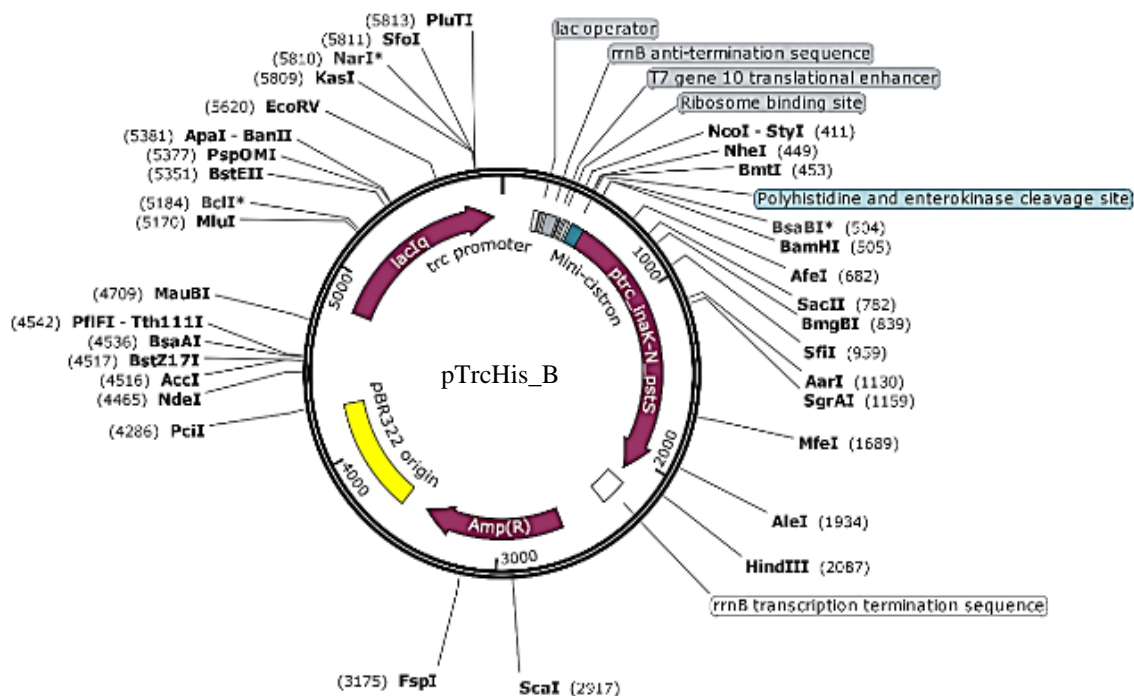


Figure A1 Gene map of recombinant plasmid pTrcHis_B. lacIq is the overexpressed lac repressor. inaK-N is the N-terminal sequence of the ice nucleation protein (INP). pstS is the phosphate-binding protein encoding gene. Amp is the ampicillin-resistant gene. The blue area is the poly-histidine peptide (His-Tag).

Table A1 provides the signal intensity of western blot bands

Table A1 Signal intensity of western blot bands for induced cells.

Location	Channel Signal		
	Red	Green	Blue
Location-1	6358	23397	35203
Location-2	38641	76181	105775
% Ratio	16.5%	30.7%	33.3%
Average % Ratio	26.8%		

Table A2 provides the functional group assignments for FTIR spectra

Table A2 Peak functional group assignments for FTIR spectra.

Wavenumber (cm ⁻¹)	Functional Group Assignment
~ 2918-2850	C-H stretching in aliphatic of cell walls (carbohydrates)
~ 1654	C=O stretching in amides associated with proteins (amide I), NH ₂ bending of amines
~ 1540	N-H bending and C-N stretching in amides associated with proteins (amide II)
~ 1455	C-H deformation of CH ₂ or CH ₃ of proteins
~ 1270	COOH and C-O-H vibrations
~ 1100	P=O stretching of phosphodiester, phosphorylated proteins or polyphosphate products
~ 976	Phosphoryl group PO ₃ ²⁻ stretching
~ 610-575	P-O-C and C-O-C bonds in phospholipids and aromatics

Appendix B Supporting Information - Chapter 4

Figure B1 describes the experimental steps for PBP expression and purification

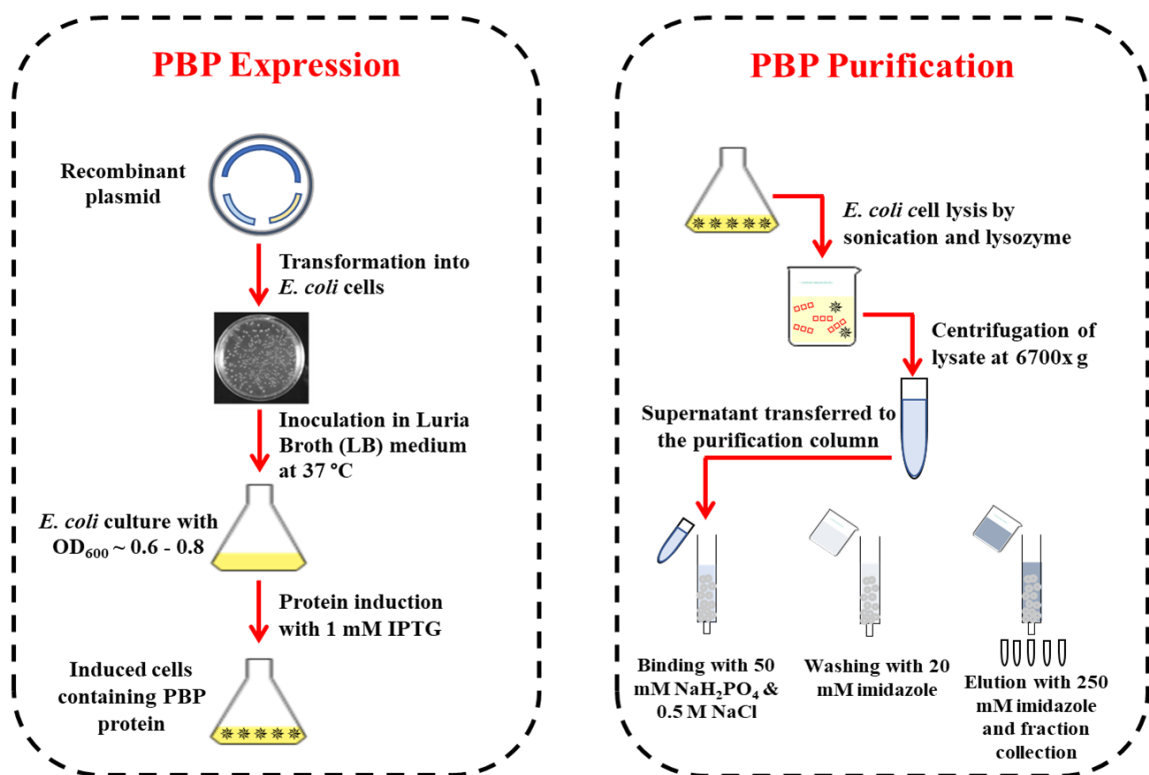


Figure B1 Schematic illustration of phosphate-binding protein (PBP) expression and purification procedures.

Table B1 provides characteristics of the tertiary wastewater effluent sample

Table B1 Characterizations of tertiary wastewater effluent (prior to de-chlorination) from the South Shore Water Reclamation Facility in Oak Creek, WI. Each measurement was performed in duplicate using approaches in accordance with Standard Methods.

Parameter	Unit	Average \pm Standard Deviation
Total Suspended Solid (TSS)	mg L ⁻¹	20 \pm 3
Dissolved Organic Carbon (DOC)	mg-C L ⁻¹	9.4 \pm 0.1
Total Hardness	mg L ⁻¹ CaCO ₃	370 \pm 10
Alkalinity	mg L ⁻¹ CaCO ₃	300 \pm 10
Chloride	mg L ⁻¹ as Cl ⁻	360 \pm 10
Ammonia	mg NH ₃ L ⁻¹	0.3 \pm 0.1
Phosphate	mg PO ₄ ³⁻ L ⁻¹	0.75 \pm 0.1
Nitrate	mg NO ₃ ⁻ L ⁻¹	3.95 \pm 0.05
Sulfate	mg SO ₄ ²⁻ L ⁻¹	224 \pm 0.13
Hydrogen Sulfide	mg S ²⁻ L ⁻¹	0
pH	---	7.25 \pm 0.1

Mathematical Models Fitting at Different Influent P_i Concentrations

Figures B2-B4 illustrate the Thomas, Yoon-Nelson and Adams-Bohart linear regression analysis and model fits at different influent P_i concentrations.

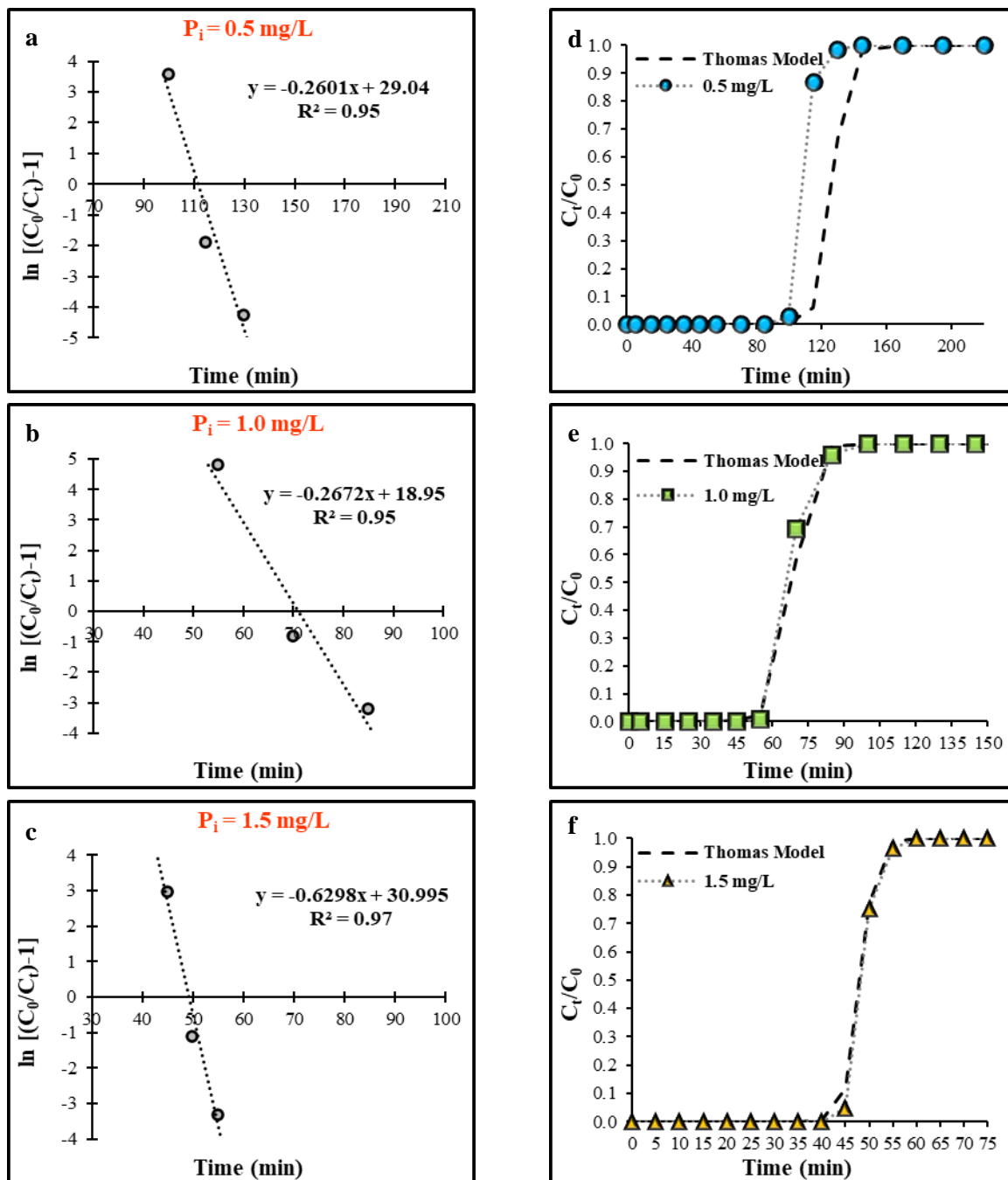


Figure B2 Mathematical modeling for breakthrough curves at different influent phosphate concentrations using the Thomas model. Panels a, b, and c show the linear regression analysis, while panels d, e, and f show the experimental data (points) in comparison to the theoretical breakthrough curves (dashed lines).

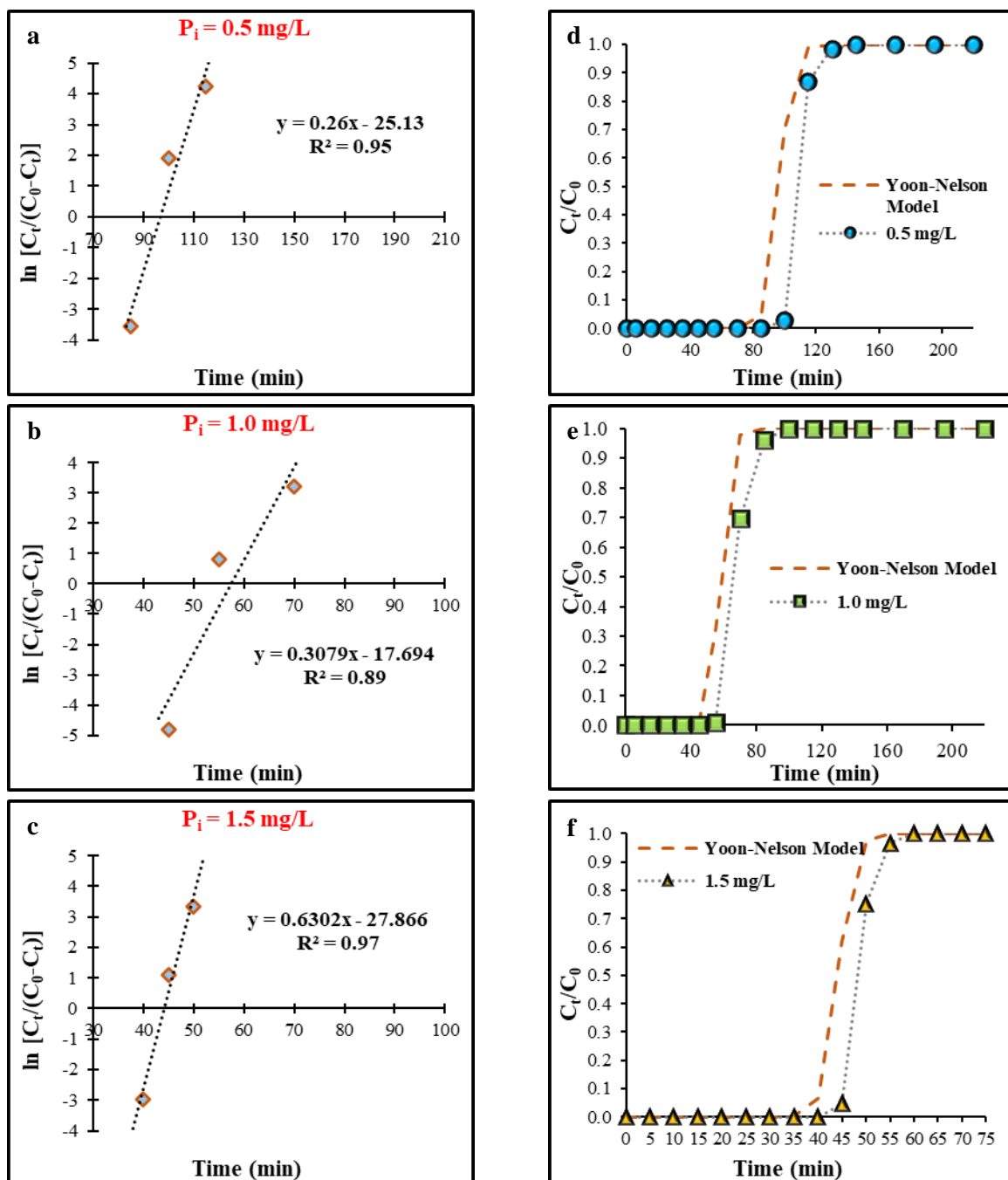


Figure B3 Mathematical modeling for breakthrough curves at different influent phosphate concentrations using the Yoon-Nelson model. Panels a, b, and c show the linear regression analysis, while panels d, e, and f show the experimental data (points) in comparison to the theoretical breakthrough curves (dashed lines).

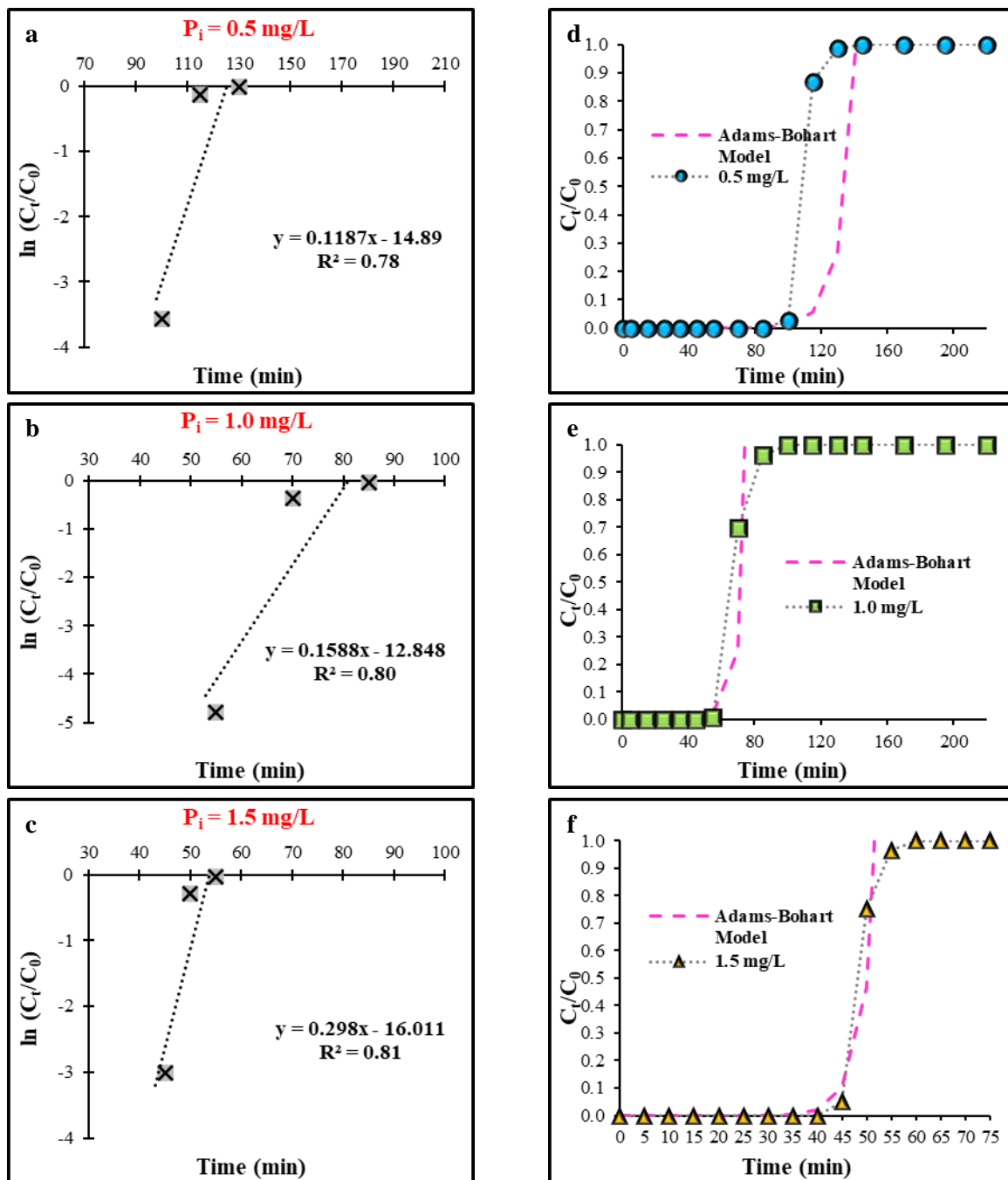


Figure B4 Mathematical modeling for breakthrough curves at different influent phosphate concentrations using the Adams-Bohart model. Panels a, b, and c show the linear regression analysis, while panels d, e, and f show the experimental data (points) in comparison to the theoretical breakthrough curves (dashed lines).

Mathematical Models Fitting at Different Bed Volumes

Figures B5-B7 illustrate the Thomas, Yoon-Nelson, and Adams-Bohart linear regression analysis and model fits at different bed volumes.

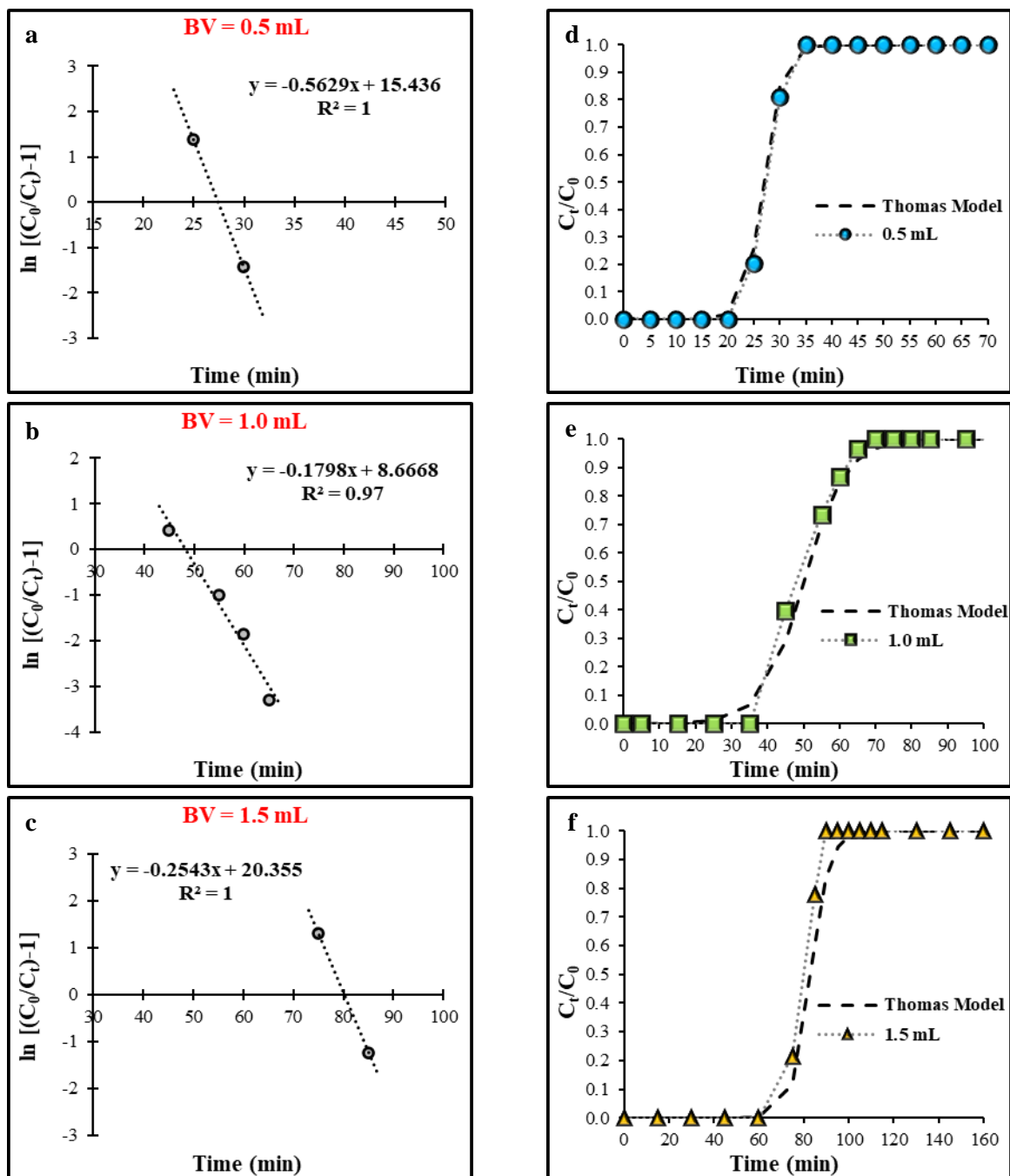


Figure B5 Mathematical modeling for breakthrough curves at different bed volumes using the Thomas model. Panels a, b, and c show the linear regression analysis, while panels d, e, and f show the experimental data (points) in comparison to the theoretical breakthrough curves (dashed lines).

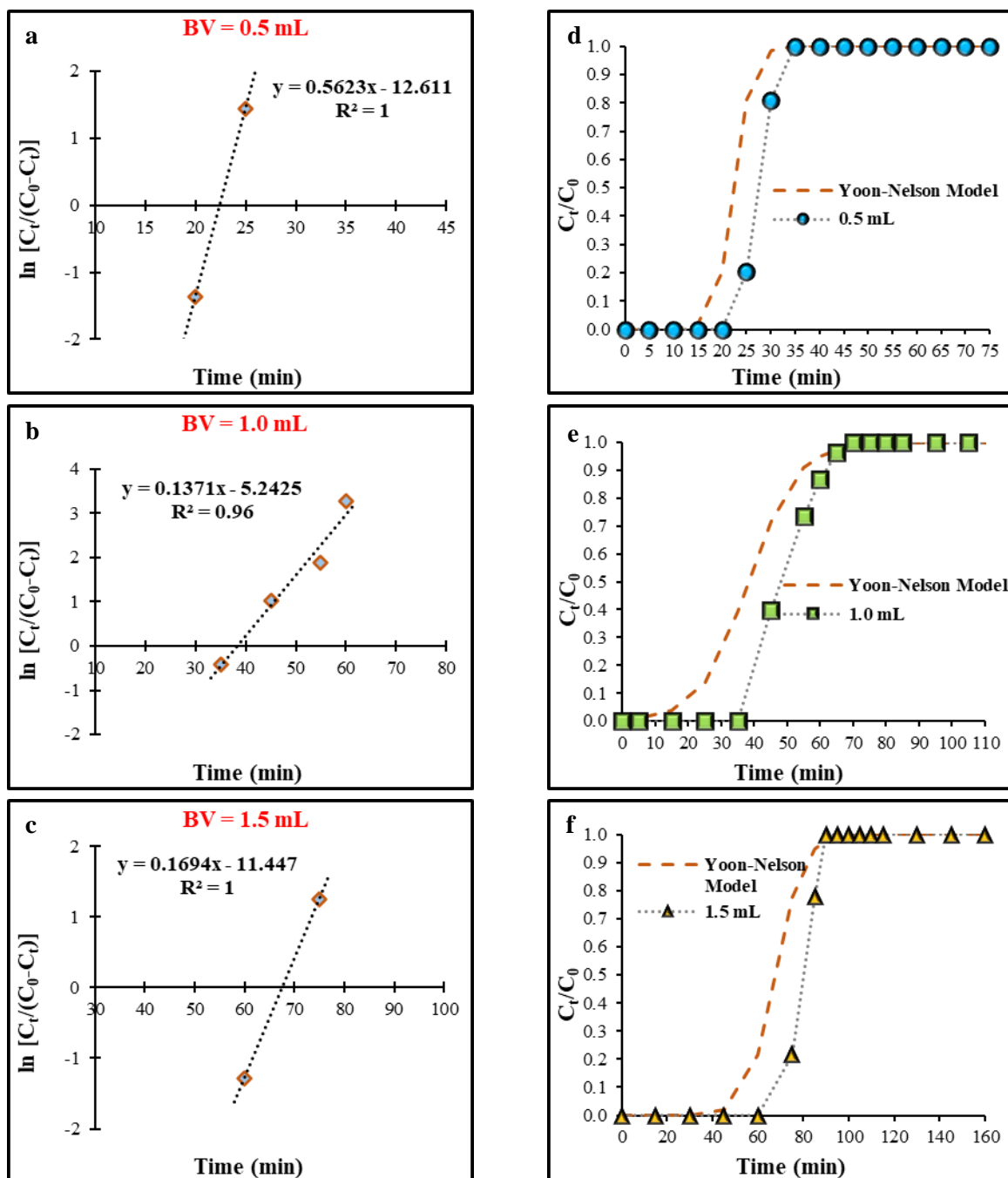


Figure B6 Mathematical modeling for breakthrough curves at different bed volumes using the Yoon-Nelson model. Panels a, b, and c show the linear regression analysis, while panels d, e, and f show the experimental data (points) in comparison to the theoretical breakthrough curves (dashed lines).

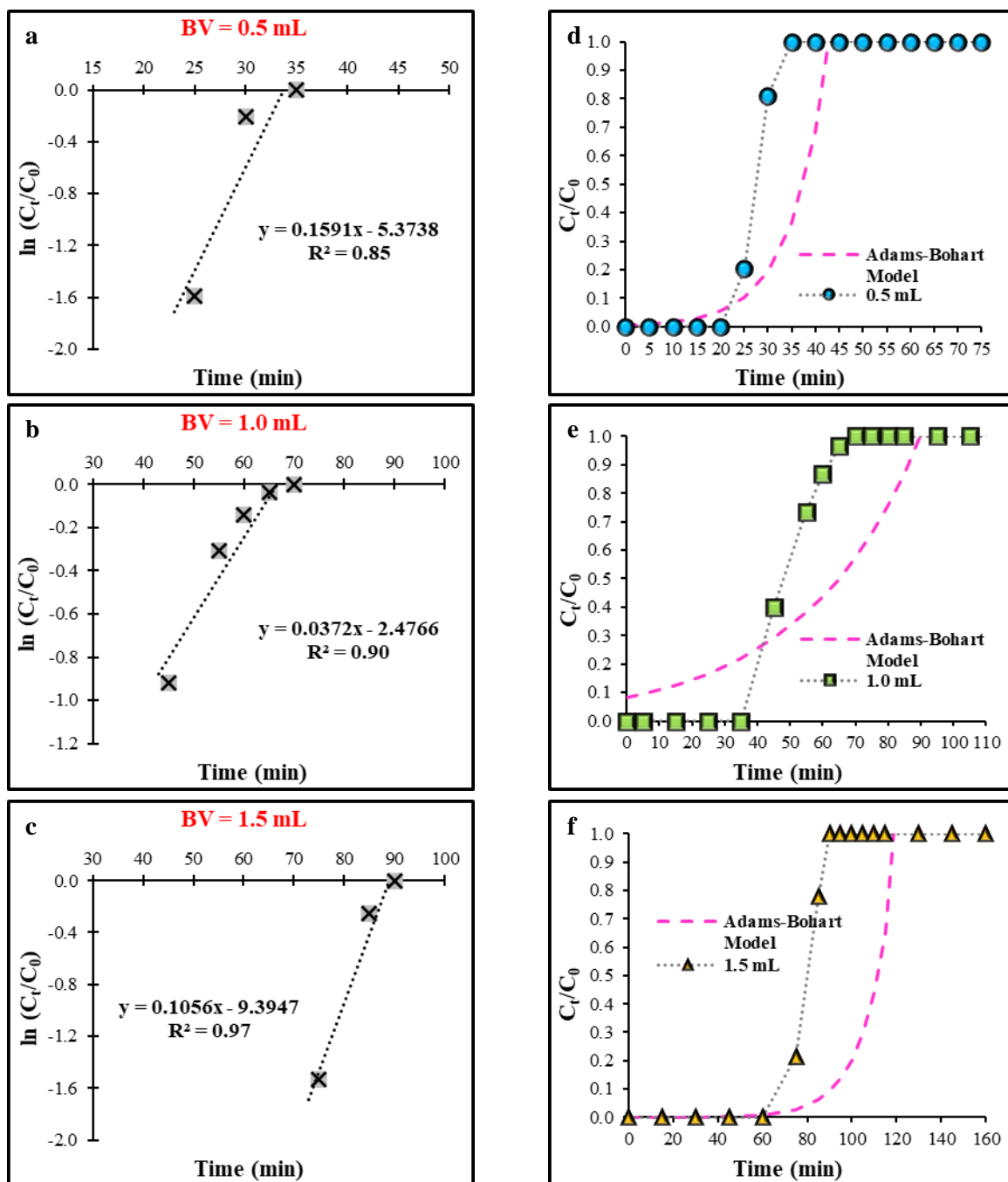


Figure B7 Mathematical modeling for breakthrough curves at different bed volumes using the Adams-Bohart model. Panels a, b, and c show the linear regression analysis, while panels d, e, and f show the experimental data (points) in comparison to the theoretical breakthrough curves (dashed lines).

Mathematical Models Fitting at Different Influent P_i Flow Rates

Figures B8-B10 illustrate the Thomas, Yoon-Nelson, and Adams-Bohart linear regression analysis and model fits at different influent flow rates.

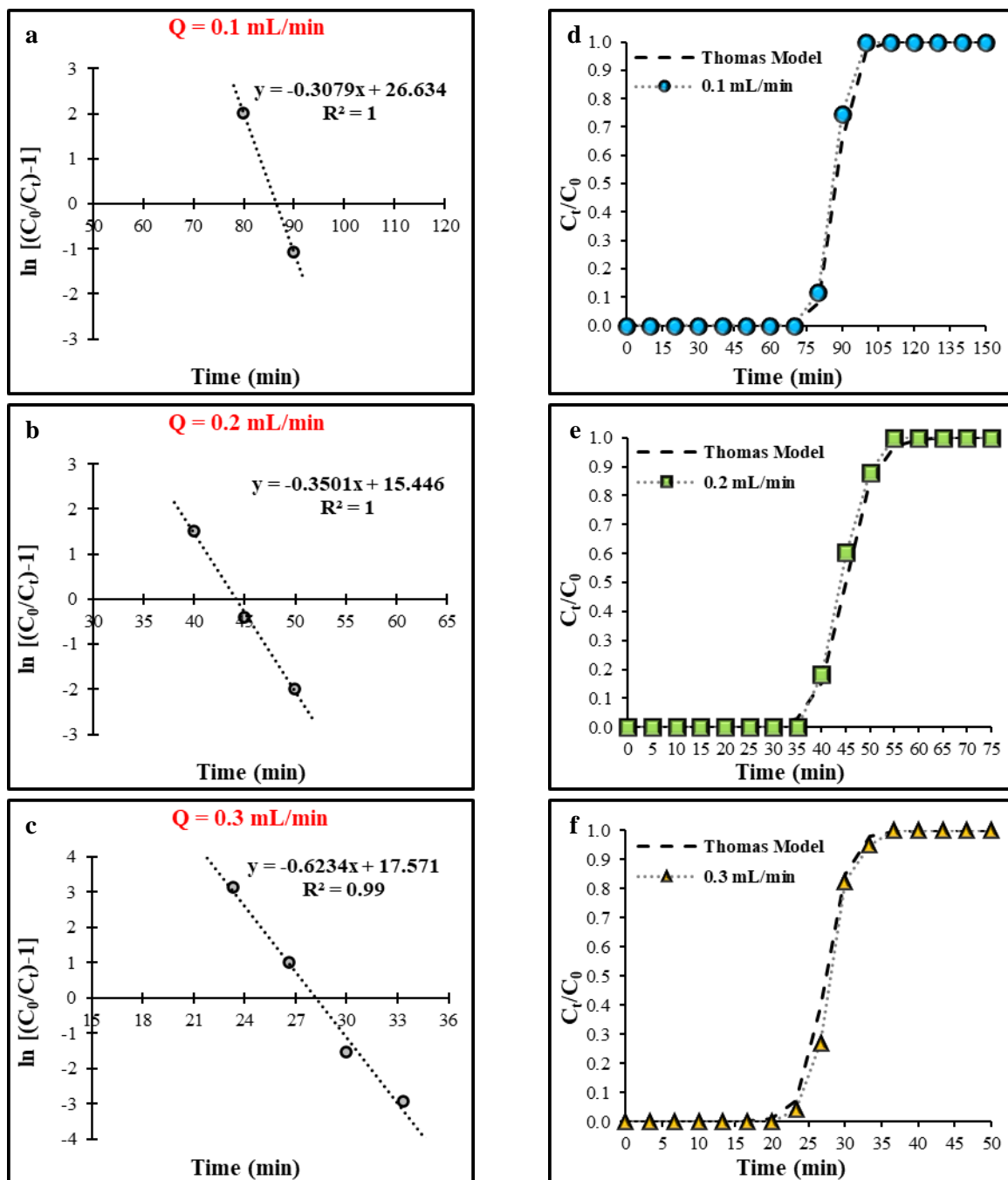


Figure B8 Mathematical modeling for breakthrough curves at different flow rates using the Thomas model. Panels a, b, and c show the linear regression analysis, while panels d, e, and f show the experimental data (points) in comparison to the theoretical breakthrough curves (dashed lines).

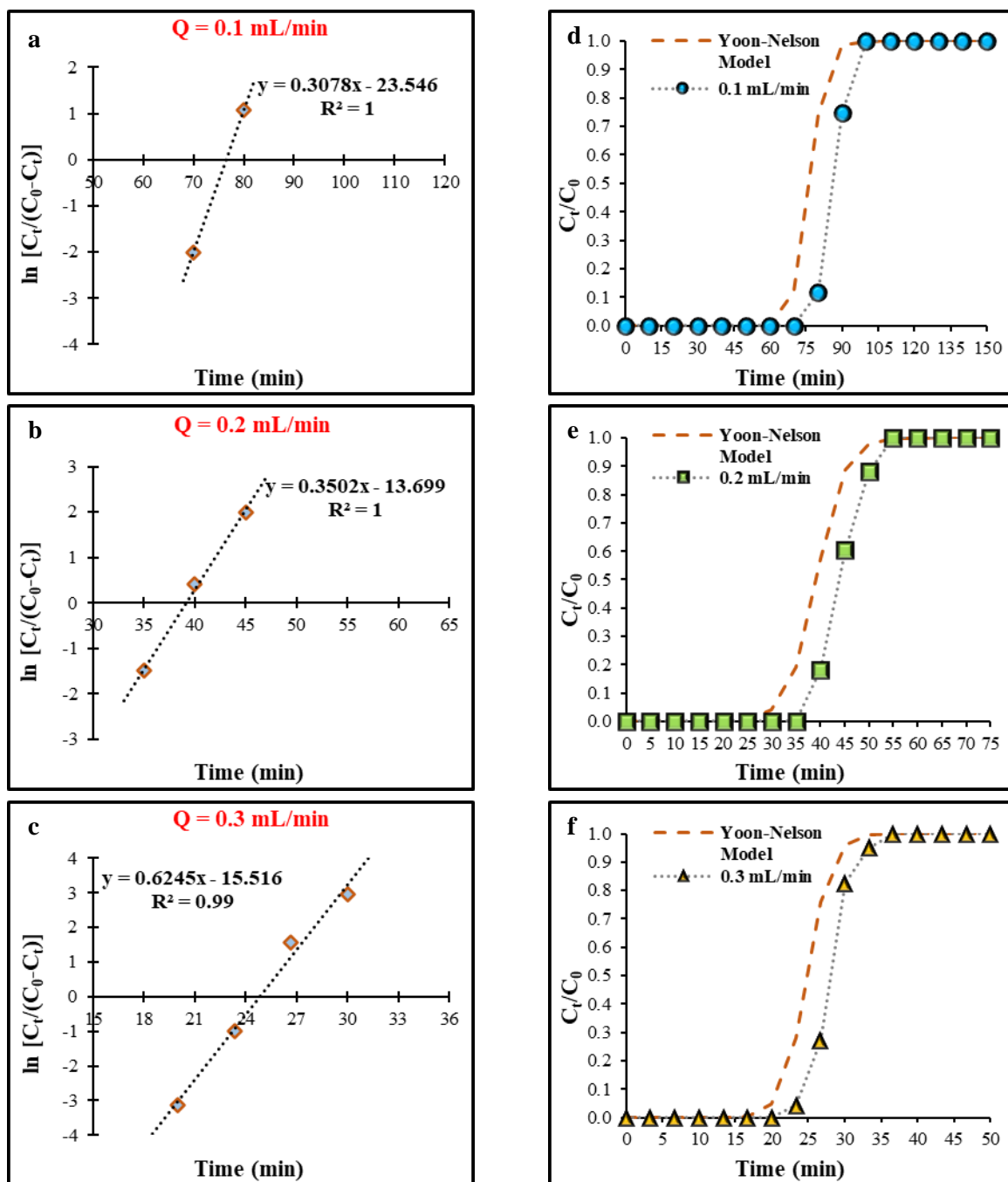


Figure B9 Mathematical modeling for breakthrough curves at different flow rates using the Yoon-Nelson model. Panels a, b, and c show the linear regression analysis, while panels d, e, and f show the experimental data (points) in comparison to the theoretical breakthrough curves (dashed lines).

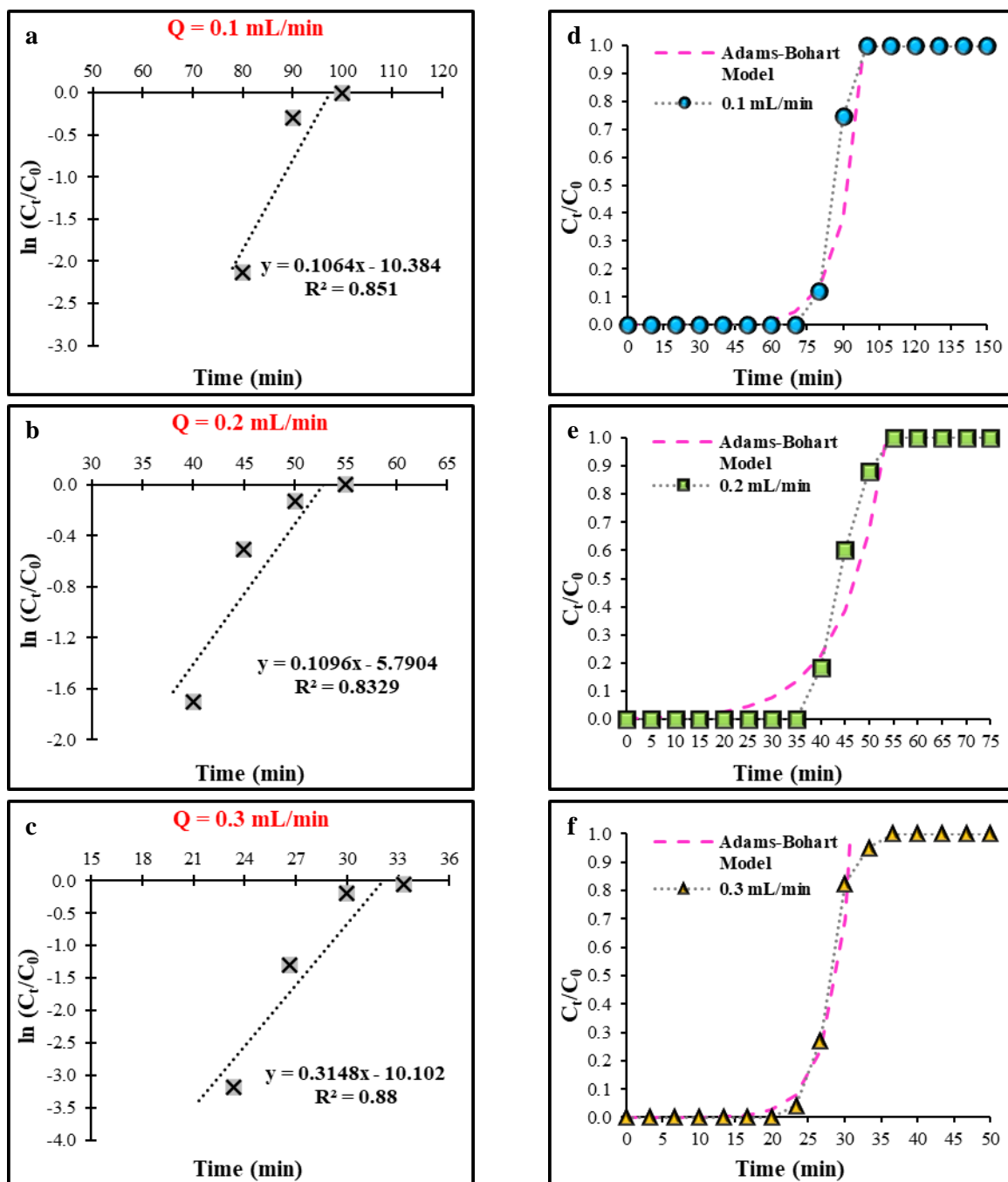


Figure B10 Mathematical modeling for breakthrough curves at different flow rates using the Adams-Bohart model. Panels a, b, and c show the linear regression analysis, while panels d, e, and f show the experimental data (points) in comparison to the theoretical breakthrough curves (dashed lines).

Application of the Bed-Depth/Service Time (BDST) Model

Figures B11-B12 illustrate the application of the bed depth service time [BDST] model at different P_i concentrations and flow rates.

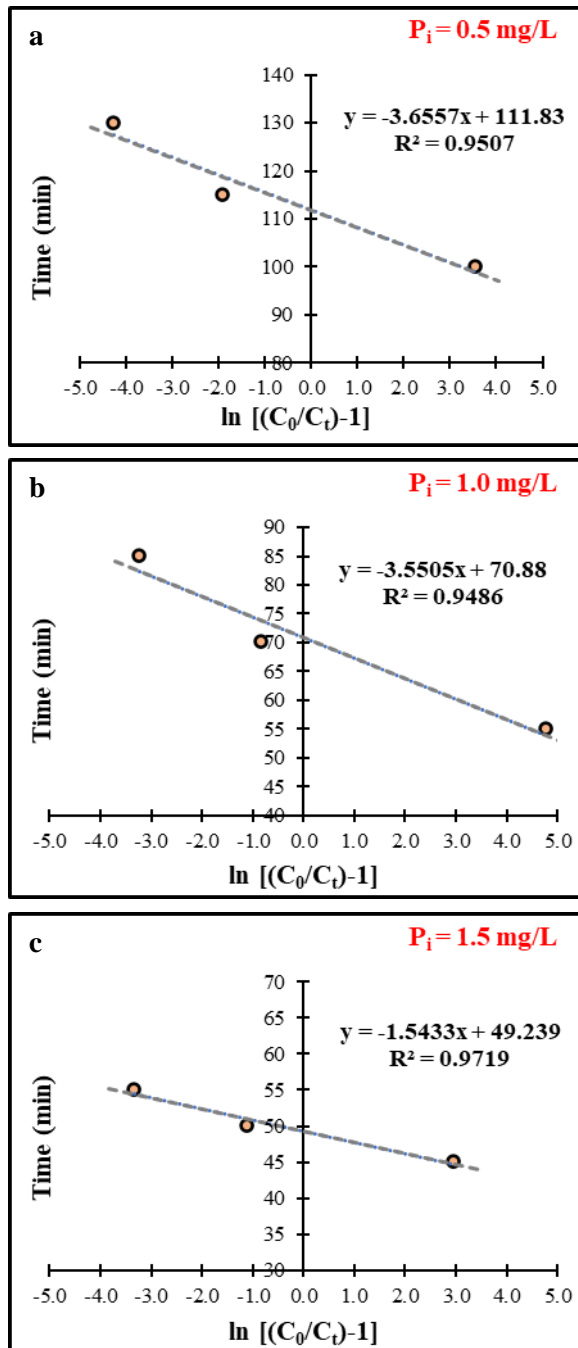


Figure B11 Experimental data fit to the BDST equation at different influent phosphate concentrations (a) $0.5 \text{ mg PO}_4^{3-} \text{ L}^{-1}$, (b) $1.0 \text{ mg PO}_4^{3-} \text{ L}^{-1}$, and (c) $1.5 \text{ mg PO}_4^{3-} \text{ L}^{-1}$.

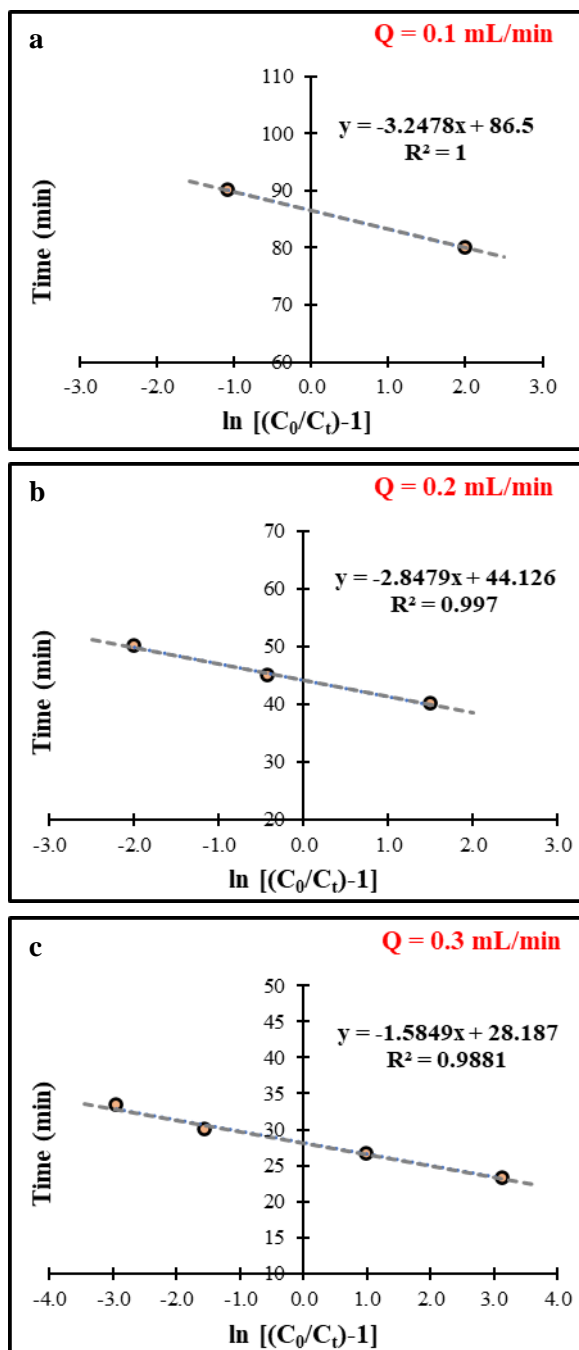


Figure B12 Experimental data fit to the BDST equation at different influent phosphate flow rates (a) 0.1 mL min^{-1} , (b) 0.2 mL min^{-1} , and (c) 0.3 mL min^{-1} .

Breakthrough Modeling for Tertiary Wastewater Effluent

Figure B13 shows the linear regression analysis and experimental data fitting for tertiary wastewater using the Thomas, Yoon-Nelson, and Adams-Bohart models.

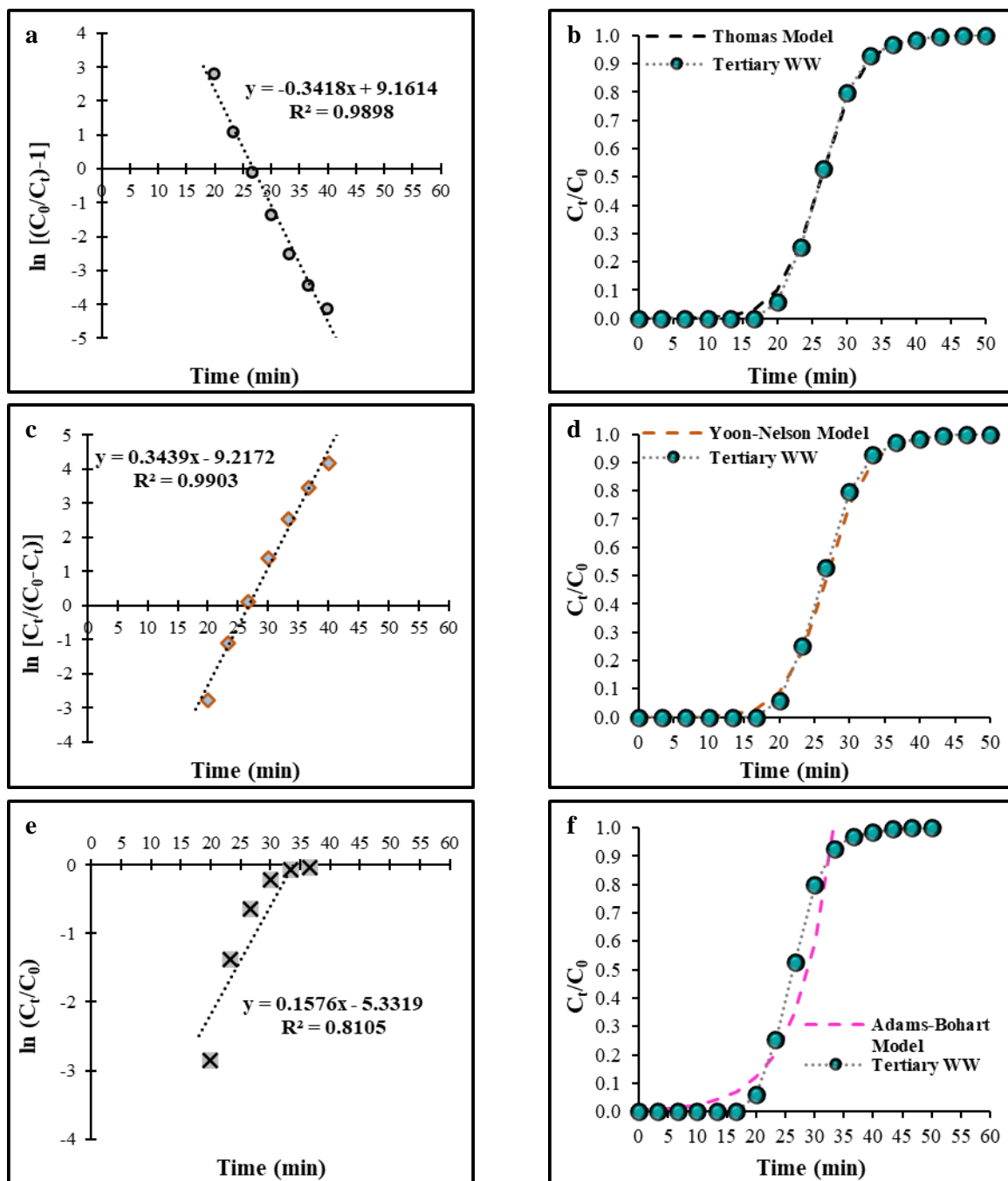


Figure B13 Linear regression analysis and experimental data fitting for tertiary wastewater effluent; (a and b) Thomas model, (c and d) Yoon-Nelson model, and (e and f) Adams-Bohart model.

Figure B14 illustrates the application of the bed depth service time [BDST] model for tertiary wastewater.

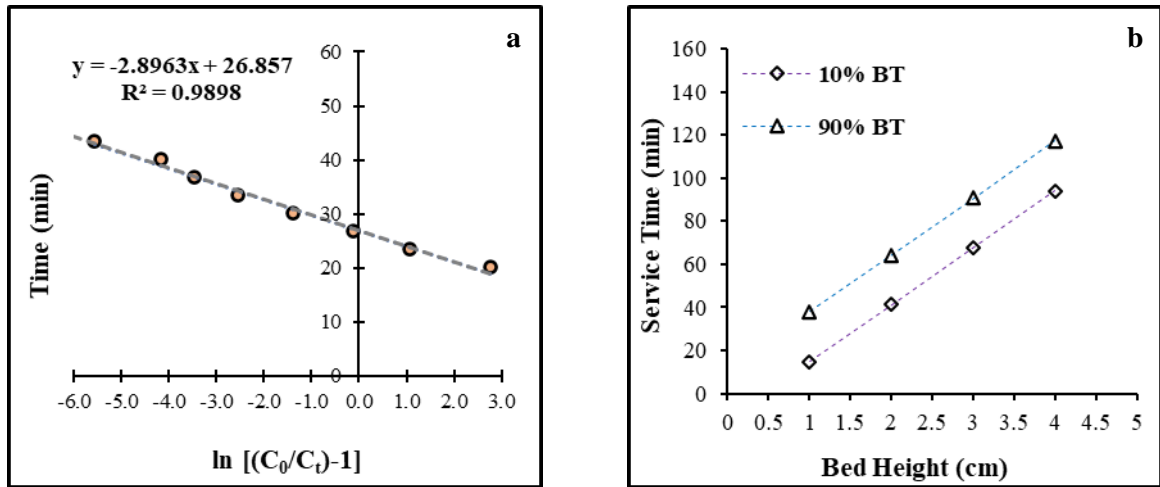


Figure B14 Application of BDST analysis for tertiary wastewater effluent: (a) experimental data fit to the BDST equation, and (b) calculated bed service time for 10% and 90% breakthrough.

Table B2 provides the Thomas, Yoon-Nelson, Adams-Bohart and the bed depth service time [BDST] model parameters for tertiary wastewater based on Figures B13-B14.

Table B2 Thomas, Adams-Bohart, Yoon-Nelson, and BDST model parameters for tertiary wastewater effluent tests.

Model	Parameter	Value
Thomas	K_{TH} (L [mg-min] ⁻¹)	0.464
	q_0 (mg g ⁻¹)	16.9
	R^2	0.99
	% ε (t _{0.5})*	1.0
Adams-Bohart	K_{AB} (L [mg-min] ⁻¹)	0.214
	N_0 (mg L ⁻¹)	15.0
	R^2	0.81
	% ε (t _{0.5})	-9.0
Yoon-Nelson	K_{YN} (min ⁻¹)	0.344
	τ (min)	26.8
	R^2	0.99
	% ε (t _{0.5})	1.0
BDST	K_{BDST} (L [mg-min] ⁻¹)	0.254
	N_0 (mg L ⁻¹)	11.9
	R^2	0.99
	% ε (t _{0.5})	2.0

* % ε (t_{0.5}), percentage error for the time required for 50% breakthrough (τ) determined using the experimental data versus the predicted models.

Scale-up Design of a PBP-NHS Column

The breakthrough results from lab-scale column tests can be used to design large-scale columns using scale-up or kinetic approaches. The scale-up approach relies on similarities in the empty bed contact time (EBCT) and hydrodynamic characteristics between lab-scale and either pilot- or full-scale column systems (Jung et al., 2017). In the kinetic approach, values for the Thomas model constants, obtained from the lab-scale column data, can be used as the basis for designing a pilot- or full-scale column (Manjunath and Kumar, 2021). Here, we use the scale-up approach as an example of large-scale column design using the lab-scale results. The filtration rate (FR) and EBCT values from the lab-scale column were used as the basis for designing the large-scale column. The calculations were made using the tertiary wastewater lab-scale column data and the equations below. The results are shown in Table B3.

$$FR = \frac{Q_L}{A_L} \quad \dots (1)$$

$$EBCT = \frac{BV_L}{Q_L} \quad \dots (2)$$

$$A_D = \frac{Q_D}{FR} \quad \dots (3)$$

$$H_{BD} = FR * EBCT \quad \dots (4)$$

$$BV_D = A_D * H_{BD} \quad \dots (5)$$

$$M_D = BV_D * \rho_{resin} \quad \dots (6)$$

$$BTV_D = t_L * Q_D \quad \dots (7)$$

$$M_{CR} = BTV_D * C_0 \quad \dots (8)$$

$$M_{AC} = \frac{M_{CR}}{q_{\max}} \quad \dots (9)$$

where:

FR = filtration rate (cm min^{-1})

Q_L = lab-scale flow rate ($\text{cm}^3 \text{min}^{-1}$)

A_L = cross-sectional area of the lab-scale column (cm^2)

EBCT = empty bed contact time of the lab-scale column (min)

BV_L = bed volume of the lab-scale column (cm^3)

A_D = cross-sectional area of the design column (m^2)

Q_D = design flow rate (assumed $500 \text{ m}^3 \text{d}^{-1}$)

H_{BD} = bed height of the design column (cm)

BV_D = bed volume of the design column (m^3)

M_D = adsorbent mass required in the design column (kg)

ρ_{resin} = density of resin (g m^{-3})

t_L = lab-scale breakthrough time (min)

BTV_D = design breakthrough volume (m^3)

M_{CR} = adsorbate consumption rate of the design column (g)

C_0 = initial P_i concentration (mg mL^{-1})

M_{AC} = amount of adsorbent consumed in the design column (kg)

q_{\max} = maximum capacity of the resin ($\mu\text{g g}^{-1}$)

Table B3 provides the parameters for scale-up design of PBP-NHS columns.

Table B3 Parameters for scale-up design of a PBP-NHS column.

Parameter	Unit	Value
Filtration rate	cm min ⁻¹	0.6
Area	m ²	57.9
Diameter	m	8.58
Empty bed contact time	min	1.67
Bed height	cm	1
Bed volume	m ³	0.58
Adsorbent mass	kg	609
Breakthrough time	min	20
Breakthrough volume	m ³	6.94
Amount of adsorbent consumed	kg	261

Appendix C Supporting Information - Chapter 5

Table C1 provides characteristics of the tertiary wastewater effluent sample.

Table C1 Characterizations of tertiary wastewater effluent from the South Shore Water Reclamation Facility in Oak Creek, WI. Each measurement was performed in triplicate using Standard Methods*.

Parameter	Unit	Average ± Standard Deviation
Total Suspended Solid (TSS)	mg L ⁻¹	16 ±3
Dissolved Organic Carbon (DOC)	mg-C L ⁻¹	9.2 ±0.1
Total Hardness	mg L ⁻¹ CaCO ₃	327 ±10
Alkalinity	mg L ⁻¹ CaCO ₃	180 ±10
Chloride	mg L ⁻¹ as Cl ⁻	460 ±10
Phosphate	mg PO ₄ ³⁻ L ⁻¹	1.2 ±0.1
Nitrate	mg NO ₃ ⁻ L ⁻¹	8.0 ±0.05
Sulfate	mg SO ₄ ²⁻ L ⁻¹	224 ±0.13
Hydrogen Sulfide	mg S ²⁻ L ⁻¹	0
pH	---	7.13 ±0.1

*TSS was measured following Method 2540D from Standard Methods for the Examination of Water and Wastewater, APHA, 2005. DOC was measured following U.S. EPA Method 415.3 using a Shimadzu TOC-VCSN. The rest of measurements were performed using Single Parameter Test Kits from Hach Company.

Figure C1 illustrates the pseudo first-order kinetic model for P_i adsorption using PBP-IOPs.

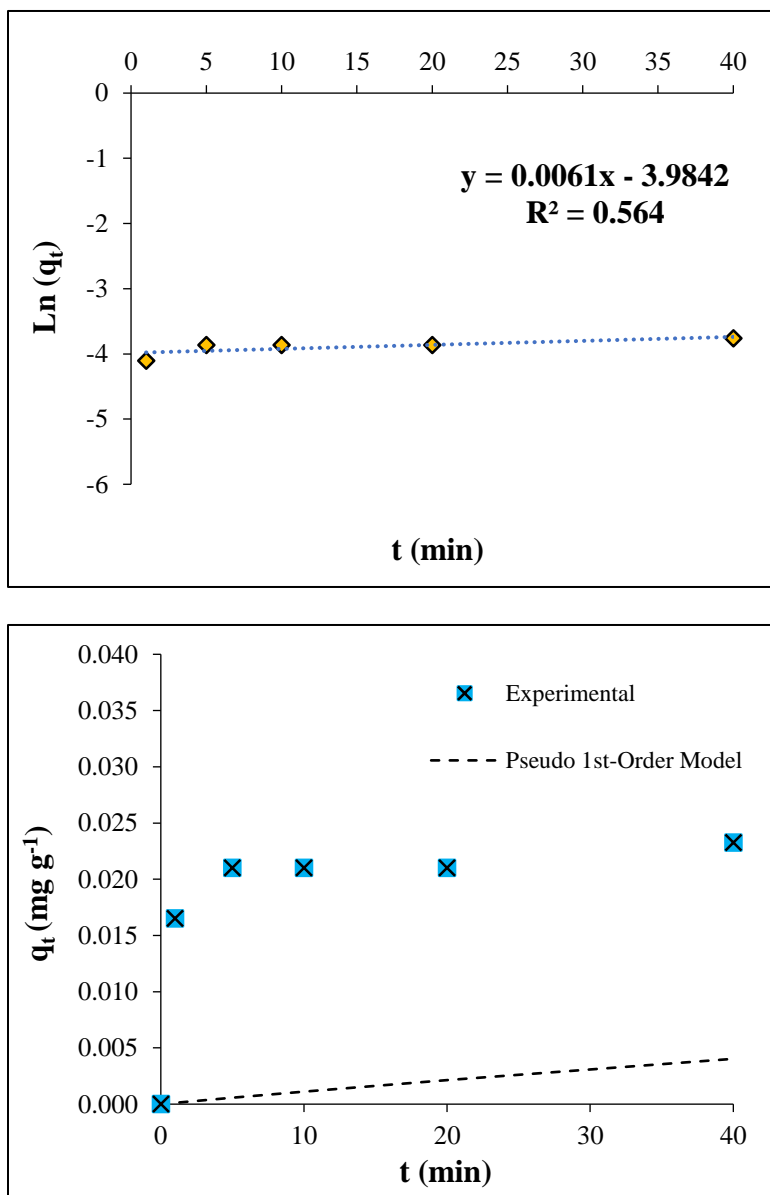


Figure C1 P_i adsorption kinetics using the PBP-IOP adsorbent at room temperature and neutral pH. (a) PBP-IOP adsorbent capacity as a function of time modeled using non-linear pseudo first-order kinetics, (b) experimental data fit to linear regression using the pseudo first-order kinetic model.